MODELING THE PROSTATE CANCER TISSUE MICROENVIRONMENT USING HYALURONAN HYDROGELS

by
Nicky W. Tam

Submitted in partial fulfilment of the requirements
for the degree of Master of Applied Science

at
Dalhousie University
Halifax, Nova Scotia
March 2020

Table of Contents

List of Tables ..... **vi**

List of Figures ..... **vii**

Abstract ..... **viii**

List of Abbreviations Used ..... **ix**

Chapter 1. Introduction **1**

1.1. Clinical Relevance of Prostate Cancer 1

1.1.1. Genetic Basis of Prostate Cancer 2

1.1.2. Relationship with Tissue Environment 3

1.2. The Tumour Microenvironment 4

1.2.1. The Extracellular Matrix 5

1.2.2. Molecular Mechanisms of Phenotypic Shifts 7

1.2.3. Anoikis 8

1.2.4. Cancer Cell Evolution 10

1.2.5. The Pre-Metastatic Niche 10

1.3. Standards for Cell Culture 12

1.4. State-of-the-Art in Model Tissues 15

1.5. Hyaluronan as a Cell Culture Environment 17

1.5.1. Cell Interactions with HA 18

1.5.2. CD44 in Cancer 19

1.5.3. HA Hydrogels 20

Chapter 2. Chemical Modification of HA **22**

2.1. Disulfide Crosslinked HA Hydrogels 22

2.1.1. Crosslinking Scheme: Materials and Methods 23
2.1.2. HA Content of the Final Hydrogel Material 25
2.2. Discussion 26
2.2.1. Choice of Chemical Modification 26
2.2.2. Protocol Optimization 27
2.2.3. Hydrogel HA Content 30
2.2.4. Molecular Weight and Degree of Crosslinking 30
Chapter 3. Material Characterization 32
3.1. Results 33
3.1.1. Power Law Dependence of Gelation on Concentration 33
3.1.2. Mechanical Stiffness of HA Gels is Much Lower than Prostate Tissue 35
3.2. Materials and Methods 36
3.2.1. Capillary Gelation Test 36
3.2.2. Compression Testing 37
3.3. Discussion 40
Chapter 4. Diffusivity and Mass Transfer 42
4.1. Results 42
4.1.1. Cell Viability Appears Limited by Access to Nutrients 42
4.1.2. Diffusivity of Small Particles is Independent of HA Content 48
4.1.3. HA Hydrogels Sequester Proteins from Medium 50
4.2. Materials and Methods 52
4.2.1. Cell Line Culture Methods 52
4.2.2. Acute Cytotoxicity Experiments 53

4.2.3. Modified Culture Configuration 54
4.2.4. Fluorescence Recovery after Photobleaching 55
4.2.5. Dot-Blots 59
4.3. Discussion 60
4.3.1. Diffusion and Systems-Level Mass Transfer 60
4.3.2. Differences in Cell Viability 63
4.3.3. Cell Aggregation 64
Chapter 5. Cells in Gels 65
5.1. Results 67
5.1.1. Decreasing ATP Content Suggests Lack of Nutrients 67
5.1.2. PC3 Cells in Hydrogel Culture Upregulate HIF1A mRNA Expression 68
5.1.3. Akt-AMPK-mTOR Activity Profile of PC3 Cells 70
5.2. Materials and Methods 74
5.2.1. ATP Content Assay 74
5.2.2. Endpoint Reverse Transcriptase PCR Analysis 74
5.2.3. Western Blot Analysis 76
5.3. Discussion 77
5.3.1. Cell Line Mutations 77
5.3.2. Expression of HIF-1 in PC3 Cells 79
5.3.3. S6K Activation amidst Metabolic Stress 79
Chapter 6. Conclusion 81
6.1. Future Directions 81
6.1.1. From 2D to 3D 81

6.1.2. ECM Additives 83
6.1.3. Comparing Cell Types 83
6.1.4. HA Hydrogels as Surgical Filler 84
6.2. Limitations of HA Hydrogels 84
6.3. Is the Future of Cancer Research 3D? 85
6.4. Final Remarks 88
References 89

List of Tables

Table 1, Correlation ratios of diffusion half-times 58

List of Figures

Figure 1, Chemical modification of hyaluronan to form a hydrogel. 23

Figure 2, CTAB turbidimetric assay for measuring HA content.. 26

Figure 3, Over-crosslinking of gels and crashing from solution. 29

Figure 4, Gelation progression as measured using a capillary gelation test. 33

Figure 5, Power law relationship between hydrogel concentration and gelation onset. 34

Figure 6, Hydrogel mechanical properties measured with compression testing. 35

Figure 7, experimental setup for compression testing.. 38

Figure 8, LNCaP acute cytotoxicity after exposure to HA hydrogels. 43

Figure 9, PC3 acute cytotoxicity after exposure to HA hydrogels. 44

Figure 10, Schematic diagram of different hydrogel cell culture configurations. 46

Figure 11, Comparison of cells cultured underneath and on top of HA hydrogels. 47

Figure 12, FRaP analysis of diffusive properties of HA hydrogels.. 49

Figure 13, Dot-blot analysis of HA hydrogel protein retention. 50

Figure 14, Dot-blot analysis of protein penetrance in HA hydrogels. 51

Figure 15, Mass transfer compartmentalization. 61

Figure 16, Akt-mTOR signaling pathway with adjacent control elements 66

Figure 17, ATP content of PC3 cells cultured in hydrogels. 68

Figure 18, Endpoint PCR analysis of HIF1A mRNA expression.. 69

Figure 19, Akt activation in PC3 cells cultured in varying concentrations of HA hydrogel. 70

Figure 20, AMPK activation in PC3 cells cultured in varying concentrations of HA hydrogel. 71

Figure 21, LC3B expression in PC3 cells cultured in varying concentrations of HA hydrogel. 72

Figure 22, S6K activation in PC3 cells cultured in varying concentrations of HA hydrogel. 73

Figure 23, Known mutations in the Akt-mTOR pathway in LNCaP cells. 78

Figure 24, Spheroids grown in agarose-HA hydrogel sandwich culture.. 82

Abstract

Prostate cancer cells exist in dynamic, evolving tissue environments and their behaviour is influenced by context-specific interactions with their surroundings. To better understand how and why prostate cancer cells behave the way they do, they need to be studied in context. To improve upon conventional cell culture techniques, I explored the use of a disulfide-crosslinked hyaluronan hydrogel as a model cell culture environment. I optimized a previously described chemical modification protocol to better suit the needs of a general life science laboratory and characterized the material properties of the resulting hydrogel. With unique diffusive properties, this hydrogel can potentially be used to model hypoxic tissues with limited diffusivity. Model prostate cancer cells cultured within this hydrogel environment exhibited increased metabolic activity despite signs of limited access to nutrients. This hydrogel has potential for use in advanced three-dimensional tissue culture and could help improve the physiological relevance of prostate cancer research.

List of Abbreviations and Symbols Used

2D	Two-dimensional
3D	Three-dimensional
Akt	Protein kinase B
AMP	Adenosine monophosphate
AMPK	5’ adenosine monophosphate-activated protein kinase
ANOVA	Analysis of variance
ATP	Adenosine triphosphate
BSA	Bovine serum albumin
BRCA1/2	Breast cancer type 1/2 susceptibility protein
CD44	Cluster of differentiation 44
CTAB	Cetyltrimethylammonium bromide
CXCL12	C-X-C motif chemokine 12, stromal cell-derived factor 1 (SDF1)
CXCR4	C-X-C chemokine receptor type 4, fusin, cluster of differentiation 184
DMEM	Dulbecco’s modified Eagle’s medium
DNA	Deoxyribonucleic acid
DTP	3,3’-Dithiobis(propanoic dihydrazide)
DTT	Dithiothreitol
ECM	Extracellular matrix
EDC	1-Ethyl-3-(3-dimethylaminopropyl) carbodiimide
EMT	Epithelial-to-mesenchymal transition
ERG	ETS-related gene
ETS	E26 transformation-specific transcription factor

F-12K	Kaighn’s modification of Ham’s F-12 medium
FBS	Fetal bovine serum
FITC	Fluorescein isothiocyanate
FOXA1	Forkhead box protein A1
FRaP	Fluorescence recovery after photobleaching
Gly	Glycine
GTP	Guanosine-5’-triphosphate
HA	Hyaluronan, hyaluronic acid
HIF-1	Hypoxia inducible factor 1
HIF1A	Hypoxia inducible factor 1, α subunit (gene)
HMBS	Hydroxymethylbilane synthase, porphobilinogen deaminase (gene)
HRP	Horseradish peroxidase
kDa	Kilodalton
kPa	Kilopascal
LC3B	Microtubule-associated proteins 1A/1B light chain 3B
LOX	Lysyl oxidase
M	Molar
MET	Mesenchymal-to-epithelial transition
miRNA	miRNA
MMP	Matrix metalloproteinase (or metalloprotease)
mTOR	Mammalian Target of Rapamycin
N	Newton
NF-κB	Nuclear factor κB

PBS	Phosphate-buffered saline
PCR	Polymerase chain reaction
PTEN	Phosphatase and tensin homolog
PVDF	Polyvinylidene fluoride
RANK	Receptor activator of nuclear factor κB
RANKL	Receptor activator of nuclear factor κB ligand
RGD	Arginylglyculaspartic acid
RHAMM	Receptor for hyaluronan-mediated motility
RIPA	Radio-immunoprecipitation assay
RUNX2	Runt-related transcription factor 2
S6K	P70 S6 Kinase
SDS-PAGE	Sodium dodecyl sulfate-polyacrylamide gel electrophoresis
SPOP	Speckle-type POZ protein
TAE	Tris-acetate-EDTA
TBST	Tris-buffered saline with 0.05% Tween 20
TCPS	Tissue culture polystyrene
TMPRSS2	Transmembrane protease, serine 2 (gene)
TP53	Tumour protein p53 (gene)

Chapter 1. Introduction

1.1. Clinical Relevance of Prostate Cancer

Prostate cancer continues to be a prominent concern for healthcare systems around the world. According to the Canadian Cancer Society, it is the most common form of cancer in men and also the 3rd leading cause of death from cancer in this population (1). As a disease often associated with old age, prostate cancer is particularly prevalent in developed countries, where life expectancy is high and populations continue to grow older. Rates of diagnosis are increasing around the world as a result of improved access to healthcare, improved diagnostic capabilities, and increasing life expectancy (2). Prostate cancer poses a significant economic burden on healthcare systems and patients due to high costs associated with initial diagnosis and treatment, as well as long-term follow-up and monitoring procedures to track possible disease progression or recurrence after treatment (3). The high prevalence of prostate cancer and the inherent risk of over-diagnosis leading to unnecessary treatment also poses a significant challenge to healthcare systems. This is especially relevant in the context of early-onset prostate cancer. The proportion of men below the age of 55 at diagnosis is increasing, and this younger cohort is more likely to undergo prostatectomy as treatment compared to their older counterparts (4,5). Well-informed risk analysis models that take into account disease progression, likelihood of recurrence, and treatment-related complications are needed to better plan for patient care and to avoid unnecessary treatments that might result in further complications.

Currently, a major issue in the diagnosis and treatment of prostate cancer is the lack of accurate risk stratification in predicting disease aggressiveness and subsequent identification of patient candidates that would respond well to medical intervention. Traditionally, various clinical algorithms have been used to assess disease progression, such as the level of prostate-specific antigen (PSA) in serum and the Gleason score, which is a morphological evaluation of prostate tissue obtained from biopsy (6–8). Studies have also looked at the effectiveness of genetic markers and circulating immunological and cell-based

biomarkers in determining risk of metastasis, severity of disease, and potential effectiveness of treatments (9–11). This has revealed a great diversity of genetic profiles and cellular phenotypes in prostate cancer, which complicates the use of current models to predict disease outcomes. This is evident in differential patient responses to cancer treatments. Even within the same tumour, the heterogeneity of cancer cells in terms of mutations, proliferative potential, malignancy, and resistance to treatment poses a significant challenge in evaluating disease state as a whole, especially given only a limited number of possible diagnostic readouts. For example, multifocal prostate cancer can behave as multiple different cancers in response to individual cancer treatments due to clonal differences (12). Moreover, the use of non-specific biomarkers, such as PSA is known to result in false positives, potentially leading to unnecessary treatment and possible patient morbidity (13). Issues of biomarker specificity and their accuracy in representing overall disease state limit the effectiveness of personalized treatment strategies for cancer patients. New personalized disease tracking models hold great promise in streamlining the identification of effective treatment options for prostate cancer patients (14–16), but operate on the assumption that disease state can be accurately, wholly, and specifically represented by monitored biomarkers in order to estimate disease progression and to inform further treatment. These models are thus limited by the lack of understanding of how biomarkers relate back to overall disease state in light of cancer cell heterogeneity and the interplay of cancer cells with the surrounding tissue.

1.1.1. Genetic Basis of Prostate Cancer

At the cellular level, prostate cancer is the uncontrolled proliferation and growth of prostate cells due to aberrant gene expression. The prostate cancer genome is complex and evolves over time with disease state through cancer cell evolution. According to Arora and Barbieri in their review of the molecular subtypes of prostate cancer (17), the disease can be loosely categorized according to present mutations or genetic alterations at the onset of the disease, which predisposes cancer cells towards specific subsequent genetic alterations. For example, one of the most common genetic mutations found in

prostate cancer cells, found in up to 50% of disease cases is the rearrangement and fusion of TMPRSS2 with members of the ETS transcription factor family (18,19). ETS transcription factors – which include ERG, a prominent oncogene, mediate many important cell processes, including cell proliferation, migration, and angiogenesis. The fusion of ERG with TMPRSS2 results in a substantial increase in the expression of ERG in response to androgen signaling mediated by its TMPRSS2 fusion pair. Other genes that can be mutated in the early stages of prostate cancer include FOXA1, which promotes androgen-dependent cell growth and SPOP, which is involved in DNA repair and protein turnover (17). Interestingly, SPOP mutations and TMPRSS2-ETS fusions appear to be mutually exclusive, suggesting early divergence in genetic subtypes of prostate cancers (18,19). Since many of these early mutations act on androgen signaling pathways, androgen deprivation therapy is an effective means of limiting cancer growth (17). As prostate cancer cells acquire new mutations, however, the disease can progress from a benign state to a malignant state. Loss of function or deletion of PTEN (20) or TP53 (21) can lead to uncontrolled cell cycle progression leading to rapid overgrowth of cancer tissue. Interestingly, mutations in these genes appear to be negatively correlated or entirely absent from cells with SPOP mutations while being enriched in cells with ETS fusions (17,22), suggesting mutational predisposition and lineage divergence. This is not, however, a reliable predictor of disease outcome (17). As the mutational burden of a prostate cancer increases, the disease can become aggressively metastatic and insensitive to androgen deprivation. Mutations in DNA repair genes like BRCA1 and 2 cause genetic instability while mutations in the androgen receptor signaling pathway can cause androgen hypersensitivity or constitutive activation of downstream processes (17,19). This shift in cancer cell biology is difficult to predict since the factors that contribute to this disease progression are not well understood.

1.1.2. Relationship with Tissue Environment

Many different aspects of overall health and lifestyle factors, on top of genetic predispositions can contribute to changes in the cancer tissue environment, which affect overall disease state. For example,

obesity has long been associated with worse disease prognosis and more aggressive cancers in general (23,24). This manifests clearly at the molecular level and can be observed as altered metabolic activity, increased inflammation, and changes in the protein composition of tissues (25–28). Dietary, occupational, and lifestyle factors can contribute to oxidative stress in tissues through the production and release of reactive oxygen species, changing the overall balance of oxidants and antioxidants as well as promoting inflammation (29). While tumour cells themselves are capable of priming their environment with oxidative species (30,31), exogenous reactivity coming from the stromal environment can contribute to changes in tissues that promote malignant transformation (31,32). Given this complex relationship between cancer cells and their environment, it is understandable that predicting disease outcomes is a challenge. Indeed, it is not fully understood how the interplay of all these factors affects the transformation of tissue from a healthy state to a cancerous state.

Ultimately, greater understanding of the underlying molecular processes of prostate cancer progression is required to improve disease monitoring and targeted cancer treatments. Accurate and detailed cell-based *in vitro* models of prostate cancer as well as *in vivo* models of human disease are both needed. Specifically, *in vitro* models need to take into account the complex relationship between cancer cells and their tissue environment. A holistic understanding of how cells influence their environment and how they are in turn influenced by their surroundings will help contribute to more efficient identification of potential risk factors that may predispose patients to recurrent, aggressive, and/or metastatic disease. Without understanding the physiological context in which a cancer grows, the disease state as a whole cannot be fully elucidated.

1.2. The Tumour Microenvironment

In their seminal review on “occult” cancers, or cancers that remain undetected in the body, and the role of tissue microenvironments in disease presentation and progression, Bissell and Hines argue that context is paramount to understanding cancer cell behaviour (33). A key point they bring up is the

apparent overriding of cell genotype with external environmental cues, as evidenced in the tissue specificity of heritable cancers despite the oncogene in question existing throughout an individual's somatic cells. The focus of Bissell and Hines' review is the chemical aspect of the tumour microenvironment, as parsed and decoded by cells by way of surface receptors such as integrins. Biochemical signals from the extracellular environment are sensed and transduced by cells, resulting in alterations in protein activity and gene transcription that drive changes in cell behaviour. However, physical and mechanical aspects of the tumour microenvironment also have effects on cell function, and there is an active and reciprocal role that cells have in shaping their surroundings. Disease presentation and progression must therefore be studied within the context of the complex and dynamic relationship that cancer cells have with their tissue environment.

1.2.1. The Extracellular Matrix

The non-cellular, structural portion of tissues is made up of an interconnected network of large secreted macromolecules, termed the extracellular matrix (ECM) (34). For most solid tissues, the ECM can be described as a hydrogel with covalent and non-covalent interactions that hold the macromolecules together, functionally crosslinking them into a stable, insoluble structure (35,36) perfused by interstitial fluid. The ECM is an integral part of tissues, providing both tissue-specific mechanical and biochemical support to its resident cells. Signaling can be derived from soluble factors, exosomes, and other materials sequestered or entrapped in the matrix (37,38), or through direct receptor binding with ECM components. Cells can gather information about their environment through various cell surface receptors that bind with specific molecular sequences. One well-studied example is the interaction between integrins and RGD sequences on the fibronectin molecule (35,39), which are now often used in engineering biomaterials to improve cell attachment (40,41). Direct ECM-binding allows cells to sense the chemical makeup of their surroundings as well as the geometry and mechanics of their environment through the spatial variation of bound receptors and mechanical reorganization of their cytoskeleton. These physical signals ultimately

get transduced into biochemical signals inside the cell which control gene expression and protein function, contributing to tissue-specific cell phenotypes (34,39,42–45). The interplay of these cell-matrix interactions is still not completely understood due to the complexity of the ECM environment. With so many different signals being integrated by cells, it is difficult to parse out the individual contributions of such interactions to cell behaviour. Reciprocally, cells can modify their extracellular environment through the expression of matrix metalloproteinases (MMPs), which break down ECM constituents, and through the laying down of new ECM materials. Dynamic, regulated ECM degradation and production is a normal part of ECM turnover and allows cells to maintain a homeostatic environment for optimal function (46–48). It is when this remodeling becomes dysregulated and cell-matrix interactions are knocked out of balance that disease processes may occur.

In cancer, the dysregulation of ECM remodeling results in changes in ECM architecture and tissue organization. Abnormal deposition of matrix components changes both the chemical and mechanical properties of the extracellular environment, modifying patterns of cell attachment, signal transduction, and cell activation (42,49–51). For example, collagen I has been found to be upregulated in various cancers, including in prostate cancer, especially in the tissue stroma (52), resulting in a denser and stiffer matrix, which affects interstitial fluid pressure and movement. The mechanical forces in this environment can facilitate the alignment of collagen fibrils, providing enhanced directional cues for cell attachment, which in turn can promote migratory behaviour via activation of the Rho-ROCK pathway (53). These environmental conditions promote the expression of a migratory cell phenotype, a characteristic that is indicative of an epithelial-to-mesenchymal transition (EMT), which is needed for metastasis (54). Moreover, the increased collagen content results in stronger integrin engagement, which can affect cell cycle progression via expression of cyclin D1 (55). Physically, the ECM acts as a barrier to limit cell motility and the diffusion of signaling molecules and nutrients (56). Abnormal MMP expression by activated cancer and cancer-associated cells can lead to disruption in the local integrity of the ECM, allowing cell invasion. This is an important aspect of intravasation into vasculature during metastasis, as specific MMPs are required to digest components of the basement membrane surrounding blood vessels

(45,52,57). Changes in the diffusive properties of the ECM can affect paracrine and autocrine signalling pathways, which help modulate cell behaviour and control cell survival. As well, the formation of concentration gradients of signalling molecules can be affected by changes in matrix properties, which can in turn affect chemotactic behaviour (58–60). The correlation between disease progression, cell behaviour, and ECM organisation is clear, but the specifics of ECM remodeling and cell signaling remain unclear. Active remodeling of the tumour microenvironment and cancer progression occur hand-in-hand, with the eventual emergence of malignant cell types and the development of an ECM environment that facilitates their spread into neighbouring tissues and distant sites of metastasis (52,57).

1.2.2. Molecular Mechanisms of Phenotypic Shifts

Though not strictly pathological, as in development or wound healing, EMT is a hallmark feature in the development of metastasis in epithelial tumours. Type III EMT, the process specifically involved in cancer is characterized by the loss of epithelial cell markers, reorganization of cytoskeletal components, and the expression of mesenchymal genes and markers which facilitate migratory behaviour and cancer cell stemness. One of the most notable changes involved is cadherin switching, in which cells downregulate E-cadherin expression – a cell adhesion molecule ubiquitously expressed in epithelial cells that is important in the formation of intact cell sheets, and upregulate N-cadherin expression, which promotes collective cell migration and is implicated in cancer invasiveness (61,62). EMT induction is largely regulated by transcription factors, which can induce changes in gene expression programs that govern cell behaviour (62,63). The tumour microenvironment plays a part in EMT induction by promoting the expression of the canonical EMT-inducing transcription factors, TWIST, ZEB, and SNAIL, among others (62). This can be achieved through cytokine or growth factor signaling, through hypoxia inducible factor 1 (HIF-1) activation in hypoxic conditions (64), and through direct cell-matrix interaction via integrin signalling (43,51). Upon EMT induction, ECM geometry and organization can promote as well as direct cell migration. Increased ECM alignment and density decreases the energy

requirement for cell migration (49) and enhances characteristics that drive migration, such as cytoskeletal tension, integrin clustering, and overall cell contractility via activation of Rho GTPases and the ROCK pathway (51). Genomic analysis of cells that have undergone EMT also shows that genes involved in ECM remodeling, including MMPs are upregulated (63), providing further evidence of the reciprocity of cell-matrix interactions and the dynamic changes that occur in cancer progression.

Mesenchymal-to-epithelial transition (MET) is less well-studied compared to EMT but is understood to be an equally important step in the establishment and stabilization of metastases. While EMT is required for dissemination of cancer cells, the observation that metastases are phenotypically similar to their primary epithelial tumour of origin suggests that metastatic cells revert to an epithelial phenotype at the site of metastasis (65). This was evident in a rat model of squamous cell carcinoma, in which TWIST activation was sufficient to induce EMT, but only reversal of TWIST activation allowed for metastatic growth (66). The tissue microenvironment of a metastatic site appears to play as important a role in cancer progression as that of the primary tumour. In breast cancer metastatic to lung, versican, an ECM proteoglycan was found to enhance metastatic cell proliferation and induce epithelial phenotype expression (67). MET was confirmed morphologically and biochemically through increased expression of epithelial cell markers, notably E-cadherin. Myeloid progenitor cells were found to be responsible for upregulation of versican in an example of pre-metastatic niche priming, which is discussed in Section The Pre-Metastatic Niche. This shows that extrinsic environmental cues play important roles throughout the progression of cancer, from the primary tumour to sites of metastasis.

1.2.3. Anoikis

Any discussion of the tumour microenvironment will invariably lead to the topic of anoikis, or programmed cell death in response to the loss of ECM attachment. Normal cells derive important pro-survival and anti-apoptotic signals from integrin and cell receptor engagement, which depend on the cell existing in the correct ECM environment for its type. Loss of these signals triggers signal cascades that

result in cell death, or anoikis, ensuring tissue organization and preventing unchecked tissue expansion (68–70). For cancer cells to metastasize, they must therefore acquire mutations that enable them to overcome anoikis before being able to detach from their native ECM environment. Apoptotic machinery can be decoupled from cell receptor engagement in a variety of ways, including through mutations or altered behaviour of downstream control elements (71,72), co-opting of pro-survival signals derived from other signal transduction pathways to replace those from cell-matrix interactions (73), and the use of autophagy and other cell survival strategies to stave off cell death (74). Talin1 overexpression, for example, provides pro-survival signals via activation of focal adhesions (72) while inhibition of Bim, a pro-apoptotic protein can prevent cell death when it would otherwise occur (68). The contrasting roles of Akt, also known as protein kinase B, and adenosine monophosphate (AMP) activated protein kinase (AMPK) are important in regulating cancer cell survival as cells detach and re-attach to ECM environments during metastasis. Acting as a metabolic switch, differential activation of the two kinases allows dormancy during matrix deprivation and metabolic reactivation upon attachment in a new tissue. AMPK is also important for promoting autophagy, which is used by cancer cells as a survival mechanism to improve metabolic efficiency (75). A great diversity of anoikis resistance mutations (as well as other cancer-driving mutations) exists, and within the context of cell heterogeneity within a primary tumour, this suggests that there are many different selective pressures within the tumour microenvironment, all selecting for cells that are uniquely capable of metastasizing. This is supported by evidence of polyclonal seeding of metastatic sites as well as metastasis-to-metastasis interactions and retrograde metastasis, in which cells derived from a metastatic site subsequently metastasize and re-seed the site of the primary tumour (76). The simultaneous existence of multiple sources of selective pressure reflects spatial and temporal variations in the tumour microenvironment as it is dynamically remodeled throughout the progression of cancer.

1.2.4. Cancer Cell Evolution

The mutational burden of a cancerous tissue and the process of cancer progression through the acquisition of new mutations is an important aspect of emergent malignancies (77) – and the tissue microenvironment plays a vital role in this as well. Adverse growth conditions, such as hypoxia or fluctuating pH, induce metabolic stresses, such as the release of reactive oxygen species, that can lead to DNA damage and genomic instability of a cell population (31,77,78). Hypoxia, in particular, is known to repress the expression of genes involved in DNA repair (79) while also directly contributing to DNA damage. If cells cannot faithfully reproduce their genetic code, the chance of mutation increases. As well, many of the pathways downstream of cell adhesion-induced signaling involve cell proliferation and survival, affecting the probability of a stable mutant line of cells taking hold in a host tissue (43,68,80). In this way, the tissue microenvironment acts as a source for mutagenesis, providing the selective pressures that can establish hardier populations of cancerous cells (81). Acquisition of mutations is random, but the tendency for certain mutations and cell phenotypes to appear again and again suggests that there must be some environmental factors selecting for or promoting their emergence. One of these is the upregulation of C-X-C chemokine receptor type 4 (CXCR4), known to be an important mediator of metastasis and cancer cell stemness in many different cancers. Cancers of the breast, lung, and kidney, but especially those of the prostate tend to metastasize to bone (82,83) and the interaction of CXCR4 with its ligand, C-X-C motif chemokine 12 (CXCL12), a chemokine highly expressed in bone tissue, facilitates the homing of metastatic cells to bone marrow (84,85). The reasons for this are not well understood (86), but if upregulation of CXCR4 begins in the primary tumour prior to migration and homing to bone tissue, then there must be environmental factors in the primary tumour selecting for or promoting this characteristic.

1.2.5. The Pre-Metastatic Niche

Organotropism, or the “targeting” of certain tissues by metastatic cells has been noted since Paget first described his “seed and soil” hypothesis in 1889 (87), but it continues to be an important topic of

cancer research today. Previous work has operated under the assumption of passive dispersion and implantation of metastatic cells, but the current paradigm has shifted towards active long-distance priming of a pre-metastatic niche that actively accepts and supports metastatic growth (88). Active ECM remodeling appears to be an important aspect of niche formation, as well as the reprogramming of resident cells and co-opting of local growth conditions to facilitate the infiltration and spread of metastatic cells. Many different secreted factors derived from primary tumours, as well as the release of exosomes and micro-vesicles have been implicated in this process. Why these factors preferentially activate certain sites of metastasis is still not well understood, though the targeting of exosomes can at least in part be explained by integrin expression (89). Exosomes released from tumour cells can be enriched with specific integrin isoforms that favour certain tissue ECM compositions. Randomly distributed throughout the body, they would preferentially attach to pre-metastatic sites that match their integrin profile. A bioinformatics study of exosome-encapsulated microRNAs (miRNAs) derived from prostate cancer patient primary cells showed that miRNAs derived from tumour cells can regulate a variety of signaling pathways involved in differentiation, proliferation, migration, and MMP synthesis. When these miRNAs were transfected into a fibroblast cell line, MMP expression was functionally increased at the protein level (90), which would encourage active ECM remodeling processes in the priming of a pre-metastatic niche. It is not well understood how environmental factors might facilitate the expression of such miRNAs in the primary tumour and what mechanisms are involved in their packaging into exosomes and release into circulation. Hypoxic conditions in the primary tumour have been singled out as an important promoter of the expression of angiogenic chemokines and enzymes involved in ECM remodeling (91–93). The release of lysyl oxidase (LOX) by breast cancer cells through activation of HIF-1 under hypoxia (91) is a particularly interesting example. LOX is an enzyme responsible for crosslinking structural ECM proteins such as collagens and elastins and is known to be an important regulator of matrix stiffness in primary tumours. In the pre-metastatic niche, it has been found to crosslink collagen IV, making the local tissue architecture more amenable to the attachment and migration of circulating bone marrow-derived cells. These recruited myeloid-type cells further remodel the ECM environment through the expression of

MMP-2 (94). It is not clear whether LOX-mediated remodeling is tissue-specific and if any tissue environmental factors contribute to its activity or if it is a probabilistic, non-specific first step in the progression of a pre-metastatic niche that can occur throughout the body. The pre-metastatic niche has the local ECM playing a central role in the development of metastases, but the ECM environment of the primary tumour clearly also has an important role in promoting or selecting for the expression of niche-priming signals.

Prostate cancer cells exist within the intricate context of the ECM, deriving biochemical, mechanical, and physical cues from their surroundings via cell surface receptors and mechanotransduction. At the heart of the complex changes involved in the progression and metastasis of cancer are the ECM and the reciprocal interactions between cells and matrix. This is important both in primary tumours and in potential sites of metastasis. Given the complexity of these environments, reductionist techniques are required in cancer research to simplify and isolate certain aspects of cancer cell behaviour. This must be carefully balanced with physiological relevance as, according to Bissel and Hines, context is the key to understanding cancer.

1.3. Standards for Cell Culture

In vitro models are vital to the understanding of cancer cell behaviour, as they provide a simplified environment that allows the control of cell growth conditions without many of the confounding factors associated with real living tissues. Traditionally, cells are cultured on standardized glass or tissue culture polystyrene (TCPS) plates. In the case of adherent cells, the adhesion of cells to TCPS surfaces appears to primarily be a result of integrin binding to serum glycoproteins, such as fibronectin and vitronectin derived from cell culture media, that have adsorbed onto the plate surface (95,96), though evidence also exists of direct electrostatic interactions between cell surfaces and surface-treated TCPS (97). This hard, stiff, two-dimensional (2D) environment does not reflect the chemical or mechanical properties of real tissues from which cells are obtained. Furthermore, cells are forced into basal-apical

polarization due to having all cell attachment molecules on the side adhering to the plate surface and the opposing side exposed to free-flowing liquid medium. This results in increased cell spreading, differences in integrin expression, perturbations to cytoskeletal organization and activation, as well as changes in gene expression when compared to cells in 3D environments as they would be *in vivo* (98,99). These differences ultimately affect morphology, differentiation, phenotypic expression, and proliferation (100). Direct exposure of the "apical" side of the cell to liquid media introduces cells to shear forces from fluid flow during media changes or physical perturbations of the culture environment. Diffusion in liquid medium is also poorly representative of the diffusive environment imposed by tissue ECM and multiple cell layers as in solid tissues, which has a molecular crowding effect resulting in localized concentration gradients of nutrient and waste material (56,60). While 2D cell models have played an invaluable role in biological research, their physiological relevance, especially in cancer research, is limited due to their inability to recapitulate the context of the tumour microenvironment and the important cell-cell and cell-matrix interactions that govern cell behaviour.

Three-dimensional (3D) cell culture models have been proposed as a way to bridge the gap between the simplicity of 2D *in vitro* models and the physiological realism of live animal models. The aim of 3D cultures is to recreate the mechanical and biochemical aspects of real tissue ECM in order to provide the necessary context for cells to behave as they might naturally in the body. While there are a variety of ways to generate 3D cell cultures, most protocols generally fall into two categories: spherical (or spheroid) culture and scaffold culture. Terminology in literature is not always clear on 3D cell structures, and the terms "spheroid" and "organoid" are sometimes used interchangeably to describe any 3D growth of cells (101). For the purposes of this thesis, "spheroid" will be used to describe an aggregation of tumour cells grown in non-adherent conditions while the term "organoid" will be used to describe a multicellular structure with some form of self-organization into a functional unit.

Spherical cell culture models rely on aggregation and cell-cell attachment to form 3D structures in the absence of an adherent substrate. Not all cell types are capable of forming spheroids, but anoikis-resistant prostate cancer cell lines lend well to this type of 3D model (102). One popular method for

forming spheroids is the hanging drop method, which involves suspending cells in a droplet of culture medium and relying on gravity to draw cells to the bottom of the droplet, where they eventually form aggregates (103). Due to the small volumes involved in hanging drop culture, this method tends to suffer from dehydration and is prone to physical perturbations from mishandling. A similar method is the liquid overlay technique, which involves coating a standard multi-well plate with an agarose hydrogel, a material for which mammalian cells have no natural receptors. Similarly to a hanging drop, this non-adherent environment favours the formation of cell-cell interactions and aggregate formation as cells are drawn to the bottom of the well by gravity (102,104). While care must be taken to ensure an even coating of agarose to prevent cells from attaching to the walls of the well, this technique is relatively robust to physical perturbation compared to the hanging drop method and can be done with a greater volume of medium, lessening the effects of evaporative losses. Over time with both methods, cells will secrete ECM components and develop as micro-tissues. Similarly to solid tumours, cells within a spheroid experience concentration gradients as nutrients and waste diffuse through the layers of cells. These gradients lead to decreasing cell viability towards the centres of spheroids, often forming necrotic cores akin to those in solid tumours (101). In spherical models, cell-matrix interactions are secondary to cell-cell interactions in that ECM materials must be produced and laid down by cells over the course of culture or introduced after spheroid formation to allow appropriate aggregate formation.

In contrast to spherical cell culture, scaffold cell culture involves providing an adherent 3D matrix environment with appropriate signaling cues to cells that allow them to attach and proliferate in the material. A variety of culture materials can be used and are available commercially, including Matrigel, a secretion of the murine Engelbreth-Holm-Swarm tumour containing ECM components representative of basement membrane (105). Cells grown in Matrigel are known to differentiate and self-organize into organoids with notable tissue-like structure (106). While Matrigel is an exciting material in terms of its ability to direct cell differentiation and organization, it is not a well-defined matrix due to its nature as a secretion from murine cells. Batch to batch variation is noted, as is the presence of non-structural ECM-adjacent materials such as growth factors and intracellular proteins, even in growth factor-reduced

Matrigel products (107). These confounding factors make it difficult to systematically study cell-matrix interactions using this material. Synthetic or recombinant materials are also used as scaffold materials and enable nearly complete definition of the material composition (108). These synthetic materials need to be engineered with molecular sequences such as RGD peptides to allow cell attachment, but can be produced with fine control of mechanical properties and matrix geometry to mimic natural ECM (42). Scaffold cultures can sometimes be sensitive to cell seeding density. With low seeding density, cells are sparsely dispersed and the contributions of autocrine, paracrine, and direct cell-cell signaling to cell behaviour are relatively small compared to cell-matrix interactions. Over time, however, as cells proliferate and populate the scaffold material, these cell-cell interactions can override matrix cues (109), illustrating the complexity of cell signaling and the interplay of cellular interactions in the tissue microenvironment.

While 3D cultures have the potential to be powerful tools for cancer research, their adoption has remained limited due to issues of practicality. Three-dimensional cell structures are difficult to image in a high-throughput capacity due to opacity and the existence of cells on multiple focal planes, requiring specialized imaging capabilities, such as confocal microscopy or histological sectioning. Lack of standardization of methods for generating 3D cultures means it is difficult to translate functional and biochemical assays optimized for 2D cultures to 3D cultures. Consistency of aggregate formation and spatial variability of cells are also prominent issues, especially when cell viability is highly dependent on position within the aggregate. While 3D cell culture is an exciting field and an important advancement in the understanding of cell behaviour in physiological contexts, more work is required to address the issue of feasibility for widespread adoption.

1.4. State-of-the-Art in Model Tissues

Considering the complexities of the tumour microenvironment, various strategies have been employed to isolate aspects of tissues in model cell culture environments. Baker et al. describe a fully synthetic ECM-mimicking fibre network composed of methacrylated dextran that they used to study cell-

matrix interactions and mechanosensing (42). Their model tissue environment allowed controllable fibre architecture with tunable mechanics via UV-mediated crosslinking. Addition of RGD peptides allowed cell attachment and provided contextual ECM cues to cells. Using this cell culture environment, they reported architecture-dependence of cell spreading and proliferation in response to matrix stiffness and the ability of cells to recruit and pull on fibres to increase ligand density and subsequent matrix-derived signaling cues. While powerful in allowing such a high level of control over culture conditions, such an environment includes exogenous materials that would not normally be found in human tissues. Even if cells do not have receptors for methacrylated dextran, its presence may have unknown effects on cells, such as electrostatic or hydrophilic/hydrophobic interactions. Using a completely different top-down approach, Piccoli et al. described a decellularized colorectal cancer biopsy sample for use as a model environment for 3D cancer cell culture (110). After noting clear structural and compositional differences between healthy colorectal tissue samples and cancerous samples, Piccoli et al. were able to show that cell lines re-seeded onto decellularized matrices show marked differences in behaviour, with over-expression of chemokines and genes related to angiogenesis and cancerous growth in cells grown in cancerous matrices compared to matrices derived from healthy mucosa. These results come with a caveat that the process of decellularization may affect ECM architecture, cause protein denaturation, and could also leave traces of cellular material that may affect subsequently seeded cells. Regardless, this model is especially interesting in preclinical research as it uses materials derived from real human tissues and would thus reflect real disease states. Another interesting model cell culture environment is described by Rodenhizer et al., who developed a platform to study spatial variations in metabolic signatures arising from concentration gradients (111). Their platform consists of a bio-composite sheet on which cells are seeded that can be rolled up to represent cell layers within a solid tumour. Diffusion of oxygen and nutrients across the device resulted in concentration gradients that were differentially sensed by cells depending on position within the construct. Unrolling the device allowed easy access to cells in different layers, enabling the study of how concentration gradients affect cancer cells as they would in solid tumours. The user-friendliness of this device in combination with its ability to recreate the diffusive

environment of solid tissues is the real highlight of this technology, as it could easily be adapted to study how chemotherapeutics diffuse through solid tissues and affect spatially varied cells. Drawbacks with the use of this device include its specialized manufacture and the extra training required to learn how to effectively use it.

The challenges of creating physiologically relevant *in vitro* disease models are particularly relevant in the study of prostate cancer. Research is greatly hampered by the lack of representative model cell lines that recapitulate the molecular aspects of disease presentation (112–114). Recent work by Sawyers et al. using primary cells derived from prostate cancer patients has demonstrated the utility of Matrigel in sustaining organoid cultures that have many of the molecular characteristics of real prostate cancers (113–115). Sawyers et al. characterized organoid lines derived from both circulating tumour cells and biopsy samples that expressed the diverse genetic profiles seen in prostate cancer including TMPRSS2-ETS fusions and SPOP mutations (113). They were also able to recreate accurate phenotype expression in rare neuroendocrine type prostate cancer cells using this method (114). *In vitro* models involving patient-derived cells are powerful tools for cancer research as they provide a broad representation of real-world disease states. The required use of Matrigel to induce accurate phenotype expression raises an interesting question, however. What aspect of Matrigel is actually required for self organization and proper phenotype expression? Given the complexities of Matrigel composition, it would be advantageous to have a bottom-up approach to growth matrix design to better understand the minimal requirements for physiologically accurate cell culture.

1.5. Hyaluronan as a Cell Culture Environment

Given the complexity of the cancer microenvironment and the difficulties in studying prostate cancer cells in physiological conditions, a bottom-up approach to augmenting standard cell culture conditions would be a good step forward in prostate cancer research. The simplest way to do this would be to introduce a layer of ECM material on top of a 2D culture (116,117). In this model, cells remain

attached to a 2D TCPS surface, but the impact of cell polarization would be theoretically lessened by receptor engagement in the presence of ECM material on the apical surface. When searching for a model ECM material in which to culture and study prostate cancer cells, hyaluronan, also known as hyaluronic acid (HA) stands out as a promising material.

1.5.1. Cell Interactions with HA

Hyaluronan is an anionic glycosaminoglycan found naturally in the human body and is ubiquitously expressed in most tissues. In cartilaginous tissues and synovial fluid, its water content and goo-like consistency provide a low-friction environment (47,118,119). Binding with proteoglycans, such as aggrecan or versican links HA with a wider ECM network, where it plays an important role in the retention of water and sequestration of soluble factors (47,120). HA is known to be overexpressed in a number of malignancies, including those of the breast, lung, prostate, and urinary bladder (80,118,121,122), and is also known to play an important role in inflammation and wound healing. When tissue is damaged, HA degradation products can be detected by cells, promoting inflammatory responses. In the newly synthesized and highly vascularized ECM of granulation tissue formed on wound surfaces, HA is thought to help promote the migration of cells and the remodeling of tissue (123,124). Cells interact with HA through two known primary receptors: cluster of differentiation 44 (CD44) and receptor for hyaluronic acid-mediated motility (RHAMM). The interaction between CD44 and HA is of particular interest, as CD44 is a known cancer stem cell marker and is used as a prognostic marker of poor disease outcomes (80,118,125). Numerous studies have reported conflicting effects of HA on cultured cells, which may be related to HA molecular weight. Smaller HA fragments present in the degradation products of damaged tissues can be endocytosed and tend to promote inflammation, cell proliferation and migration. In contrast, large HA molecules present in normal healthy tissues tend to act as a physical barrier to cell movement and expansion (123,124,126). Differences in the function of HA signaling also appear to be related to cell type, which suggests differences in signal transduction or HA uptake

(80,127,128). Experiments with free, unbound HA oligomers have revealed that HA binding by CD44 is cooperative, with stronger avidity as the number of engaged, adjacent receptors increases (129). This provides a potential mechanism for differential cell activation based on HA molecule size and could also explain differences in cell behaviour based on CD44 expression in different cell types. While cell interactions with free, oligomeric HA and downstream CD44-mediated signal transduction are well-documented, the effects of large HA molecules and ECM-bound HA on cell behaviour are less clear. HA in the tumour microenvironment would have two-fold effects on cells by influencing the material properties of tissues while also directly engaging cell receptors. Thus, it would be important to study how HA in the prostate tumour can affect cancer progression in an ECM-mimicking environment.

1.5.2. CD44 in Cancer

CD44 is known to be expressed as numerous isoforms depending on alternative splicing of the CD44 gene and expression of variant exons. Association of specific CD44 splice variants with cancer aggressiveness, cell stemness, drug resistance, and overall disease outcome has made CD44 expression a prominent prognostic marker and a target for therapeutic research in numerous cancers (121,130,131). For prostate cancer specifically, CD44v5 is associated with benign prostate cells whereas the standard variant, CD44s is upregulated in neoplastic cells (132). Isoforms that contain the v6 region of the CD44 gene are implicated in increased metastatic potential (133).

CD44 can bind to and interact with a variety of other materials besides HA, including collagens, fibronectin, and other ECM components (121) as well as MMPs and growth factors (130). These interactions can directly trigger numerous cell processes that can facilitate the progression of cancer. CD44 forms a complex with MMP-9 on the cell surface, which facilitates the activation of MMP-9, allowing matrix degradation and inducing migratory behaviour in cells (134). CD44 can also phosphorylate runt-related transcription factor 2 (RUNX2), which targets it for nuclear localization, facilitating the transcription of a number of different genes involved specifically in bone metastasis (135).

One of these genes is that of receptor activator of nuclear factor κB ligand (RANKL), a cytokine that promotes the priming of metastatic niches in bone tissue through osteoclast differentiation and activation. RANKL can also have a paracrine effect on adjacent prostate cancer cells expressing receptor activator of NF-κB (RANK), which can have a wide range of effects via NF-κB mediated protein expression (136). Acting through ankyrin and Rho GTPases, CD44 signaling can activate cytoskeleton dynamics, leading to altered cell adhesion and increased migration (137). CD44 can be cleaved, producing an intracellular domain that localizes to the nucleus and directly acts as a transcription factor (138). This CD44-mediated transcription can activate the canonical stem cell transcription factors Nanog, Sox2, and Oct4, promoting self-renewal and metastatic behaviour (139). CD44 thus has a wide range of functions and its signaling plays an important role in the progression of cancer.

1.5.3. HA Hydrogels

Using HA as a primary ECM material in which to culture prostate cancer cells serves to recreate an ECM environment that might be found in a malignant or pre-metastatic tumour in which it would be upregulated (122). As a material found naturally in the ECM, HA is not expected to pose any issues towards cell viability at physiological concentrations and would be a material that can provide contextual ECM signaling cues via CD44 and RHAMM. As a single-component semi-synthetic material, an HA hydrogel would have a well-defined chemical composition, circumventing many of the issues involved in the use of Matrigel. The main issue with HA as a culture environment is its handling properties. In its reconstituted high-molecular weight form, HA is a highly viscous liquid that does not lend well to standard liquid handling procedures using pipettes. Cell culture with liquid HA would also put shear stresses on cells during media changes or physical perturbations, which would not be reflective of the mechanical environment of solid prostate cancer tissue. Chemical modification of HA into a hydrogel material is a popular method of addressing these issues in the fields of biomaterials and tissue engineering (140–144). Chemical modification of HA to enable crosslinking improves the mechanical properties of

the material, making it more similar to the crosslinked structure of natural ECM without having to introduce other ECM materials that would naturally bind HA. By growing cells within a crosslinked HA matrix, medium exchanges can be performed without disturbing the cells, preventing bulk-flow mixing and exposure to shear stresses. Thus, the use of a HA-based hydrogel material in cell culture would allow the study of prostate cancer cell interactions with HA in an environment that is mechanistically similar to, but biochemically simpler than prostate cancer tissue ECM.

The goal of this research is to find a suitable HA-based hydrogel material to use as a cell culture environment and to use it to study prostate cancer cell behaviour. By using a semi-synthetic hydrogel system based on HA, cells will be provided contextual ECM binding cues while maintaining well-defined material composition and characterization. Functional characterization of the hydrogel environment will help tease apart the individual contributions of physical, mechanical, and biochemical properties that influence cell behaviour within the system. In mimicking the mechanical properties of tissue ECM, the hope is to better understand how ECM-bound HA contributes to cell signaling, cancer cell migration and invasion, and phenotype expression. Using a bottom-up approach, a secondary goal of this project is to augment and improve upon existing 2D cell culture models and move towards a more physiologically relevant 3D model of prostate cancer tissue. Not only will this improve on the performance of 2D tissue models, but this would also help in transferring established experimental procedures developed for 2D systems to 3D systems.

Chapter 2. Chemical Modification of HA

2.1. Disulfide Crosslinked HA Hydrogels

After reviewing a number of published HA crosslinking protocols available in literature (140–144), I chose a carbodiimide-based modification procedure first proposed by Shu et al (143). The procedure appeared straightforward and involved relatively mild reagents and reaction conditions, which would be important for maintaining cell viability. Their thiol-modified HA material is available commercially (Glycosil®, Advanced BioMatrix; HyStem®, Sigma-Aldrich) and is incorporated in a number of hybrid copolymer hydrogel systems (142,145). Briefly, 3,3'-dithiobis(propanoic dihydrazide) (DTP), a palindromic molecule with a central disulfide bond is coupled to carboxyl groups on adjacent HA chains via carbodiimide-hydrazide chemistry, resulting in a hydrogel material. The central disulfide bond can be broken through reduction, solubilizing the material, and subsequently reformed through oxidation in air. This allows *in situ* gelation of the material at physiological conditions. The hydrogel can also be broken down enzymatically with exogenous or cell-expressed hyaluronidases. Though not mentioned in the original paper (143), a subsequent paper using the thiol-modified HA material in a copolymer hydrogel system mentions preparing the hydrogel under a blanket of nitrogen gas to prevent premature crosslinking (145). I decided to attempt the procedure myself and optimize it for production and use in a typical life science lab, which may not have access to equipment for chemical process control described in the previous studies. My optimizations include decreasing batch size to improve mixing of the reaction volume and ensuring even crosslinking, decreasing the amount of dithiothreitol (DTT) needed to reduce the disulfide bond and solubilize the material by 64%, and removing the need to conduct the reaction under nitrogen by introducing a final addition of glutathione to prevent premature crosslinking.

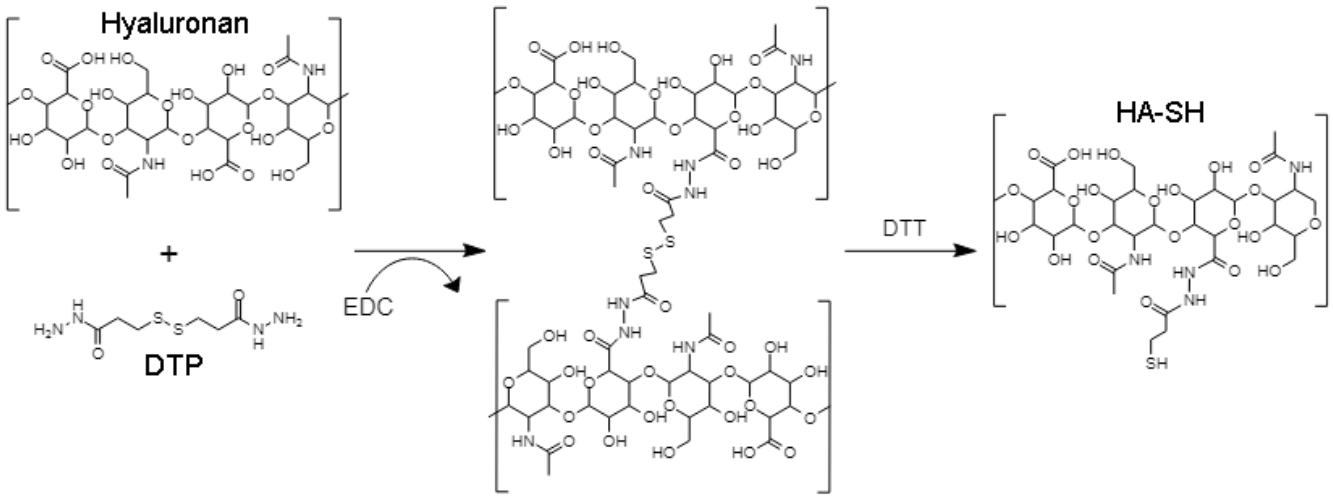

Figure 1, Chemical modification of hyaluronan to form a hydrogel. DTP is coupled to HA chains with carbodiimide-hydrazide chemistry to form a chemical crosslink. DTT is then used to break the central disulfide bond to solubilize the material, resulting in a thiol-modified HA material.

2.1.1. Crosslinking Scheme: Materials and Methods

First, high molecular weight HA must be degraded in acidic conditions. Though the purpose of this step is not mentioned by Shu et al., this acidic degradation greatly decreases the viscosity of the HA, making it easier to work with and ensures a soluble end product. Initial attempts at hydrogel synthesis without prior acid degradation all resulted in insoluble final products. In the optimized protocol, 1g of fermentation-derived HA from Streptococcus equii (Sigma-Aldrich) is dissolved in 100mL of distilled water on a hot plate set to 35°C. Once fully dissolved, 4M HCl is added until the solution reaches a pH of 0.5. Maintaining the temperature at 35°C with stirring at 130rpm, the mixture is allowed to degrade for 24 hours. Degradation is stopped by raising the pH to 7 using 1M NaOH and the mixture is put into dialysis tubing (standard regenerated cellulose, 6-8kDa pore size; Spectra/Por®) and dialysed against distilled water for 4 days, changing the dialysis bath every day. The mixture is then removed from the dialysis tubing, frozen at -80°C in 50mL conical tubes, and lyophilized (AAPPTec Sharp Freeze -110). This lyophilisation step allows subsequent rehydration of the low molecular weight HA for synthesis at the appropriate concentration and this step cannot be skipped, even if the molar ratios of the other reactants

are kept constant. Attempts at using the dialyzed low molecular weight HA solution directly in the crosslinking reaction resulted in final hydrogel products that over-crosslinked and crashed out of solution.

An example of the amounts of reagents used in the crosslinking reaction is as follows: 0.5g low molecular weight HA is dissolved in 50mL of distilled water, making sure a homogeneous solution is obtained. A total of 50mL is the largest reaction volume I have attempted that has resulted in a soluble final product. Larger volumes are associated with problems I discuss later in Section Protocol Optimization. Next, 0.6g DTP (Frontier Scientific) is added to the mixture as a dry powder and the pH of the reaction is adjusted to 4.75 with additions of 1M HCl. Once an appropriate pH is achieved, 0.48g N-(3-dimethylaminopropyl)-N'-ethylcarbodiimide hydrochloride (VWR) is added to the solution as a dry powder, starting the crosslinking reaction. The pH is maintained at 4.75 with additions of 1M HCl as the reaction progresses. The solution will begin thickening as crosslinks are formed, eventually forming a gelatinous mass. The reaction is stopped after 10 minutes by adjusting the pH to 7 using 1M NaOH. At this point, the material can hold its shape and can be cut; visible cleavage planes imply that the material will not reform a single mass if remixed. To re-solubilize the material, 0.9g DTT (VWR) is added as a dry powder and the pH is raised to 8.75 with 1M NaOH. This is left to stir overnight before being put into dialysis tubing and dialyzed. Dialysis is done in a solution of 11.69g NaCl dissolved in 2L distilled water and 600µL 1M HCl (pH 3.5) for one day, then in a solution of 600µL 1M HCl in 2L distilled water (pH 3.5) for three days, changing dialysis baths once a day as needed. According to Shu et al., the dilute acidic dialysis conditions prevent crosslinking of the material while also ensuring the HA backbone does not hydrolyze. After dialysis, 0.9g reduced glutathione (VWR) is added as a final measure to prevent crosslinking before being lyophilized. Because of the dialysis in an acidic bath, the resulting lyophilized product is acidic upon rehydration and requires aliquots of NaOH to bring it to neutral pH for use in cell culture or other experiments.

2.1.2. HA Content of the Final Hydrogel Material

Due to the potential loss of material during dialysis and the addition of glutathione, the final HA content of the material is unknown. To correct for this, I use a turbidimetric assay described by Oueslati et al. (146) to quantify HA content of the final material. This assay utilizes the specific formation of a precipitate between cetyltrimethylammonium bromide (CTAB) and HA regardless of state of crosslinking or molecular weight and provides a quantitative measurement of HA content. During initial testing, I confirmed that DTP, DTT, and glutathione were non-reactive to the CTAB solution. By comparing the absorbances of hydrogel test solutions with that of a pure HA standard curve, I can calculate the purity of the final material. In general, I am able to achieve an average HA content by mass of 44±6% in the final product following my optimized synthesis protocol. The remainder is likely glutathione and salts leftover from dialysis.

The procedure for the CTAB turbidimetric assay is as follows: CTAB reagent is made by dissolving 1.25g CTAB in 50mL 0.5M NaOH; a pure 0.6mg/mL HA standard stock is made by dissolving 30mg HA in 50mL phosphate buffer; a hydrogel test solution is made by dissolving 6mg hydrogel material of unknown HA content in 10mL phosphate buffer. In a standard flat-bottom 96-well plate, both the standard solution and test solution are serially diluted with phosphate buffer, with final volumes of 50µL in each well, done in triplicate. The three blank wells receive 50µL pure phosphate buffer. Each well then receives another 50µL phosphate buffer, bringing the volume in each well to 100µL. This is left to incubate at 37°C for 15 minutes. Next, 100µL of the CTAB reagent is pipetted into each well and gently shaken. The precipitate forms instantly, but will begin to disappear over time, so the absorbance must be measured within 30 minutes of adding the CTAB reagent. The absorbance at 595nm of each well is measured using a Filtermax F5 Microplate Reader. The absorbance data are plotted against concentration for both sets of data and the slopes are found using least-squares linear regression. By dividing the slope of the test solution data by the standard solution data, the percent HA content can be found. An example is shown in Figure 2.

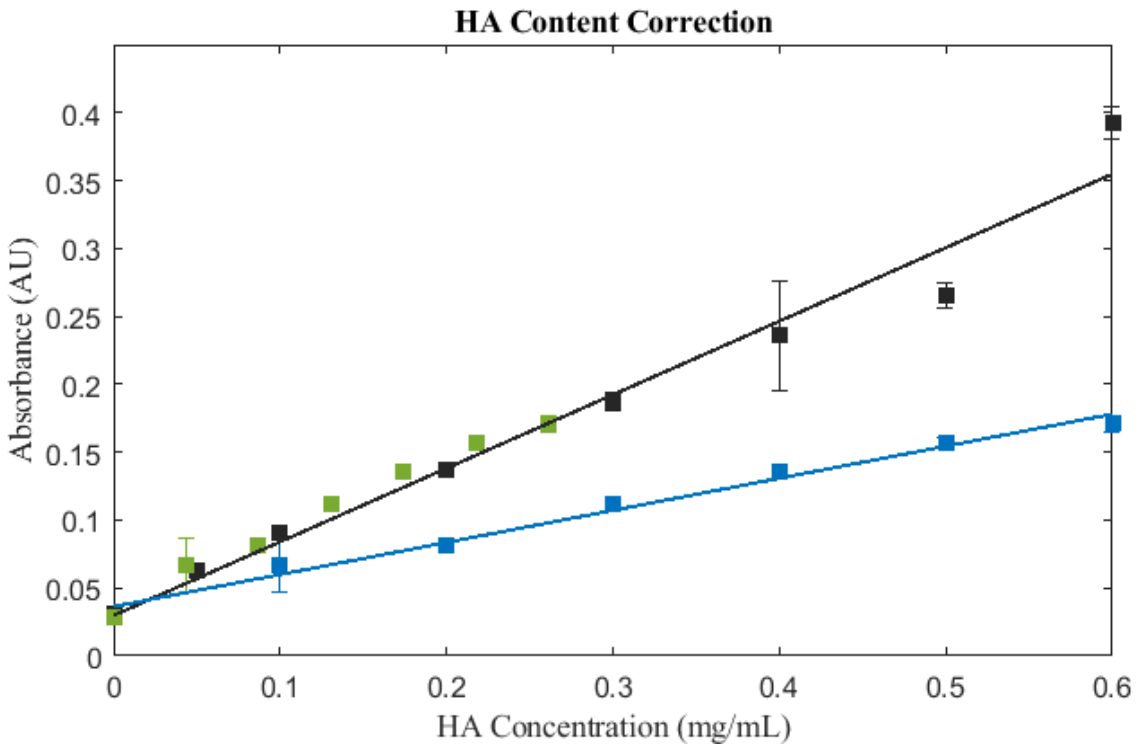

Figure 2, CTAB turbidimetric assay for measuring HA content. Pure HA standard curve in black with, test solution with estimated concentrations in blue, and test solution with corrected HA content in green. The correction is done by finding the slopes of the standard and test data with least-squares fitting, dividing the slope of the original test solution data by that of the standard curve, and then multiplying the estimated concentrations by this ratio. In this example, the test solution has an HA content of 43.6%.

2.2. Discussion

2.2.1. Choice of Chemical Modification

A number of chemical modification schemes have been described for the crosslinking of HA into a hydrogel (141–144,147,148). Among these, methacrylated HA has specifically been used to emulate the HA-rich environment of the stem cell niche to culture embryonic stem cells (147). Phenol-functionalized HA hydrogels, on the other hand, have been used to aid in cell sorting and enrichment of cells expressing CD44 (148). I chose the chemical modification procedure by Shu et al. over others because it is relatively simple and used relatively mild reagents and reaction parameters. Other hydrogels that require the addition of a crosslinking agent such as glutaraldehyde have the possibility of having unreacted reagent

interfering with cell viability or behaviour. Hydrogels that require exposure to ultraviolet light for photopolymerisation would also have issues with cell viability, as cells would be exposed to the light and may incur DNA damage. The simplicity of having the gel form through oxidation in air is an attractive selling point for me, as it allows forming of the gel *in situ*, encapsulating cells in an ECM-mimicking environment. The crosslink molecule used is available commercially, so the initial crosslink synthesis steps described by Shu et al. can be skipped. With this protocol, my hope was to make the procedure more accessible for a general cancer research audience that may not have the facilities required in the original protocol, such as the capability to work under nitrogen gas.

2.2.2. Protocol Optimization

My optimizations are simple, but have a great effect on material usage and feasibility. Shu et al. report that a five-fold excess of DTT compared to initial HA by weight is needed to fully solubilize the hydrogel material prior to dialysis and lyophilisation. In reducing the reaction volume and conducting synthesis in smaller batches, I am able to shorten the crosslinking reaction time from two hours down to ten minutes and reduce the amount of DTT required in the solubilisation step by 64%. In vivo, HA is an important material for sequestering soluble factors and thus has a strong molecular crowding effect in solution (47,120). Large reaction volumes would suffer from uneven reactions due to this crowding. To prevent uneven reaction pockets, the original protocol probably would have required intense mixing, which would incorporate air into the reaction, causing oxidation and premature gelation. This would further increase the amount of reducing agent needed to solubilize the crosslinked material. Working in smaller batches means the reaction volume can be more easily mixed at lower speeds. Reagents would more readily disperse through the material, ensuring an even reaction. Less air would be incorporated during mixing, minimizing the risk of oxidation. The final addition of glutathione also ensures that the material remains uncrosslinked during freezing and lyophilization. Without glutathione, I find that the final material after lyophilization tends to be insoluble. Using less glutathione tends to result in faster

gelation and higher initial viscosity after rehydrating the material. I chose to use glutathione as opposed to more DTT because glutathione is an antioxidant naturally found *in vivo* and is generally much milder with low cytotoxicity (149).

An interesting phenomenon that occurs with this material if the crosslinking reaction proceeds for too long or if the concentration of reagents in the reaction volume is too low (as it would be if dialyzed acid degradation product is used directly in synthesis, skipping the first lyophilisation step) is over-gelation of the final rehydrated material and its crashing out of solution. This over-crosslinked material readily dissolves in phosphate buffered saline (PBS) and cell culture media, but over the course of gelation, it shrivels up, squeezing the solvent out of the matrix and becoming a stiff and opaque mass, as seen in Figure 3. This occurs to a greater extent if reconstituted at higher concentrations, usually above 1% (w/v). There are a few possible reasons for this. If the carbodiimide-hydrazide reaction proceeds for too long, the HA material will become saturated with crosslinks, resulting in a very stiff matrix. I have also noticed this in large reaction volumes in which the reagents are not well-dispersed, resulting in uneven reaction pockets. My experience with the material has been that a ten-minute reaction is sufficient to achieve desirable material qualities for cell culture. If reagent concentration is too low, the reaction is slow, requiring extended amounts of time to achieve a gel of comparable mechanical properties compared to the gel formed as described in Section Crosslinking Scheme: Materials and Methods. The resulting hydrogel, however, is formed at a far lower HA concentration and a greater degree of crosslinking would be required to have the same mechanical properties. Upon reconstitution at 1% or above, as used in subsequent experiments, this hydrogel would have more crosslinks per unit volume, leading to over-crosslinking and crashing from solution.

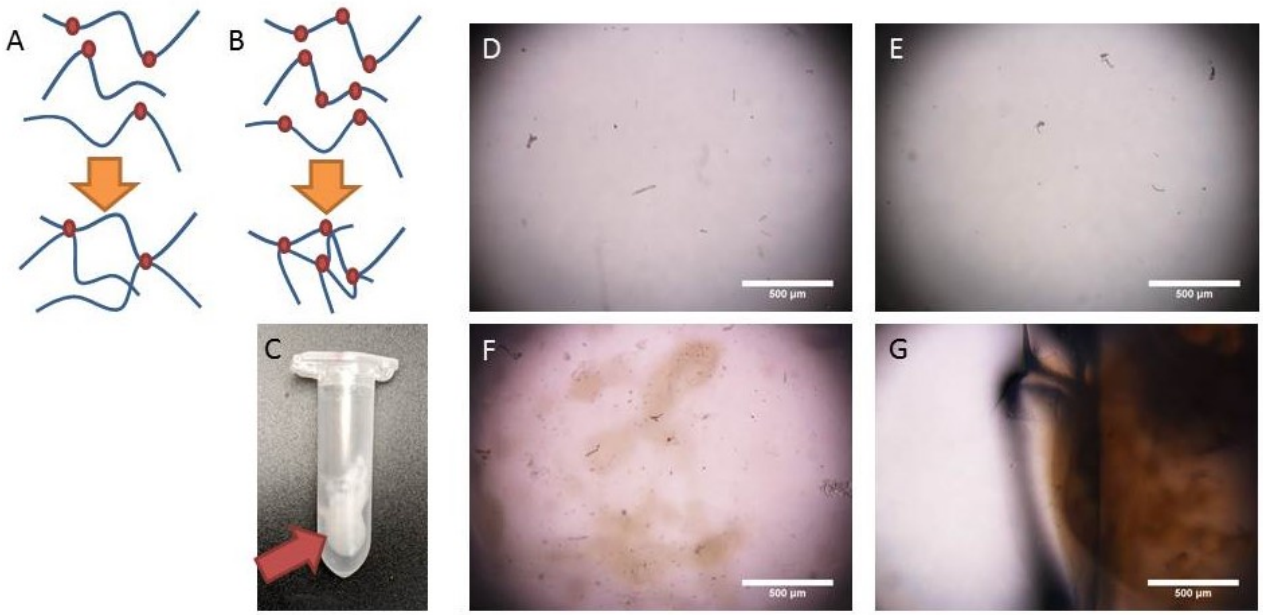

Figure 3, Over-crosslinking of gels and crashing from solution. Following the procedure in Section 2.1 results in adequate crosslinking (A), but allowing the reaction to progress for too long will result in too many active thiol groups per unit volume, which causes the material to over-crosslink upon rehydration (B). Having a low initial HA concentration will also result in over-crosslinking because more crosslinks are required to obtain a hydrogel with comparable mechanical properties. Upon rehydration, an over-crosslinked hydrogel will "crash" out of solution, squeezing the solvent out of the matrix (C). D and E show successful hydrogels at 1% and 1.5% w/v, respectively under the microscope (4X objective, scale bar is 500µm), which are optically clear. This is compared to F and G, which show over-crosslinked and crashed hydrogels at 1% and 1.5%, respectively. In F, the hydrogel has not fully crashed, but has coalesced into scattered translucent aggregates. In G, the higher concentration (and thus greater number of crosslinks per unit volume) has caused the hydrogel to separate from solution, forming a single semi-opaque mass. The edge of the mass is shown.

One drawback of my optimizations is that the reduction in reaction volume greatly decreases the potential for large-scale synthesis of the material. The ratio of reactants would likely not scale linearly, as increasing the reaction volume would lead to issues with reaction uniformity, as discussed earlier. While this would not be ideal in an industrial setting, the amount produced per batch would be sufficient for a general cancer research laboratory environment on a monthly basis. Regarding the addition of glutathione, any reduced glutathione remaining in the final material could have some protective effects on

cultured cancer cells. This would be especially relevant when testing chemotherapeutic drugs, radiotherapy, or other cancer treatments that rely on the generation of oxidative molecules. One way to address this would be to extensively wash the hydrogels after rehydration and gelation to gradually elute the glutathione.

2.2.3. Hydrogel HA Content

The average final HA content of the hydrogel material I can achieve is 44±6% by weight, as measured by the CTAB turbidimetric assay. The remainder is the glutathione that is added after dialysis and possibly salts derived from the acidic dialysis bath. Assuming all HA is conserved through the reaction and dialysis, the addition of glutathione should result in a maximum theoretical purity of about $\frac{0.5g\ HA}{0.5g\ HA+0.9g\ glutathione} = 36\%\ HA$. While salt content and pH can affect the assay by interfering with precipitate formation (146), their contribution in this case would be negligible due to being highly diluted in buffer. I confirmed that DTP is unreactive to the CTAB reagent on its own, but this apparent inflation of HA content suggests that the DTP crosslink contributes to precipitate formation, lacking alternative explanations. Oueslati et al. note the insensitivity of this assay to HA molecular weight, suggesting that the interaction with CTAB relies on the material bulk rather than on individual molecules (146). Therefore, as a functional group covalently attached to the HA chain, the DTP crosslink is likely adding to the bulk mass of the material, which gets reflected in this inflated concentration reading.

2.2.4. Molecular Weight and Degree of Crosslinking

Aspects that I have not addressed in the material synthesis are the molecular weight of the HA and the degree of crosslinking in the material. Shu et al. have described these aspects in their original paper, conducting detailed chemical analyses, and note the use of reaction time and pH to control both the molecular weight of HA during the initial acid degradation prior to crosslinking and the degree of crosslinking during synthesis. While my decreased reaction volume affects the reaction time and thus the

degree of crosslinking, I have maintained constant reaction time from batch to batch and evaluated the progression of the crosslinking reaction based on qualitative visual and mechanical criteria (e.g. whether the material is still capable of flowing, whether it can hold its shape, whether stirring the material results in visible cleavage planes, etc.). These methods have resulted in fairly consistent hydrogels, as evidenced in later mechanical testing and diffusivity data, but there is some variability due to the crudeness of using reaction time and qualitative assessment to monitor reaction progress. As for the molecular weight, again there is some variability stemming from the acid degradation as well as the crosslinking and dialysis in acidic conditions. This aspect may not be relevant to the final material, however, since the crosslinking of HA appears to result in a consistent bulk material. The average molecular weight of the material is likely lower than that of natural HA found *in vivo,* which can exist in the 1000-8000kDa range but could, however, be representative of low molecular weight HA degradation products found in wound repair and inflammatory processes (47,118). How cells might differentiate between low and high molecular weight HA in the context of a chemically crosslinked matrix remains unclear. This would require further investigation, but previous tests of crosslinking high molecular weight HA without prior acid degradation resulted in an insoluble material. Thus, a different strategy would be required to determine the effects of molecular weight on matrix properties and cell behaviour. The DTP crosslink is probably poorly representative of the HA-binding ECM proteins found in vivo, both due to its relative size as well as its non-specificity in reacting with carboxyl groups on HA chains (120).

Chapter 3. Material Characterization

Much of the material characteristics of this disulfide-crosslinked HA hydrogel have been previously described by Shu et al., including reaction kinetics, crosslinking efficiency, gelation, and swelling ratio (143). The goal of my material characterization was to understand its functional properties relating back to its use as a model cell culture environment. I wanted to see how the mechanical properties of HA on its own would compare to those of real tissues made up of a complex mix of ECM proteins. My hypothesis was that since the hydrogel material did not contain any fibrous structural ECM elements, such as collagen or elastin, it was highly unlikely that I would achieve comparable mechanical stiffness to real tissue. I conducted mechanical testing to obtain the elastic modulus of the material and also used simple measurements based on rheology to better understand the transition kinetics involved in the gelation process.

Though my protocol optimizations would not have fundamentally changed the carbodiimide-hydrazide chemistry from the original protocol by Shu et al., I wanted to see how the addition of glutathione would affect the gelation of the material upon rehydration since the disulfide linkage in the crosslink requires oxidation to reform and the glutathione would change the redox balance. Previous studies have shown that the gelation of reversibly and covalently-interacting biopolymers is dependent on concentration according to a power law relationship with a negative exponent value (150,151). I hypothesized that the addition of glutathione as a reducing agent would slow the gelation process by inhibiting the oxidation of the disulfide crosslink. Only once the reduced glutathione is spent would the disulfide bond be able to form stably. The power law relationship would likely still be intact, since the molecular interaction governing gelation would not change. My hydrogels would have longer gelation times compared to the values reported by Shu et al. in their original paper, however.

3.1. Results

3.1.1. Power Law Dependence of Gelation on Concentration

Shu et al. originally determine onset of gelation using a test tube inversion method and report that the speed at which HA hydrogels solidify is dependent on the pH of the final gel solution and the reactivity of thiol groups (143). Their data, however, was not collected with enough time intervals to be able to calculate a gelation time. I decided to use a method described by Xu et al. (152) based on capillary action of liquids to characterize the onset of gelation of four different concentrations of hydrogel solution: 0.5%, 1%, 1.5%, and 2% w/v. Using this data, I could then characterize the power law relationship between gel time and concentration and compare my gelation times to those reported by Shu et al. If my hypothesis about the glutathione addition was correct, the predicted gelation time for a 3% HA hydrogel using my gelation data should be appreciably longer than the observed gelation time reported by Shu et al.

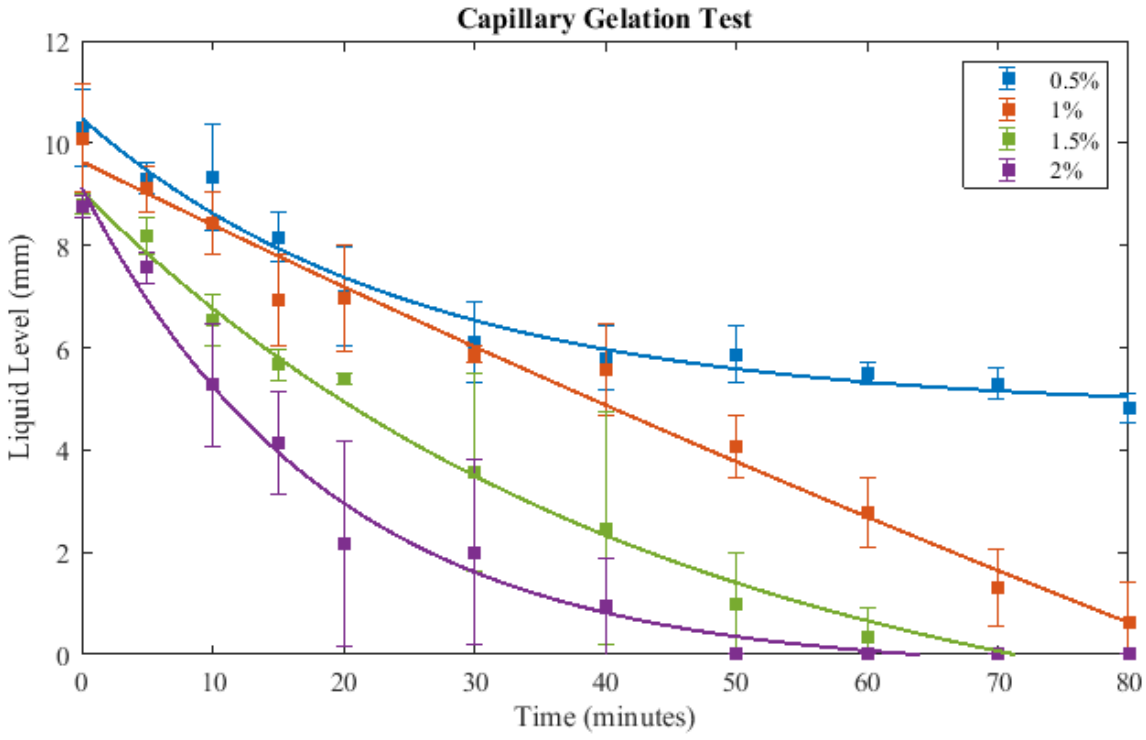

Figure 4, Gelation progression as measured using a capillary gelation test. Data were fitted to exponential curves to show time trends using least-squares regression. Hydrogel solutions of 0.5% (w/v) do not fully stabilize into gels and remain liquid, hence the plateau in the data presented.

Above 0.5% w/v, hydrogel solutions fully stabilize and form gels. At 0.5% and below, however, the little amount of HA in solution is unable to fully stabilize into a gel (Figure 4), and therefore, the HA remains a viscous liquid. This is the approximate the critical gelling concentration of the HA hydrogel. Variability in gelation curves is likely due to inconsistencies in gel synthesis and imprecision of the capillary gelation assay.

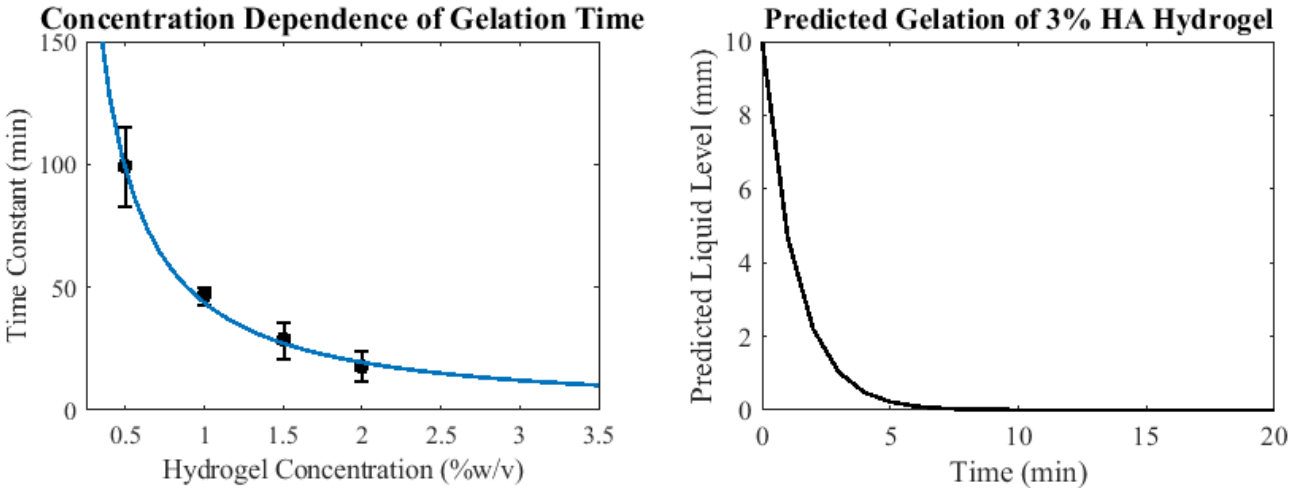

Figure 5, Power law relationship between hydrogel concentration and gelation onset. Left: exponential time constants obtained from gelation curves in Figure 4 (black) were fitted to a power law function with least-squares regression (blue) with an exponent of -1.148; R-square = 0.9977. Right: the predicted gelation curve of a 3% HA hydrogel, obtained by extrapolating a time constant of 1.3 minutes from the fitted power law function. According to this predicted curve, a 3% w/v HA hydrogel would be fully gelled within 5-10 minutes.

The gelation times of the hydrogel solutions appear to follow a power law relationship according to concentration (Figure 5). Due to the viscosity of the hydrogel solution, it is too difficult to homogeneously rehydrate the material above 2% w/v. Extrapolating from the fitted power law, it appears that a 3% w/v hydrogel would fully gel in less than 10 minutes. Shu et al. report onset of gelation for a 3% hydrogel within 15 minutes at a pH of 7 with their original protocol, though their experiment did not include any earlier time points. Counter to my hypothesis, this suggests that the gelation of the material may not be affected by the presence of glutathione, since the predicted gelation time is comparable to what was reported

3.1.2. Mechanical Stiffness of HA Gels is Much Lower than Prostate Tissue

Compression tests were used to characterize the mechanical properties of the hydrogels. The hydrogels show clear concentration-dependent stiffness as expected, both due to greater overall material density at higher concentrations, as well as a greater number of crosslinks per unit volume with increasing concentration (Figure 6). A study by Ahn et al. report an average elastic modulus of 24.1±14.5 kPa for cancerous prostate tissues (153). This is much higher than that of the HA hydrogels and is expected, since HA would not contribute significantly to the mechanical strength of real tissues compared to structural ECM proteins like collagen or elastin. Although the 0.5% hydrogel solutions did not form solid gels, I was able to obtain a non-zero modulus, suggesting that the 0.5% solutions are not fully liquid and can exhibit gel-like behaviour under compression.

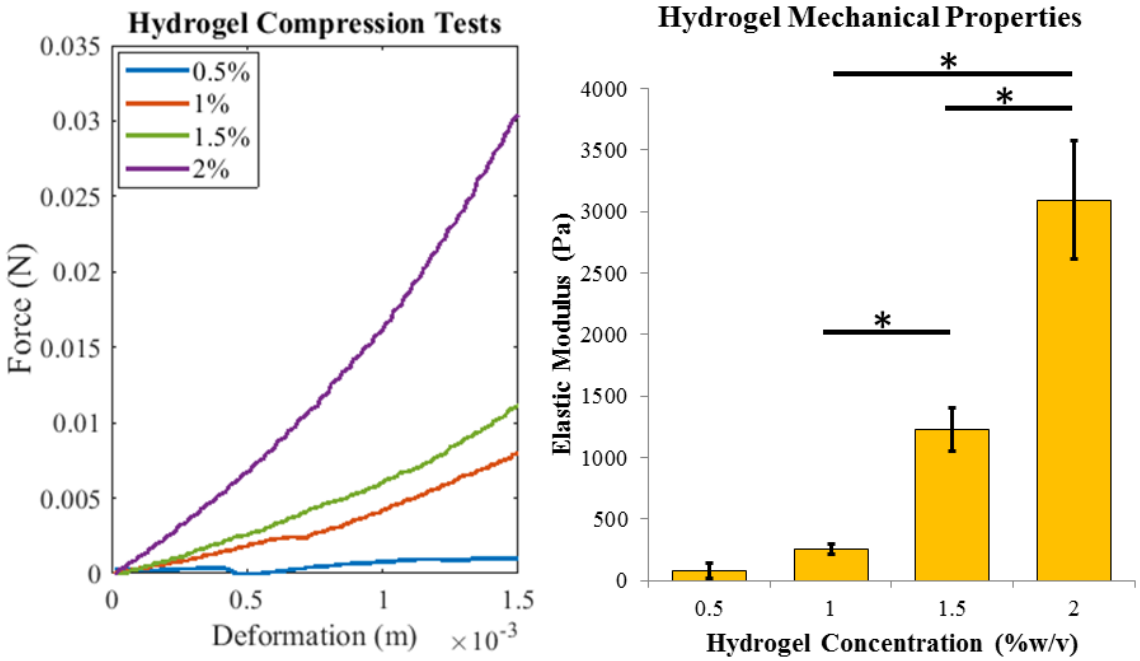

Figure 6, Hydrogel mechanical properties measured with compression testing. Left: representative force vs deformation curves of the different hydrogel concentrations tested. Right: elastic moduli, as calculated using a flat, rigid axisymmetric punch model up to 5% deformation. Error bars show standard deviation. * indicates statistical significance as computed using one-way ANOVA and pairwise Tukey-Kramer post-hoc analysis, $p<0.01$.

3.2. Materials and Methods

3.2.1. Capillary Gelation Test

Ideally, quantitative rheological measurements would provide the most precise characterization of the mechanics involved during gelation. Lacking access to a rheometer compatible with small volumes, I opted to use a method described by Xu et al. (152) to qualitatively characterize the gelation process. Liquid is wicked up the narrow lumen of a glass capillary due to attractive intermolecular forces between the hydrogel solution and the capillary wall. As the hydrogel solution gels, however, its viscosity increases and its ability to be wicked up the capillary decreases. Once the hydrogel is fully set, it is incapable of flowing and cannot be wicked up by capillary action.

The procedure for the capillary gelation test with representative amounts of materials used is as follows: an HA hydrogel solution is made by dissolving 0.049g of 47% HA content hydrogel material in 1.0mL PBS. The HA content was found using the CTAB turbidimetric assay previously described. The mass of material used was equivalent to 0.023g pure HA. To bring the solution to neutral pH, 100µL 1M NaOH is added, bringing the liquid volume to 1.1mL. The solution is topped up to 1.15mL with an addition of 50µL PBS, bringing the final HA concentration to 2% w/v. This solution is serially diluted with PBS to make up the other concentrations as follows: 700µL of 2% solution is added to 233µL PBS to make a 933µL 1.5% solution; 483µL of 1.5% solution is diluted with 241µL PBS to make a 724µl 1% solution; 274µL of 1% solution is diluted with 274µL PBS to make a 548µL 0.5% solution. The remaining 450µL of each solution is pipetted into the wells of a standard 96-well plate, making up 5 gels for each concentration, each 80µL in volume. At chosen time points, a 1.5mm-diameter borosilicate glass capillary (Kimble Chase) is inserted into each hydrogel solution. The liquid level is allowed to equilibrate before the capillary is removed and the liquid level is measured using a caliper. A different gel is sampled per concentration at each time point, cycling back to the first gel upon running out of fresh gels to sample. This is to try and minimize the possibility of breaking up the gel matrix structure by sampling a gel too often, leading to over-estimation of liquid level and gelation time.

Time constants were obtained from exponential curves fitted to the gelation data using the following form

$$y = e^{\frac{-t}{\tau}} \quad (1)$$

Where y is the liquid level in the capillary tube, t is the time in minutes, and τ is the time constant. Time constants were then plotted against hydrogel concentration and fitted to a power law relationship of the following form

$$\tau = kC^{-n} \quad (2)$$

Where C is the concentration of the hydrogel solution, n is the power law exponent, and k is a constant of proportionality. All fitting was done with least-squares regression in MATLAB.

3.2.2. Compression Testing

To characterize the mechanical properties of the hydrogel material, I used a compression test to obtain force vs deformation curves of hydrogels with the following concentrations: 0.5% 1%, 1.5%, and 2% w/v. The hydrogels were formed in the wells of a custom 3D printed holder, consisting of cylindrical 8mm-diameter, 22mm-deep wells. A 2% w/v HA hydrogel solution was made with PBS, pH adjusted using 1M NaOH, and serially diluted with PBS to make up the other concentrations, with 750µL of each solution used in each well. This corresponded to an approximate gel height of 1.5cm. The custom holder with the gels inside was then placed on a Mettler Toledo XS105 analytical scale. A syringe pump (KD Scientific) was propped up vertically and a metal 1m-long metal rod was placed in the holder of the pump mechanism (Figure 7). The threads of a small plastic screw were filed down to make a smooth cylindrical probe, 3.8mm in diameter. The probe was attached to the end of the metal rod with double-sided tape and lowered towards the surface of the gel in the holder on the scale. The syringe pump was set and calibrated to depress at a constant 0.1mm/s speed. Once the scale was tared, the syringe pump was turned on, with the probe moving towards the gel surface and subsequently into the gel. Measurements were made at 10

samples/s using the interval weighing protocol from the LabX instrument interfacing software (Mettler Toledo) as the gel was depressed by the probe.

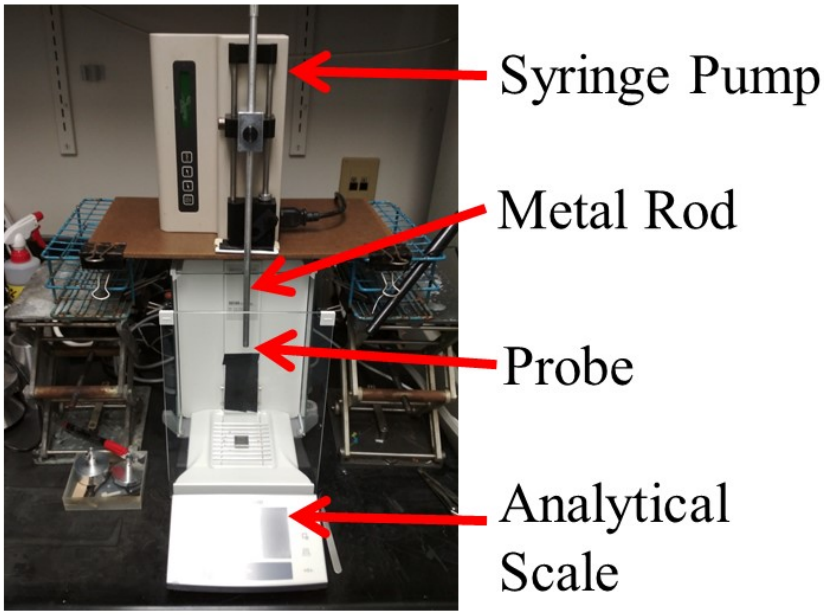

Figure 7, experimental setup for compression testing. An analytical scale is used to record mass measurements, which are converted into force readings. A syringe pump is used to depress a probe attached to a metal rod at constant speed into hydrogels placed on the scale.

Mass measurements from the scale were converted into force readings by multiplying the masses by 9.81m/s^2, the acceleration by gravity, according to Newton's Second Law. Since the software recorded at 10 samples/s and the syringe pump had a constant speed of 0.1mm/s, each sample corresponded to a deformation of 1.0×10^{-5}m. Force readings were plotted against deformation and each curve was visually inspected to determine the onset of compression as the probe made contact with the gel surface. The first 75 data points after the onset of compression, corresponding to a total deformation of 0.75mm, or 5% of the total gel height were taken and fitted with least-squares linear regression to obtain the slope. Only these data were considered because they were relatively linear in this region and would be more representative of the mechanical forces that cells would encounter in real tissues. Limiting the amount of

deformation of the sample would also help emulate the ideal conditions of a flat, rigid axisymmetric punch on an infinite elastic half-space (154). This model is given by

$$\delta = \frac{F(1-\nu^2)}{2Er} \quad 3$$

Where δ is the deformation, F is the measured force, ν is Poisson's ratio of the tested material, E is the elastic modulus, and r is the radius of the cylindrical probe (1.9mm). Since the HA hydrogel is mostly water, its Poisson's ratio can be approximated to be that of water, hence $\nu \approx 0.5$. Rearranging Equation 3 gives:

$$E = \frac{1-0.5^2}{2r}\left(\frac{F}{\delta}\right) \quad 4$$

$$E = \frac{0.75}{0.0038m}\left(\frac{F}{\delta}\right) \quad 5$$

$$E = 197.37m^{-1}\left(\frac{F}{\delta}\right) \quad 6$$

where F/δ is the slope of the force vs deformation curve. Equation 6 was used convert the slope into elastic modulus. Despite the fact that the diameter of the hydrogel sample was on the same order of magnitude as that of the probe, I felt confident in using a flat, rigid axisymmetric punch model for this analysis because I was only using data up to 5% deformation. At small enough deformation, the pressure distribution in the hydrogel sample would decay before reaching the edge of the sample, approximating the ideal condition of an infinite elastic half-space.

Statistical significance between hydrogel moduli was determined using one-way ANOVA with pairwise Tukey-Kramer post-hoc analysis, $p<0.01$ on MATLAB.

3.3. Discussion

While crude compared to rheological data obtained from a rheometer, the capillary gelation assay provided qualitative kinetic data based on the mechanical processes involved in gelation. The advantage of this assay over traditional rheological measurements was that very little test material was required with no need for specialized equipment. I was able to confirm a power law dependence of gelation time on hydrogel concentration, as had been previously reported in other biopolymer systems (150,151). Using this relationship, I found that the predicted gelation time of a 3% hydrogel solution was less than 10 minutes. Shu et al. reported a gelation time of 15 minutes, but did not have earlier time points for testing gelation onset. While it was not possible to confirm without more data, it appeared that my predicted gelation time did not disagree with what was reported. Interestingly, the added glutathione did not appreciably affect gelation onset upon rehydration of the hydrogel material, counter to my initial hypothesis. It is possible that the redox potential of the glutathione relative to the disulfide bond in the HA material in solution made it ineffective as a reducing agent, though this is unlikely because prior attempts at processing the hydrogel without glutathione resulted in insoluble products. This would suggest that most of the reduced glutathione was spent during lyophilisation to prevent gelation and so was no longer active upon rehydration. Given the crudeness of the capillary gelation assay, another possibility is that the effect of glutathione was too small to be detected. There was variability in the gelation data, and this could be evidence of the effect of glutathione on gelation. Because of the final dialysis in the production process, there was risk of losing materials smaller than the 6-8kDa molecular weight cut off of the dialysis tubing. This was not taken into account prior to the addition of glutathione, which would have resulted in variable glutathione-to-HA ratio in the final material, even after correcting with the CTAB turbidimetric assay. Variability also arose both from the crudeness of the capillary gelation assay as well as other batch-to-batch variations in the hydrogel material.

For mechanical testing, I showed that the elastic moduli of HA hydrogels increased with concentration, but were far smaller than the average elastic moduli of cancerous (24.1±14.5 kPa) and non-

cancerous (17±9 kPa) prostate tissues previously reported by Ahn et al. (153). Given that the mechanical properties of tissues are largely determined by fibrous ECM proteins that are missing from the hydrogels, such as collagen or elastin (34), this is not surprising. This seems to suggest that HA, as a component of tumour ECM that is tethered and functionally crosslinked to structural elements does not contribute much to the overall stiffness of tumour tissue. At the degree of crosslinking I set through qualitative control of reaction parameters, the resulting hydrogels were very soft. Even if the degree of crosslinking were to be increased to improve on stiffness, the resulting material is unlikely to resemble real tissue without the addition of structural ECM components. There is also the issue of the material's tendency to crash out of solution and become opaque at high degrees of crosslinking, as discussed in section 2.2.2. What was encouraging in the mechanical data was that the moduli between concentrations were significantly different. This would suggest that the crosslinking protocol was fairly consistent, even with qualitative control measures, and that the CTAB turbidimetric assay could be used to accurately correct for HA content in the final material.

Chapter 4. Diffusivity and Mass Transfer

Continuing with my functional characterization of disulfide-crosslinked hyaluronan hydrogels, I was next interested in studying the diffusive environment in the hydrogels. In solid tissues, mass transfer of nutrient and waste materials occurs via diffusion through a heterogeneous material environment, resulting in localized concentration gradients (56). It is well known that HA plays a role in this, as it has a strong molecular crowding effect and is capable of sequestering soluble factors *in vivo* (47). Thus, I wanted to study the diffusive environment imposed by a crosslinked HA hydrogel, as that could affect cellular access to nutrients and local concentrations of metabolites.

4.1. Results

4.1.1. Cell Viability Appears Limited by Access to Nutrients

Initially, I ran a short-term cell viability assay, simply with the HA hydrogel introduced on top of a standard monolayer cell culture to ensure that the HA hydrogel did not pose any issues with cytotoxicity at the concentrations I would use for subsequent experiments. I decided to run the experiment with two different cell lines: LNCaP (Figure 8), which is representative of a moderately-malignant prostate adenocarcinoma (155) and PC3 (Figure 9), which is a highly malignant model prostate cancer cell line with characteristics similar to a small cell carcinoma of the prostate (156). In testing the two cell lines and comparing them, I wanted to get a better understanding of how cells of different characterized phenotypes would behave in the hydrogel environment. As would be expected of more aggressive and hardier cells, the PC3 cells appear more robust against increasing hydrogel concentration compared to the less aggressive LNCaP cells. Overall, the hydrogel had negligible cytotoxic effects at low concentrations, up to 2% w/v. The 2% hydrogel, however, caused a large increase in cell death after 3 days of culture in both cell lines.

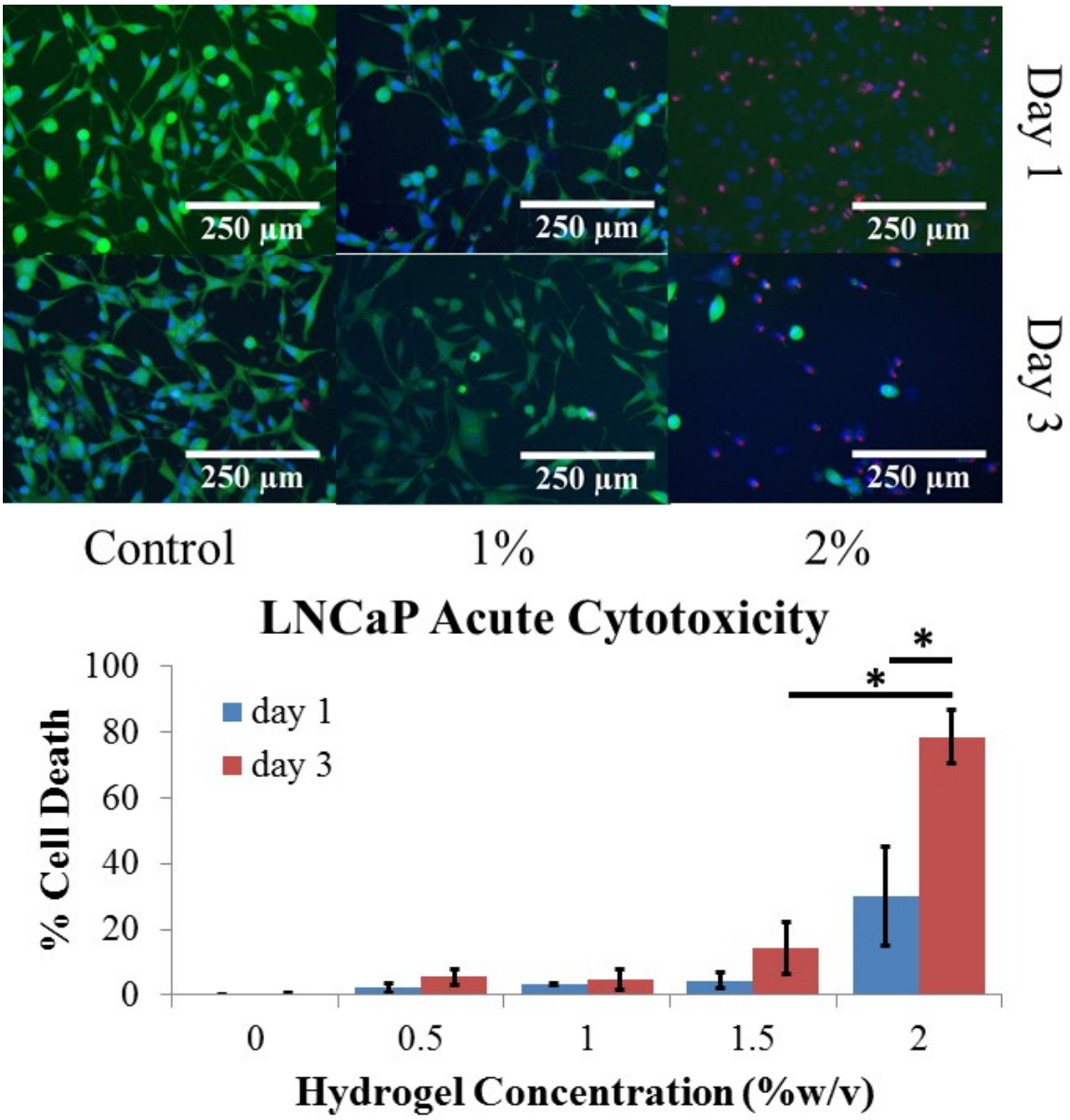

Figure 8, LNCaP acute cytotoxicity after exposure to HA hydrogels of varying concentration. Top: representative images of LNCaP cells cultured underneath HA hydrogels of different concentrations over one and three days. Viable cells were stained green with Calcein-AM and dead cells were stained red with propidium iodide. Hoechst was used to visualize nuclei to help with cell counting. Scale bars represent 250µm. Bottom: average percentage of dead cells across one and three days of culture in hydrogels of different concentrations. Error bars show standard deviation. * denotes statistical significance determined with two-way ANOVA and pairwise Tukey-Kramer post-hoc analysis, $p<0.05$.

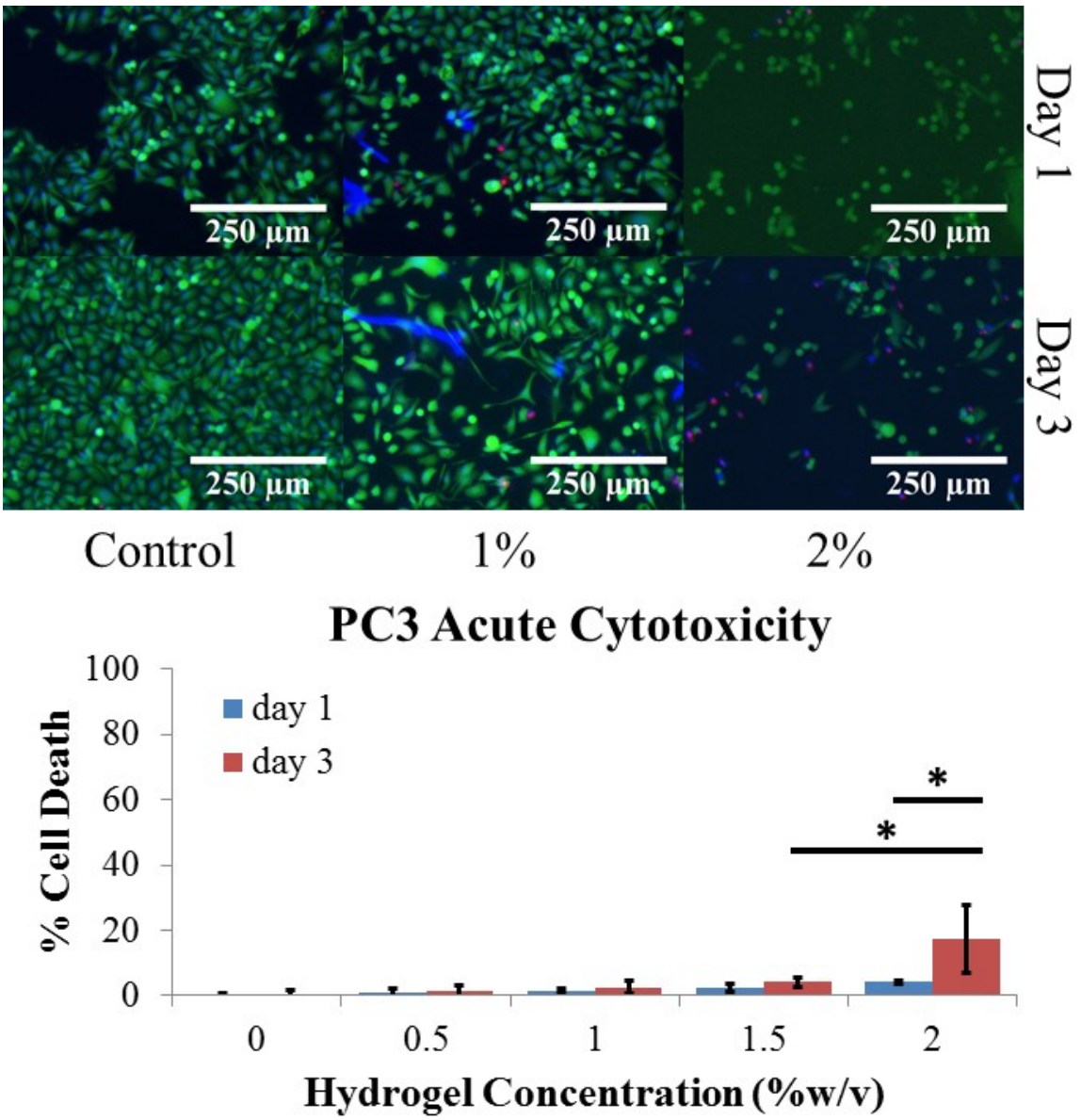

Figure 9, PC3 acute cytotoxicity after exposure to HA hydrogels of different concentrations. Top: representative images of cells cultured underneath hydrogels of different concentrations over one and three days. Viable cells were stained green with Calcein-AM and dead cells were stained red with propidium iodide. Hoechst was used to visualize nuclei to help with cell counting. Scale bars represent 250µm. Bottom: average percentage of dead cells after one and three days of culture under hydrogels of different concentrations. Error bars represent standard deviation. * denotes statistical significance determined with two-way ANOVA and pairwise Tukey-Kramer post-hoc analysis, $p<0.05$.

Interestingly, cell death is only statistically significant after three days of culture in a 2% w/v hydrogel for PC3 cells, and not at one day of culture. Even in the LNCaP cells, the cell death observed after three days of culture in the 2% hydrogel is far greater compared to that after one day of culture, and I was not convinced that this was purely due to toxicity from exposure to the hydrogel. Had this been the case, I would have expected to see more comparable cell death between days one and three instead of the dramatic spike seen only on day three of culture.

Because the cells used were model prostate cancer cell lines, there was a possibility that the cell death observed after three days of culture in the 2% hydrogel was not due to direct cytotoxicity of the material, but instead due to limits on diffusivity in the system. Rapidly dividing cells would quickly use up nutrients in their immediate surroundings, and any limitations in the ability of materials to diffuse would result in lack of nutrients and buildup of metabolic waste materials. This process would take time and cell death would be drawn out, as was observed in the data instead of appearing immediately. To test this hypothesis, I repeated this cell viability assay, but in a different cell culture configuration (Figure 10, Schematic diagram of different hydrogel cell culture configurations.). Using LNCaP cells, the more sensitive of the two cell lines used, I cultured cells on top of a layer of 2% HA hydrogel and compared cell viability with that of cells cultured underneath the hydrogel, as before. A layer of medium was added on top of the cells cultured on top of the hydrogel to allow direct access to liquid medium and freely diffusing nutrient materials. For consistency, liquid medium was also added on top of the hydrogel for the cells cultured underneath.

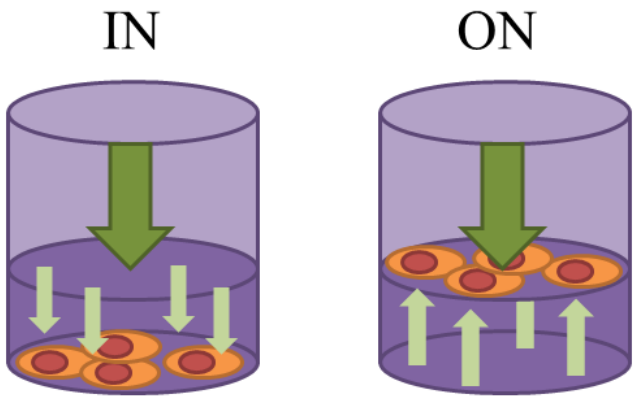

Figure 10, Schematic diagram of different hydrogel cell culture configurations. Cells were cultured "in" the hydrogel, as before, in a standard monolayer configuration with the HA hydrogel layered on top or "on" the hydrogel, with a layer of hydrogel coating the bottom of a well and the cells seeded on top. In the "on" configuration, cells remain in direct contact with the hydrogel, but also have access to free-flowing liquid media, whereas cells in the "in" configuration only have access to whatever is able to diffuse through the hydrogel.

I again quantified cell death in both conditions and also decided to measure adenosine triphosphate (ATP) content, which is the "energy currency" used by cells. The amount of ATP present in cells would be representative of the amount of nutrients the cells had access to in each culture system. I found that cell death was significantly higher in cells cultured underneath hydrogels compared to cells cultured on top (Figure 11). I also found that cells cultured on top of hydrogels had more ATP and therefore better access to nutrients than cells cultured underneath hydrogels. Taken together, this evidence supported my hypothesis that cells were not dying due to direct cytotoxicity from the hydrogel material – cells were in direct contact with the material in both culture conditions. Instead, it appeared that the cells were dying of starvation, possibly from essential serum proteins, amino acids, or sugars.

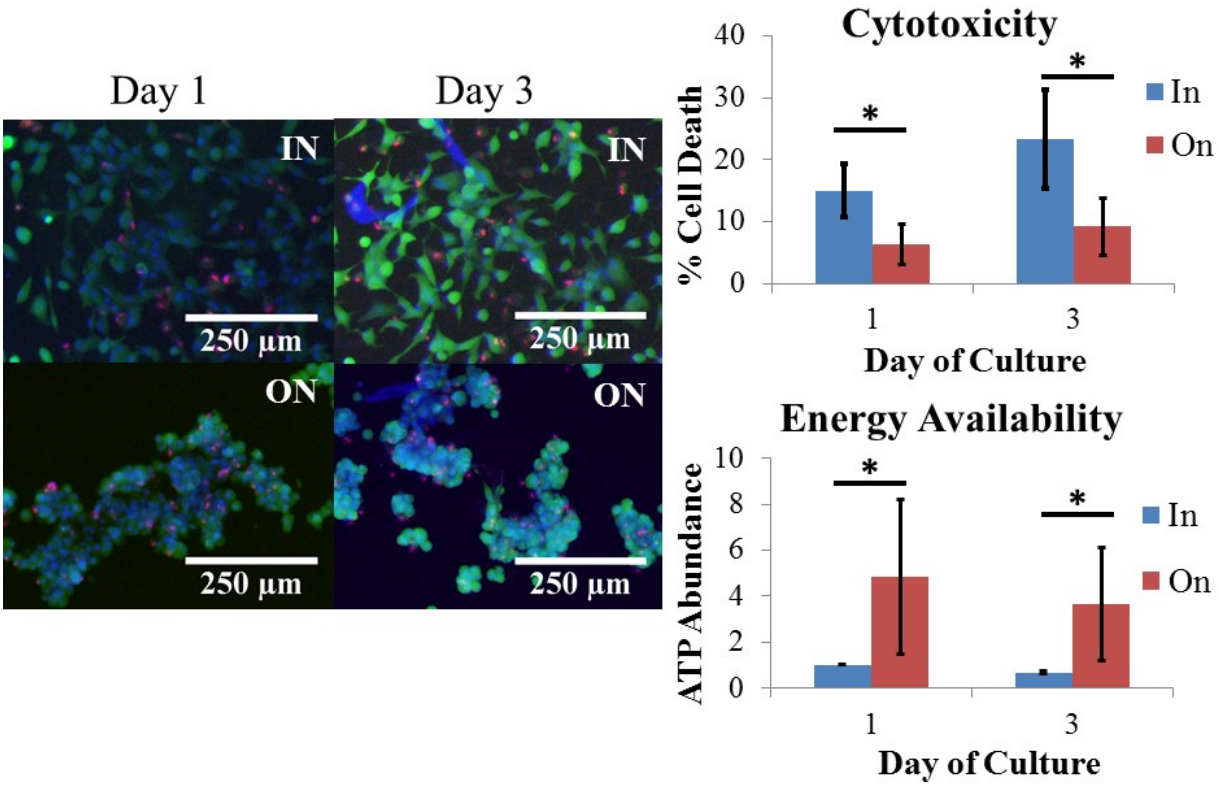

Figure 11, Comparison of cells cultured underneath and on top of HA hydrogels. Left: representative images of LNCaP cells cultured underneath (IN) and on top (ON) of 2% w/v HA hydrogels, over one and three days of culture. Viable cells were stained green with Calcein-AM, dead cells were stained red with propidium iodide, and nuclei were visualized with Hoechst to help with cell counting. Scale bars represent 250µm. Top right: cytotoxicity, as measured by percentage of dead cells cultured underneath (in) and on top (on) of 2% w/v HA hydrogels. Bottom right: ATP content of cells as a proxy for access to nutrients, as measured using CellTiter-Glo Assay normalized to cell count. Error bars represent standard deviation. * indicates statistical significance as determined with two-way ANOVA and pairwise Tukey-Kramer post-hoc analysis, $p<0.01$.

Moving forward, I was now interested in characterizing the diffusive environment of the HA hydrogels to better understand how the physical properties of the material environment affected access to nutrients and the formation of concentration gradients.

4.1.2. Diffusivity of Small Particles is Independent of HA Content

I used fluorescence recovery after photobleaching (FRaP) to study the ability of particles of different sizes to diffuse through the hydrogel material. If diffusivity was the limiting aspect for cell viability in culture underneath the hydrogel, there would be differences in the diffusion rates of dye particles within hydrogels of different concentrations. Even a subtle difference in diffusion rate could affect the formation of concentration gradients and I expected to see such differences particularly between the 2% w/v hydrogel compared to the lower concentrations, as it was in this condition that I saw the greatest difference in cell death. I was also interested in seeing how particles of different sizes would differ in their ability to diffuse through the hydrogel system. This would be an indirect method for determining pore size of the hydrogel material, as particles on the order of or larger than the effective pore size would be impeded from diffusing within the matrix while smaller particles would diffuse with relative ease. I hypothesized that dye particles in the 2% w/v hydrogel would have significantly higher diffusion half-times compared to lower hydrogel concentrations across dye particle sizes. This limitation on diffusivity would explain the lack of resources leading to starvation I observed in my cell viability experiments.

Interestingly, diffusion half-times for particles 125kDa and smaller are not significantly different across all concentrations of hydrogels tested, as determined by two-way ANOVA. Even when compared with liquid PBS and the 0.5% hydrogel solution, which is functionally liquid in that it is capable of flowing, the half-time does not appear to change. This would suggest that for small enough particles, diffusion rates are independent of HA content, at least for the hydrogel concentrations tested. Only for the 500kDa dye particle does hydrogel concentration appear to have any impact on diffusion rate, where diffusion through the 2% hydrogel was found to be significantly different from the other hydrogels and PBS (Figure 12). This would suggest that the 2% HA matrix has a functional pore size on the order of or smaller than the 500kDa dye particle, which has a hydrodynamic coil radius of 15nm (157), thus impeding its movement.

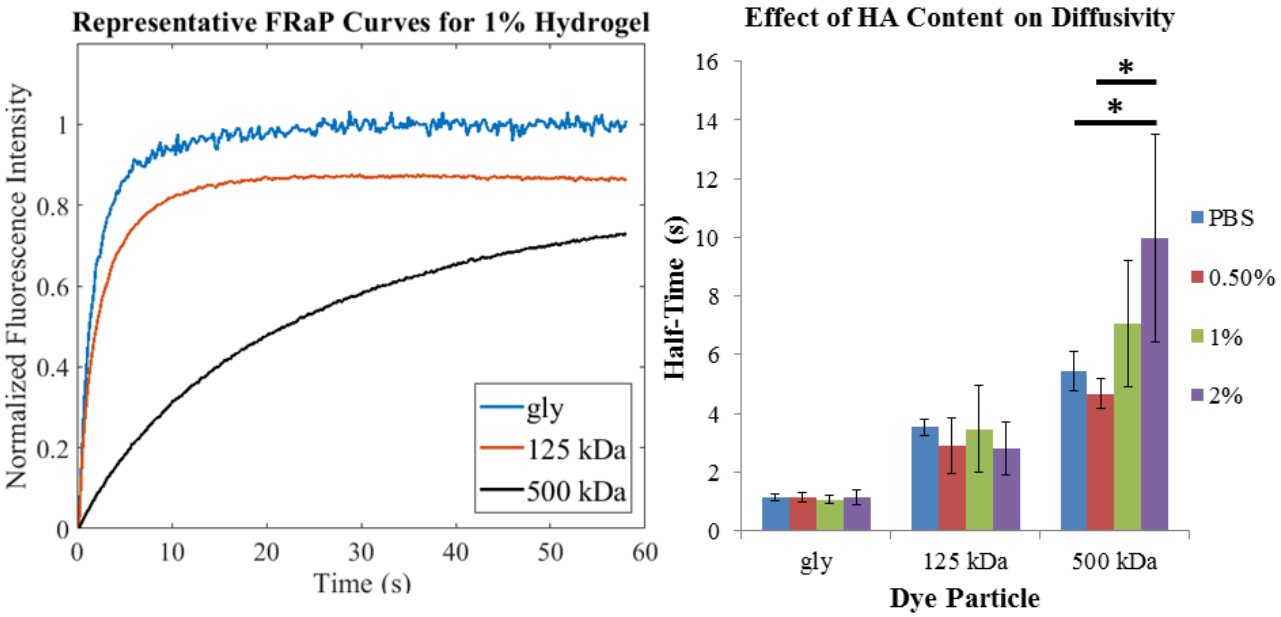

Figure 12, FRaP analysis of diffusive properties of HA hydrogels. Left: representative FRaP curves of dyes of different molecular weights in a 1% w/v HA hydrogel. Right: comparison of average diffusion half-times obtained from FRaP curves across hydrogels of differing HA content and dye particles of differing sizes. Dye particle size was found to have an effect on diffusion half-times, but not hydrogel concentration for dye particles below 125kDa in size, as determined by two-way ANOVA, $p<0.05$. A separate one-way ANOVA with Fisher's least significant difference post-hoc analysis on the half-times of the 500kDa dye particle showed that the 2% hydrogel was significantly different from the PBS and 0.5% conditions, $p<0.05$, as indicated by *.

These results were interesting, as they were not what I was expecting. Though there appears to be a difference in the ability of dye particles 500kDa or greater to diffuse through 2% hydrogels compared to the lower concentrations, the difference is subtle and does not exist for smaller particles. This challenged the idea that cells lacked access to nutrients, as most nutrient materials such as glucose and amino acids are even smaller than the fluorescein-tagged glycine that I used as my smallest dye particle. Following these results, I was interested in seeing if another material property of the HA hydrogels was responsible for limiting cellular access to nutrients.

4.1.3. HA Hydrogels Sequester Proteins from Medium

In vivo, HA is known to have strong molecular crowding effects and is responsible for sequestering important soluble factors. Shu et al. originally showed that the disulfide-crosslinked HA hydrogel can be loaded with blue dextran, which cannot be released from the hydrogel unless the crosslinks are broken or the hydrogel is enzymatically degraded with hyaluronidase (143). I was interested in seeing if the same effect could be observed with essential serum proteins derived from cell culture medium. I developed a procedure to determine whether hydrogels made up with conditioned medium could retain their protein content after extensive washing with PBS. What I found is that the hydrogels indeed prevent proteins from being washed out (Figure 13). Hydrogels between 1% and 2% concentration have similar protein retention capabilities. Moreover, while 0.5% w/v hydrogel solutions were prone to bulk mixing and being pipetted off during liquid transfer, the solution was still capable of retaining proteins to some extent. This seems to suggest that this protein sequestration has less to do with physical state of gelation or matrix geometry and more to do with molecular interaction.

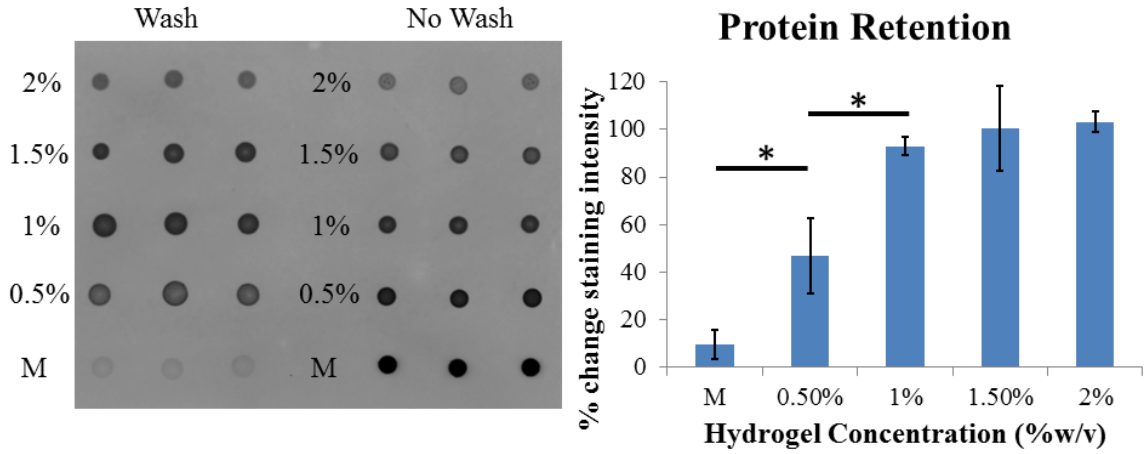

Figure 13, Dot-blot analysis of HA hydrogel protein retention. Left: representative dot-blot; each dot represents a sample taken from a hydrogel that was either washed extensively with PBS or not washed. The blot was stained with Coomassie Blue to detect protein content. Right: protein retention, as measured by change in Coomassie Blue staining intensity. Error bars represent standard deviation. * denotes statistical significance as determined with one-way ANOVA and pairwise Tukey-Kramer post-hoc analysis, $p<0.05$.

It was clear that medium-derived proteins were not able to leave the HA hydrogel matrix, but I was interested in seeing if they were able to enter it. This would be particularly important for this material's use as a long-term cell culture environment that would require medium changes. If culture medium components were unable to penetrate the matrix, cells cultured within would eventually starve. I used a similar dot-blot procedure as before, this time looking at the amount of protein that was able to enter hydrogels made with PBS during thirty minutes of incubation with conditioned medium. The results, shown in Figure 14 show that medium-derived proteins can enter HA hydrogels, but in a limited capacity. Again, hydrogels between 1% and 2% have similar protein penetrance and the 0.5% HA hydrogel solution showed intermediate penetrance, owing to bulk mixing of the solution with the conditioned medium.

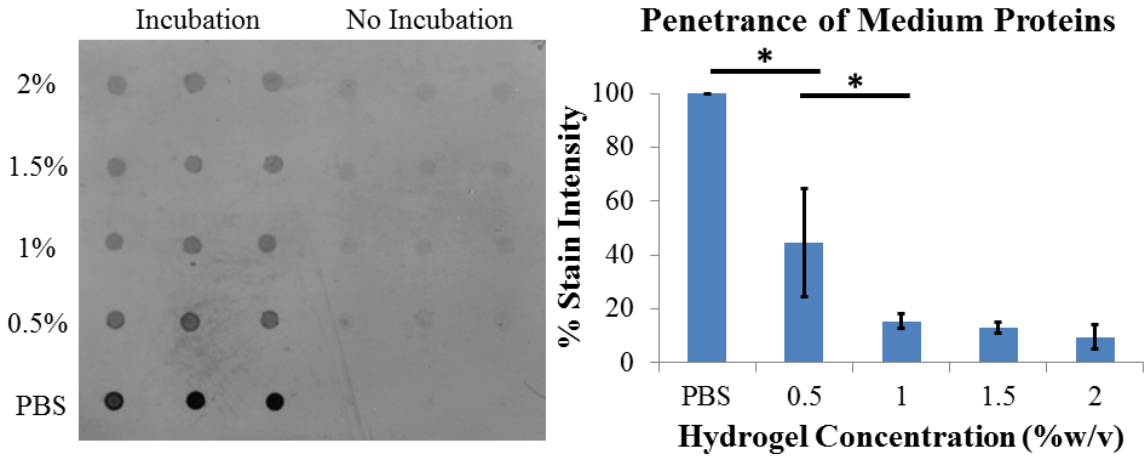

Figure 14, Dot-blot analysis of protein penetrance in HA hydrogels, or the amount of medium-derived protein that was able to enter the hydrogels during incubation. Left: representative dot-blot with samples derived from hydrogels made with PBS and either incubated with conditioned medium or without incubation. Right: protein content of hydrogels after incubation with conditioned culture medium, measured as Coomassie Blue staining intensity. Data were normalized to the PBS condition, in which pure liquid PBS was mixed with conditioned medium during incubation. Error bars show standard deviation. * denotes statistical significance as determined by one-way ANOVA and pairwise Tukey-Kramer post-hoc analysis, $p<0.05$.

4.2. Materials and Methods

4.2.1. Cell Line Culture Methods

I used the model prostate cancer cell lines LNCaP (ATCC CRL-1740) and PC3 (ATCC CRL-1435) for my cell viability experiments and LNCaP alone for culture on top of hydrogels, as they were the more sensitive of the two. Both cell lines were confirmed with Short Tandem Repeat analysis at the Centre for Applied Genomics at SickKids (Toronto, Canada). The LNCaP cells I used had 89% match with expected alleles and the PC3 cells had 100% match.

Both cell lines were cultured in standard 100mm by 22mm tissue-culture treated culture dishes (Falcon) and kept in an incubator at 37°C with 5% CO_2. Dulbecco's Modified Eagle's Medium (DMEM; Sigma-Aldrich) was used for LNCaP cells, supplemented with 10% fetal bovine serum (VWR) and 1% antibiotic antimycotic solution (Sigma-Aldrich). This was used as opposed to what is suggested by the American Type Culture Collection, as the cells had been previously cultured with DMEM prior to my acquisition of them. Complete culture medium for PC3 cells was composed of Kaighn's Modification of Ham's F-12 Medium (F-12K; Corning), supplemented with 10% FBS and 1% antibiotic antimycotic solution. Culture medium was replaced every 3-4 days.

Subculture and passaging was done at 70-90% confluency for both cell lines. First, medium is removed and the culture dish is rinsed with sterile PBS. Next, 2mL of 0.05% trypsin and 0.53mM EDTA in Hank's balanced salt solution (Corning) is added to the dish and the dish is placed in an incubator at 37°C to incubate for 5-10 minutes. Plates are visually inspected to assess cell detachment from the dish surface. Once detached, the trypsin is quenched with 3mL complete cell culture medium of the appropriate type and the dish contents are transferred to a 15mL conical tube (Greiner). Tubes are centrifuged at 200 times the force of gravity for 5 minutes to pellet the cells. The supernatant is removed and the pellet is re-suspended in fresh cell culture medium before being added to new culture dishes or seeded into plates for subsequent experiments.

4.2.2. Acute Cytotoxicity Experiments

To test cell viability, cells were detached from tissue culture plates, as described above and seeded into 96-well plates at a density of 10000-12000 cells/well. After letting the cells attach overnight, HA hydrogel solutions were made up in the appropriate complete cell culture medium, adjusting the pH to 6.5-7 using of 1M NaOH. To ensure consistency of hydrogels across concentrations, a large batch of 2% w/v hydrogel solution was made and serially diluted with culture medium to make the 1.5%, 1%, and 0.5% solutions. Old culture medium was removed from the 96-well plate 80µL of hydrogel solution was added on top of cells in each well. For the control, the old medium was replaced with 80µL fresh culture medium without any HA hydrogel. Plates were returned to the incubator at 37°C and 5% CO_2 and allowed to culture for one and three days.

At one and three days of culture, cells underwent viability testing. The following is an example of the amounts of reagents used for analyzing fifteen wells of cells. A dye mixture was made with 4.5µL 1005µM Calcein-AM (Biotium), 3µL 1500µM propidium iodide (Sigma-Aldrich), and 1µL bisbenzimide Hoechst #33342 (Sigma-Aldrich), diluted with 71.5µL PBS for a total volume of 80µL. Each well containing 80µL of hydrogel or culture medium received 5µL of the dye mixture. The plate of cells was then incubated for 20 minutes at 37°C to allow the dyes to penetrate the hydrogels and reach the cells underneath before being visualized. Representative images were taken using a Nikon Eclipse Ti Epifluorescence Microscope and later processed with ImageJ to obtain live and dead cell counts.

I chose a hydrogel volume of 80µL for this experiment because greater gel volumes, especially at 2% w/v concentrations were difficult to image through and required long incubation times with the dyes. I found that using the Hoechst stain to visualize nuclei made it easier to use the semi-automated cell counting algorithm in ImageJ, especially for highly confluent wells.

Statistical significance for all cell viability data was determined with two-way ANOVA and pairwise Tukey-Kramer post-hoc analysis with $p<0.05$ in MATLAB.

4.2.3. Modified Culture Configuration

To test whether cells were dying from direct hydrogel cytotoxicity or starvation due to lack of access to nutrients, cells were cultured on top of hydrogels and compared to cells cultured underneath. These two conditions had to be tested separately, but in parallel due to logistical issues of allowing time for hydrogels to gel and cells to attach.

For growing cells on top of hydrogels, first a 2% w/v hydrogel solution was made with DMEM supplemented with 10% FBS and 1% antibiotic antimycotic solution, with the pH adjusted to 6.5-7 using additions of 1M NaOH. Each of the centre 40 wells of a standard 96-well plate received 80µL of the hydrogel solution, with the bordering wells filled with 100µL of PBS to maintain humidity and minimize evaporation. The solutions were allowed to fully gel overnight in an incubator at 37°C and 5% CO_2. The next day, LNCaP cells were detached from their culture dish, as described in section 4.2.1 and seeded on top of the 2% hydrogels at a density of 5000 cells/well, with each well topped up with 50µL liquid medium to prevent cells from dehydrating. These plates were returned to the incubator and underwent cell viability and ATP content testing after one and three days of culture.

For growing cells underneath hydrogels, the procedure is similar to the original cell viability assay, but with minor alterations to keep consistency with the cells grown on top of gels. First, LNCaP cells were seeded into the middle 40 wells of a 96-well plate at a density of 5000 cells/well and allowed to attach overnight. I reduced the amount of cells in each well from before to ensure the cell death observed was not an artefact from seeding density. Bordering wells were filled with 100µL PBS to maintain humidity and prevent evaporation. The next day, the old medium in each well was replaced with 80µL of 2% w/v hydrogel solution, which was allowed to gel for 2 hours. Once set, 50µL of DMEM was added on top of the hydrogels. These cultures were returned to the incubator and underwent cell viability and ATP content testing after one and three days of culture.

The cell viability assay was as before, using the same ratio of dyes, but now using 8.5µL of the final dye mix in each well. For the ATP content assay, culture plates were placed on ice and 50µL of

CellTiter-Glo 2.0 Cell Viability Assay reagent was added to each well. Hydrogels were broken up mechanically by pipetting up and down and scraping the bottom of the wells to disperse the reagent. Luminescence in each well was analyzed using a Filtermax F5 Microplate Reader. These readings were then normalized to average viable cell counts obtained from the Calcein-AM and propidium iodide experiments to obtain average ATP content per cell.

Statistical significance for cell viability comparisons between culture underneath or on top of gels, as well as ATP content assays was determined with two-way ANOVA and pairwise Tukey-Kramer post-hoc analysis, $p<0.01$ using MATLAB.

4.2.4. Fluorescence Recovery after Photobleaching

I used FRaP to study diffusivity in hydrogel environments of differing concentrations. For simplicity, I compared the measured diffusion half-times of dye particles of known molecular weight, to which the corresponding diffusion constants are inversely proportional according to the numerical models described by Axelrod et al. (158) and Soumpassis (159).

The following is an example of the amounts of reagents used to make hydrogels for FRaP analysis. First, a suspension of microbeads was made by adding 1mg of polystyrene latex beads (3µm mean particle size, Sigma-Aldrich) to 500µL PBS. These microbeads aided in focusing the confocal microscope onto a plane in the middle of the hydrogel samples. Next, 35mg of 45% HA content hydrogel material, corresponding to 15.8mg pure HA was dissolved in 700µL PBS and the pH was adjusted to 6.5-7 with 50µL 1M NaOH. To this mixture, 10µL of the microbead suspension and 20µL fluorescein 5-isothiocyanate (FITC) conjugated dextran (125 or 500kDa; Sigma-Aldrich) was added. The final volume was topped up to 790µL with PBS to make a 2% w/v HA hydrogel solution, doped with dye and microbeads. Approximately 750µL of solution was dispensed into a 35mm Matsunami glass bottom culture dish (VWR). A similar process is used to make up other gel concentrations and with different sized dye particles.

For the smallest dye particle size, I wanted to use pure FITC, but as it is reactive to amines, I needed to quench it, so I conjugated it to glycine. For this, 2mg FITC (TCI Chemicals) is dissolved in 2mL dimethyl sulfoxide (Thermo Fisher) and in a separate 50mL conical tube, 20mg glycine (VWR) is dissolved in 10mL PBS. Next, 20mL borate buffer is added to the glycine solution. For the borate buffer, 0.62g boric acid, 0.44g NaCl, and 0.95g sodium tetraborate are dissolved in distilled water and the pH is adjusted to 8.4. The FITC solution is then added to the glycine, the conical tube is wrapped in aluminum foil, and the mixture is incubated in the dark at 37°C for 90 minutes. I did not confirm whether all the FITC was conjugated, so there was a possibility that the FITC would have conjugated to the HA matrix. If this were the case, the immobile fraction would be affected, since a portion of the FITC would not be able to diffuse away, but the time constant would not be affected, as other quenched dye particles would still be able to diffuse through the matrix. Given that I used a two-to-one excess of glycine to FITC and that I only looked at the half-time of diffusion during analysis and not immobile fraction, the effect of this would have been negligible.

For FRaP, samples in glass bottom culture dishes were visualized under confocal microscopy with 488nm laser illumination and 40X objective. The presence of microbeads allowed focussing on a plane within the gel to obtain an even laser bleach spot. Ten initial pictures were collected before the bleaching to obtain a baseline fluorescence reading. After this, a circular 5x5μm region of interest was bleached with a 488nm laser. Data were collected at 200ms intervals over a minute. To analyze the data, the fluorescence intensity in the region of interest was measured and was corrected for photobleaching from the imaging laser by subtracting the signal obtained from a reference spot away from the FRaP region of interest. This was repeated 6 times per gel sample. The data obtained was then processed in MATLAB, normalizing the fluorescence intensity with the baseline measurements and then removing the baseline measurements to obtain just the exponential FRaP curve. The data were fit with exponential curves of the following form using the curve fitting toolbox in MATLAB:

$$f(x) = a\left(1 - e^{-bx}\right)e^{-cx} \qquad 7$$

where *a* is the immobile fraction, *b* is the exponent constant of the FRaP recovery curve, and *c* is a correction term for the effects of photobleaching. Although the preliminary data processing included correcting with data from a reference point outside of the FRaP region of interest, I found that there were residual effects of photobleaching from the imaging laser. I thus used the extra exponential decay correction term to obtain a better fit to the data. To obtain half-times, the following relationship with the time constant was used. Given an arbitrary exponential function, $f(t)=e^{-bt}$ with exponent constant *b,* the ratio of the function evaluated one half-time, t_{half} after an initial time, *t* to the function evaluated at *t* is given by

$$\frac{f(t+t_{half})}{f(t)} = \frac{e^{-b(t+t_{half})}}{e^{-bt}} = \frac{1}{2} \quad 8$$

$$e^{-b(t+t_{half})+bt} = \frac{1}{2} \quad 9$$

$$e^{-bt_{half}} = \frac{1}{2} \quad 10$$

$$-bt_{half} = \ln\left(\frac{1}{2}\right) \quad 11$$

$$t_{half} = \frac{\ln(2)}{b} \quad 12$$

Thus, half-times were obtained with Equation$t_{half} = \ln(2)b$

12 from the measured exponent constants.

Differences in half-times across hydrogel concentrations for dye particles smaller than 125kDa were determined to not be statistically significant with two-way ANOVA, $p>0.05$. A separate one-way ANOVA with Fisher's least significant difference test ($p<0.05$) was computed on the 500kDa dye particle half-times, which showed that the only significant differences were between the 2% hydrogel and the 0.5% solution and the 2% hydrogel and PBS. I decided to use a less conservative statistical test to see if there was any possibility of the diffusion half-time being affected by hydrogel concentration. This was computed using MATLAB. Analyzing the correlation ratios of diffusion half-times, the variability in the data was determined to arise predominantly from inter-replicate variation, i.e. variation between hydrogel

samples as opposed to intra-replicate variation (Table 1). The correlation ratio is the ratio between the standard deviation across different replicates and the standard deviation of the ensemble data in all replicates.

Correlation Coefficients of Diffusion Half-Times				
Dye Particle	**PBS**	**0.5%**	**1%**	**2%**
FITC-gly	0.7031	0.6840	0.7067	0.8441
125kDa	0.4754	0.8889	0.9667	0.9173
500kDa	0.2440	0.9458	0.9832	0.7725

Table 1, Correlation ratios of diffusion half-times to determine source of variability in data. Coefficients for HA hydrogel conditions are larger than those for the PBS conditions. The coefficients for the FITC-gly dye particle appears relatively constant across gel and PBS conditions.

The high values seen in the gel conditions compared to the PBS conditions suggest that the variability in the hydrogel measurements most likely derives from differences in the hydrogels rather than from systematic measurement error or variability in the FRaP analysis. Since the PBS samples all came from the same stock, as did the dye solutions, measurement error in those cases would have a greater contribution to overall variability, hence the smaller coefficients. The FITC-gly dye is an interesting case, because the correlation ratios are fairly constant across the hydrogel and PBS conditions and is also fairly high compared to the other PBS conditions. This could stem from variability in the dye mixture, such as not having fully quenched the FITC with glycine, leading to FITC binding to the HA and affecting diffusion. Another possibility is uneven FITC binding, whereby some glycine molecules are being bound by more than one FITC molecule.

4.2.5. Dot-Blots

The procedure I developed to study the sequestration of proteins by HA hydrogels is as follows. First, conditioned medium was obtained from LNCaP cells cultured for 3 days in DMEM supplemented

with 10% FBS and 1% antibiotic antimycotic solution. HA hydrogels were then made with this conditioned medium, first at 2% w/v with the pH adjusted to 6.5-7 using additions of 1M NaOH, and then serially diluted to form solutions of 1.5%, 1%, and 0.5%. Next, 80µL volumes of hydrogel solution were added to a 96-well plate and allowed to gel overnight. For the control, 80µL of pure conditioned medium was used. The next day, half of the gels (and medium controls) were subjected to five washes, 10 minutes each with 100µL PBS while the other half was left unwashed as references.

For the other experiment involving protein penetration into hydrogels, 2% w/v hydrogels were made up in PBS, pH adjusted to a pH of 6.5-7 with 1M NaOH, and serially diluted to form 1.5%, 1%, and 0.5% hydrogel solutions. Volumes of 80µL were added to a 96-well plate and the hydrogels were allowed to gel overnight. The control consisted of 80µL of pure liquid PBS. The next day, half of the gels and PBS controls received 100µL of LNCaP-conditioned DMEM and were left to incubate at room temperature for 30 minutes on an orbital shaker. The rest of the hydrogels and controls did not receive any medium and served as references. After incubation, the media were removed from the incubated gels and they were washed briefly with 100µL PBS. This was to remove any media from the surface of the gels.

For both dot-blot experiments, a solution of 0.2g/mL DTT dissolved in PBS is made, and 40µL is dispensed into each well, for every condition, including the controls. I found that DTT was not only required to solubilize the gels, but also to denature the medium-derived proteins in order for them to properly attach to the blotting membrane and allow Coomassie Blue staining. The gels were left to incubate with the DTT solution for 10 minutes and then broken up mechanically with a pipette tip and by pipetting the hydrogel solution up and down. For the blot, 2µL samples of each solubilized hydrogel and control were spotted onto a polyvinylidene fluoride (PVDF; Millipore Sigma) membrane and left to dry overnight. Once the spots had fully dried, the blotting membrane was rinsed with Tris-buffered saline with 0.05% Tween 20 (TBST). A Coomassie Blue staining solution was made by dissolving 6mg Coomassie Brilliant Blue G (Sigma-Aldrich) in 30mL TBST. Staining solution was added to the blot, just enough to cover and left to incubate at room temperature on an orbital shaker for 10 minutes. The stain

solution was then removed and the blot was washed extensively with TBST. I found that the PVDF appeared intensely blue while the membrane was still wet and translucent. When left to dry, however, the PVDF became opaque, making the blue less pronounced and the contrast between the dots and the membrane made the blots easier to see. I thus allowed blots to dry overnight before imaging using an Azure c300 imaging system (Azure Biosystems). Images were processed with ImageJ to measure average integrated pixel intensity of the dot-blots.

4.3. Discussion

4.3.1. Diffusion and Systems-Level Mass Transfer

Taken altogether, my experimental results seem to raise conflicting conclusions about diffusion and mass transfer in the HA hydrogels. While diffusion within the hydrogels, as observed with FRaP appears to be unimpeded by HA content, at least for small enough particles, the results from the dot-blot experiments show that HA sequesters medium-derived proteins and prevents them from diffusing out. To reconcile these results, I would look at this problem from a systems-level point of view, as illustrated in Figure 15.

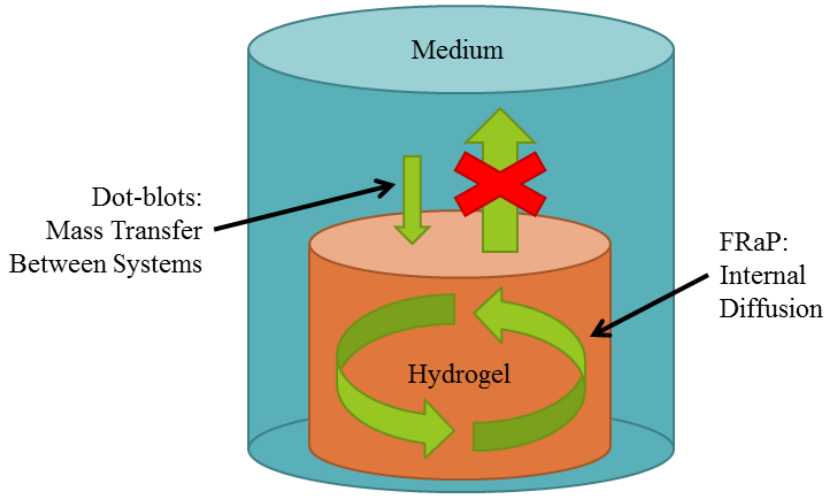

Figure 15, Mass transfer compartmentalization. Whereas FRaP looked at internal diffusion within the hydrogel material, the dot-blot experiments looked at mass transfer between the hydrogel and an external

liquid phase. Thus, diffusion within the hydrogel can occur relatively unimpeded while movement of materials into and out of the hydrogel is limited.

FRaP provides a microscopic internal view of diffusion within the hydrogel system, whereas the dot-blot experiments describe a higher-level mass transfer between the hydrogel system and an external liquid phase. With this compartmentalized model, the sequestration of proteins by the hydrogel can be described as one-way mass transfer. Swelling of the hydrogel material in the presence of culture medium allows medium-derived proteins to enter the hydrogel. Whatever is already in the hydrogel, however, is sequestered and is not able to leave the hydrogel system, as was observed with the PBS washes and in a drug-release experiment described by Shu et al. in their original paper (143). Once in the hydrogel, materials freely diffuse throughout the hydrogel volume, as was observed with FRaP. Interestingly, sequestration appears to be independent of matrix geometry or gel stability, as it can be seen to some extent with the 0.5% w/v hydrogel solution, which is functionally liquid. It is likely that even in this solution, the HA molecules are crosslinking, but without enough ensemble interactions to allow stable matrix formation. The blue dextran loading experiment for studying drug release conducted by Shu et al. also suggests that intact disulfide crosslinking is required for material sequestration, as blue dextran was observed to be released by the hydrogel upon reduction of crosslinks. Release was also seen when the hydrogel was enzymatically degraded with hyaluronidase, so it could also be related to molecular weight of individual HA chains. Non-crosslinked HA molecules or HA after enzymatic degradation would be too small to hold together, whereas crosslinking would increase overall molecular weight, allowing individual crosslinked constructs to sequester materials. It remains unclear whether unmodified but functionally crosslinked, ECM-integrated HA also has this ability.

It is important to note that the results from my dot-blot experiments are fairly non-specific. I am only able to conclude that HA is capable of sequestering proteins in general and this provides no information on the types of proteins being sequestered, nor whether other nutrient materials are being sequestered. The fact that Shu et al. showed that blue dextran can be sequestered, however, suggests that this phenomenon is likely not due to electrostatic attraction. Dextran has a net anionic charge and at least

some proteins in media would have positive charge or polar interactions via amine groups, so they should have opposite electrostatic interactions with HA, which has a net anionic charge in physiological conditions (47). It may be interesting to repeat the FRaP experiments with dye particles with net cationic charge to see if particles can still freely diffuse with little impedance or if they would start to interact with the HA matrix. To determine the protein species being sequestered by HA matrices, the PBS washing experiment or the conditioned medium incubation experiment could be repeated, with the hydrogels solubilized with DTT and run through gel electrophoresis for Western Blot analysis.

In terms of my theory on cell starvation, it is still not clear what exactly cells cultured underneath the hydrogel are lacking, though it is clear that the HA hydrogels at 2% concentration are limiting their access to these materials to a greater extent than the other concentrations. Likely it is the denser packing of HA molecules that causes this, whether through entanglement in HA chains, increased electrostatic interaction from higher charge density, or a combination of different molecular interactions. Under culture conditions, the cells would form an external compartment relative to the hydrogel, with limited transfer of materials. This would prevent cells from getting access to materials inside the gel, as well as cause the buildup of metabolic waste materials. There is also the possibility of other molecules being prevented from diffusing through the hydrogel leading to cell death, such as oxygen (the possibility of which is explored later in Section 5.1.2) or hydrogen ions. The latter would derive from the Warburg effect, in which cancer cells prefer lactic fermentation over aerobic respiration for ATP production, thus causing buildup of metabolic lactic acid and the acidification of their immediate environment (160). In this regard, these material characteristics may be exploited to model specific tissue environments in which there is limited diffusion, such as the inside of solid tumours or perhaps metastases in cartilaginous tissues (161,162), in which HA is an important component (118).

The mass transfer characteristics and resulting effects on cell viability I have described in this HA material have not previously been reported in other HA hydrogel materials including methacrylated HA (144,147) and phenol-functionalized HA (148). There are a number of possible reasons for this, primarily having to do with differences in experimental setup, materials, and cell culture environment. For some

studies, HA hydrogels were not used to encapsulate cells – in particular, cells exposed to the phenol-conjugated HA were merely seeded on top of the hydrogels (148). Thus, cells were not cultured in the same diffusive environment. Other studies involving HA hydrogels may have used lower molecular weight HA in hydrogel synthesis or had lower final crosslink density, resulting in looser gels that may not be as efficient at sequestration of materials as the disulfide crosslinked hydrogels that I produced. A final possibility is the interaction of diffusing materials with the disulfide crosslink, either sterically or electrostatically. This would require further study with direct comparisons between hydrogel formulations of equal degree of crosslinking and HA molecular weight.

4.3.2. Differences in Cell Viability

LNCaP and PC3 cells displayed differences in viability in response to culture in HA hydrogels of varying concentration. This could be due to PC3 cells simply being more resistant to adverse growth conditions, but there are other possible reasons involving cell signaling pathways. Of particular interest is that of CD44 signaling. It is known that PC3 cells, as a model small cell carcinoma of the prostate express CD44 while LNCaP cells more reminiscent of a standard adenocarcinoma do not (133,156). PC3 cells can therefore exploit CD44 signaling to promote survival responses while LNCaP cells would not have this capability. LNCaP cells are also androgen-sensitive with intact androgen receptor signaling whereas PC3 cells are not (155,156). Neither cells were treated with androgen during the cytotoxicity experiments. Thus, LNCaP cells were missing an important signaling element important for cell growth and proliferation as well as survival. Some important signaling molecules may have been present in serum which was added to the whole cell culture media, but these molecules may not have reached cells due to being sequestered in the HA hydrogel.

4.3.3. Cell Aggregation

An interesting phenomenon I noticed when culturing LNCaP cells on top of 2% w/v hydrogels was that the cells grew in aggregates (Figure 11). Compared to cells grown underneath the hydrogel, which had spread-out spindle-like and cobblestone-like morphologies, the cells grown on top of the hydrogels had a rounded morphology and were growing in clumps. This would suggest that the cells had greater affinity for cell-cell attachment than attachment with the hydrogel substrate. This is not surprising, given that the main cell attachment molecule for HA is CD44, which is not expected to have as strong a binding effect as the integrins that make up focal adhesions or the cadherins that make up adherens junctions. Cell aggregation on HA suggests that HA could be used as a non-adhesive environment for the culture of 3D cell structures, such as spheroids.

Chapter 5. Cells in Gels

With a better understanding of the mechanical and diffusive properties of disulfide-crosslinked HA hydrogels, I wanted to see how culture within the hydrogel environment would affect cell behaviour. In particular, I was interested in understanding how cell metabolism would respond to the lack of resources imposed by limited mass transfer of nutrients and waste. One of the main signaling pathways involved in nutrient sensing and directing cell growth and proliferation is the Akt-mTOR pathway, as illustrated in Figure 16. Akt is a central integrator of numerous growth and nutrient signals and its activity is often upregulated in cancer cells (75,163). Downstream of Akt is mammalian target of rapamycin (mTOR), an important effector element that controls protein synthesis, cell growth, proliferation, and metabolism via activation of the ribosomal protein p70 S6 kinase (S6K) (164). Parallel to the Akt-mTOR axis is adenosine monophosphate-activated protein kinase (AMPK), which is an energy sensor that, when activated, is responsible for downregulating anabolic activities and upregulating energy scavenging and survival mechanisms, including autophagy (75).

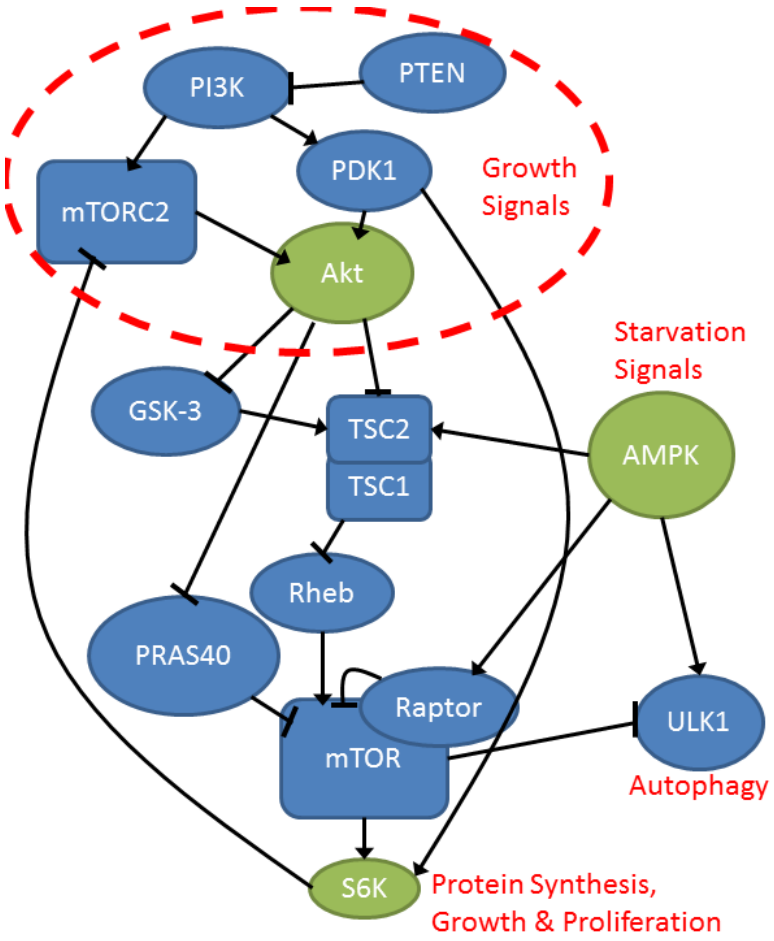

Figure 16, Akt-mTOR signaling pathway with adjacent control elements. Elements in green were studied with Western blot analysis. Akt is an integrator of numerous upstream growth signals (red dotted oval) and has a number of effector elements that control a wide variety of cell activities. One of these effector elements is mTOR, which controls protein synthesis, metabolism, and cell growth and proliferation via activation of the ribosomal protein, S6K. Parallel to the Akt-mTOR axis is AMPK, which is responsive to the ratio of AMP to ATP, which would indicate nutrient availability and energy content. When active, AMPK downregulates energy-consuming processes, including the mTOR pathway. AMPK also upregulates autophagy and energy-scavenging processes as survival mechanisms.

Altered signaling involving the Akt-mTOR axis is often implicated in numerous cancers, including that of the prostate. As a central control element that mediates cell growth, proliferation, and protein synthesis, Akt activity is often affected by upstream mutations, such as knockdown of PTEN or hyperactivation by PI3K (163). This results in Akt hyperactivity, driving cell survival and proliferation. This has been directly implicated in the growth and progression of prostate cancer (165). Many mutations that confer anoikis resistance act through Akt to provide pro-survival signals to replace those normally derived from ECM attachment (50,72,75). As a downstream controller of protein synthesis, mTOR is also a common signaling element that is affected by oncogenic mutations. By decoupling mTOR from upstream growth signals or disconnecting feedback signals to Akt, mTOR can be made constitutively active (166). The risk of using up cell resources in unchecked mTOR-mediated protein synthesis is often balanced by AMPK activity, which induces autophagy (75). In activating energy scavenging mechanisms like autophagy, AMPK can increase the energy efficiency of cells and allow continued mTOR activity. This complex signaling behaviour allows cancer cells to survive and multiply even in adverse growth conditions.

To study how this metabolic network is affected by hydrogel culture conditions, I decided to look at protein activation at key control points, namely Akt, AMPK, and S6K. This would provide a general idea of the metabolic state of the cells.

5.1. Results

5.1.1. Decreasing ATP Content Suggests Lack of Nutrients

Repeating the ATP content assay from Section 4.1.1, I looked at energy content of PC3 cells in varying hydrogel concentrations over one and three days of culture. I found that ATP content appeared to decrease over time and with increasing hydrogel concentration, as seen in Figure 17. This was most prominent in the control condition, in which cells were cultured in a standard configuration with liquid medium, as well as in the 0.5% hydrogel solution. The fact that the cells in the 0.5% hydrogel solution

followed the same trend as the control group, whereby ATP content dropped over time, supports my initial hypothesis that cell death was related to starvation due to limits in diffusion and mass transfer. There was little change in energy content between days for cells cultured in hydrogels, which would suggest that right away, the cells in hydrogels had less access to nutrients compared to cells in the control.

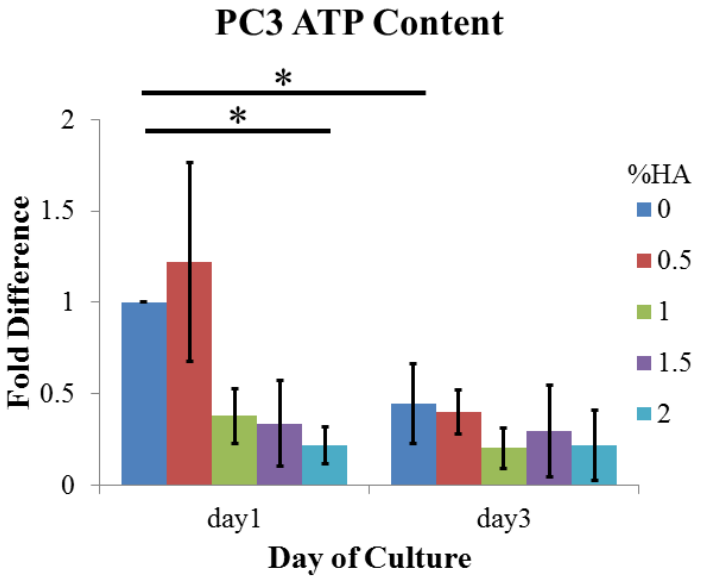

Figure 17, ATP content of PC3 cells cultured in hydrogels. ATP content decreases with day of culture and hydrogel concentration. * indicates statistical significance as determined with two-way ANOVA and pairwise Tukey-Kramer post-hoc analysis, $p<0.05$.

5.1.2. PC3 Cells in Hydrogel Culture Upregulate HIF1A mRNA Expression

Hypoxia inducible factor 1 (HIF-1) is the primary transcriptional control element in cells that responds to a lack of oxygen. Under hypoxic conditions, HIF-1 upregulates various genes, including vascular endothelial growth factor (VEGF), which induces angiogenesis (91). This is particularly relevant in metastatic cancers, as HIF-1 upregulation is implicated in promoting metastasis and priming of the metastatic niche (64,91,94). I was interested in how culture of PC3 cells in the diffusive environment of the HA hydrogels would affect the expression of HIF-1α, a subunit of HIF-1. Using endpoint reverse transcriptase PCR, I quantified HIF1A (the gene encoding HIF-1α) mRNA expression in cells cultured

under varying hydrogel concentrations. I also looked at mRNA expression of the HMBS gene, which encodes porphobilinogen deaminase. This enzyme is involved in the biosynthesis of heme and its mRNA expression levels have previously been found to be stable across states of differentiation and metabolism in hepatic carcinoma cells, macrophages, and bone cells. Thus, its expression is suitable for use as a normalization factor for PCR analysis (167,168). Using HMBS as a reference gene representing overall metabolic state, I found that the ratio between HIF1A and HMBS expression increased with hydrogel concentration in PC3 cells (Figure 18). This would imply that the cells are under hypoxic stress and are upregulating HIF1A expression as a survival response.

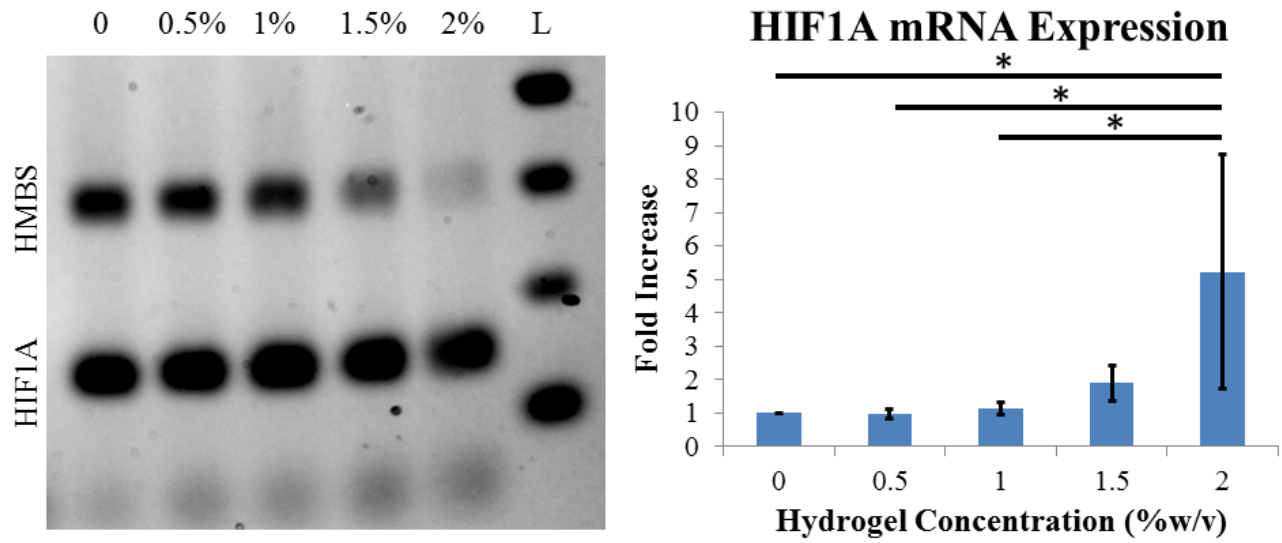

Figure 18, Endpoint PCR analysis of HIF1A mRNA expression. Left: representative DNA gel electrophoresis of HIF1A and HMBS transcripts from reverse transcriptase PCR, with RNA samples derived from PC3 cells cultured under hydrogels of varying concentration. Right: ratio between HIF1A and HMBS, showing increasing ratio with increasing gel concentration. Error bars represent standard deviation. * denotes statistical significance as determined by one-way ANOVA and pairwise Tukey-Kramer post-hoc analysis, $p<0.05$.

5.1.3. Akt-AMPK-mTOR Activity Profile of PC3 Cells

I used Western blot to analyze protein activation of key control elements in the Akt-AMPK-mTOR signaling network to see how cells were responding to hydrogel culture conditions. In PC3 cells after three days of culture in 0.5%, 1%, 1.5%, and 2% w/v hydrogels, no significant differences in Akt activation were found among culture conditions (Figure 19). This is not particularly surprising, as by day 3, cells in all conditions had comparable ATP content, suggesting similar nutrient availability. While the apparent hypoxic conditions of the 2% hydrogel environment might have affected the ability for another cell type to undergo aerobic respiration, PC3 cells likely would not be as sensitive due to the Warburg effect, i.e. the switching of cell metabolism from aerobic to anaerobic respiration.

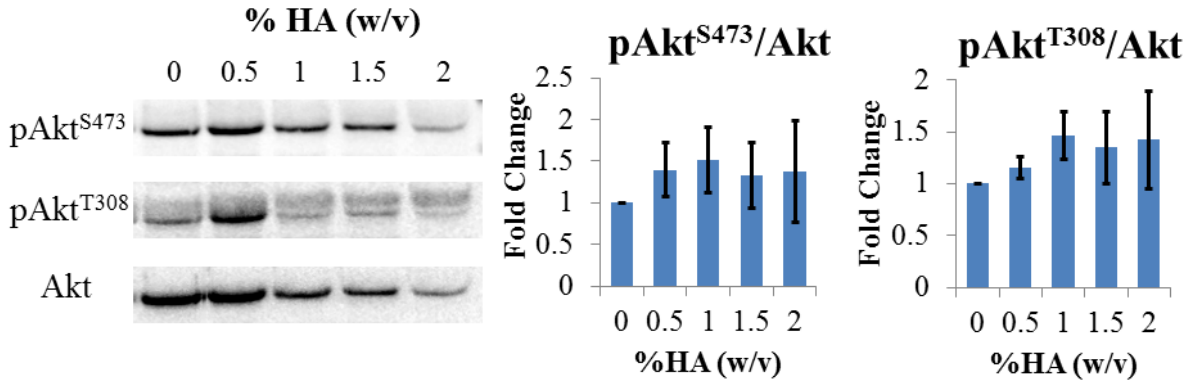

Figure 19, Akt activation in PC3 cells cultured in varying concentrations of HA hydrogel. Left: representative Western blots of Akt and two of its phosphorylated forms. Middle: ratios of Akt phosphorylated at its serine 473 residue to whole Akt protein content. Right: ratios of Akt phosphorylated at its threonine 308 residue to whole Akt protein content. No significant differences were found between conditions using one-way ANOVA, $p>0.05$. Error bars represent standard deviation.

Parallel to Akt, I looked at AMPK activity, which should line up well with measurements of ATP content. Again, I found that similarly to ATP content after 3 days of culture, AMPK activation was not significantly different across hydrogel concentrations (Figure 20). Certain anoikis-resistant cancer cell types have constitutively active AMPK, which prevents apoptotic signaling by promoting autophagy (74,75). This also improves energy efficiency by breaking down aging cell components.

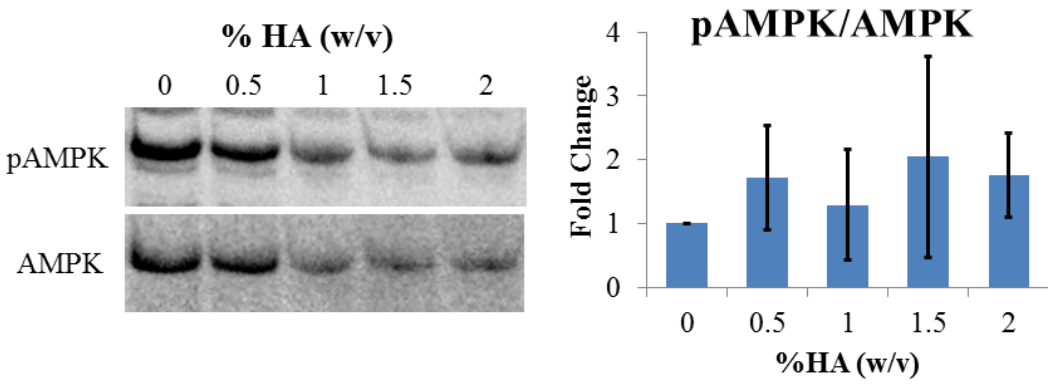

Figure 20, AMPK activation in PC3 cells cultured in varying concentrations of HA hydrogel. Left: representative Western blots of AMPK and phosphor-AMPK. Right: ratios of phosphor-AMPK to whole AMPK protein content. No significant differences were found between conditions using one-way ANOVA, $p>0.05$. Error bars show standard deviation.

To check if PC3 cells were undergoing autophagy as a result of AMPK activation, I used Western blot to look at LC3B expression. LC3B is used as a marker of autophagy and is detected as a double band in Western blot. The lower band, as seen in Figure 21, represents an active form of LC3B that has been post-translationally modified and is a component of autophagic membranes. The upper band represents an inactive form of the protein. Looking at LC3B-II (the lower band) content, there were no significant differences between conditions. Finding LC3B-II expressed at all, however, is indicative of active autophagy taking place, which matches AMPK activity in all conditions. It is interesting to note that neither AMPK nor LC3B activation appear to be affected by the apparent hypoxia, as reported by HIF1A mRNA expression. Previous work has shown that hypoxia induces an autophagic response via HIF-1 activity (169). It is possible that the hypoxic response requires more time to be expressed at the levels of AMPK or LC3B expression. It is also possible that the cells are in active 'autophagic flux' whereby LC3B-II is dynamically being synthesized and degraded during autophagy. In this case, Western blot would only provide a snapshot of LC3B content and not be reflective of the active process of autophagy.

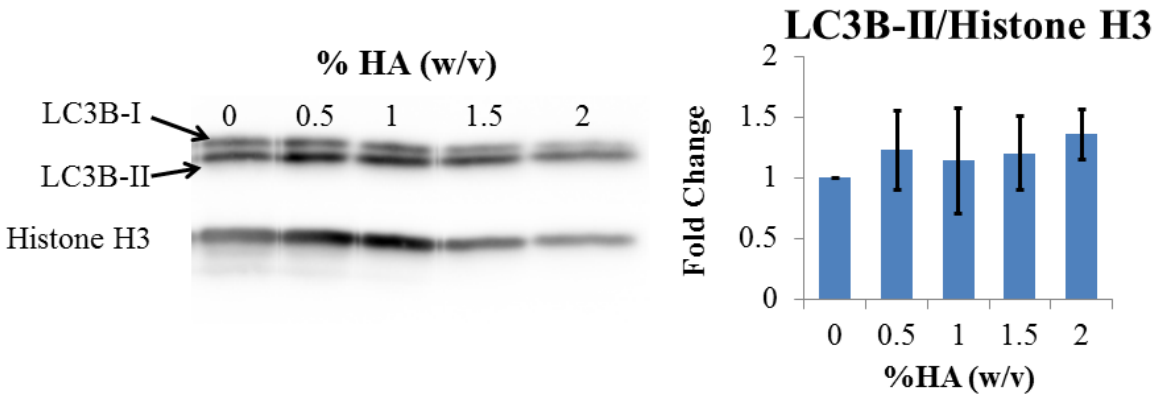

Figure 21, LC3B expression in PC3 cells cultured in varying concentrations of HA hydrogel. Left: representative Western blots of LC3B and histone H3, which is used as a normalization factor. LC3B is detected as a double band, with the top band representing an 'inactive' form and the bottom band representing a post-translationally modified active form found in autophagic membranes. Right: LC3B-II content normalized to histone H3 content of cells cultured for 3 days in HA hydrogels of varying concentration. No significant differences were found between conditions, as determined with one-way ANOVA.

The final protein I assayed, and the final effector protein in the Akt-mTOR pathway is S6K. This ribosomal protein is used as a marker for mTOR activity, being its main substrate for phosphorylation. It is an indicator for cell growth and proliferation. I found that S6K activation in PC3 cells after 3 days of culture in the 2% hydrogel environment was significantly higher than that in the control condition, as illustrated in Figure 22. This is an interesting outcome, as all prior data would suggest that S6K activity would decrease or be the same as the control condition. Likely what is happening, since this data represents 3 days of culture in the hydrogel environment, is that S6K activation is having a negative feedback effect on Akt, thus decreasing its activation levels. Meanwhile, this feedback likely has not permeated back down the signal cascade to affect S6K itself. Another possibility is that the upregulated HIF-1 expression is driving protein synthesis and thus activating S6K.

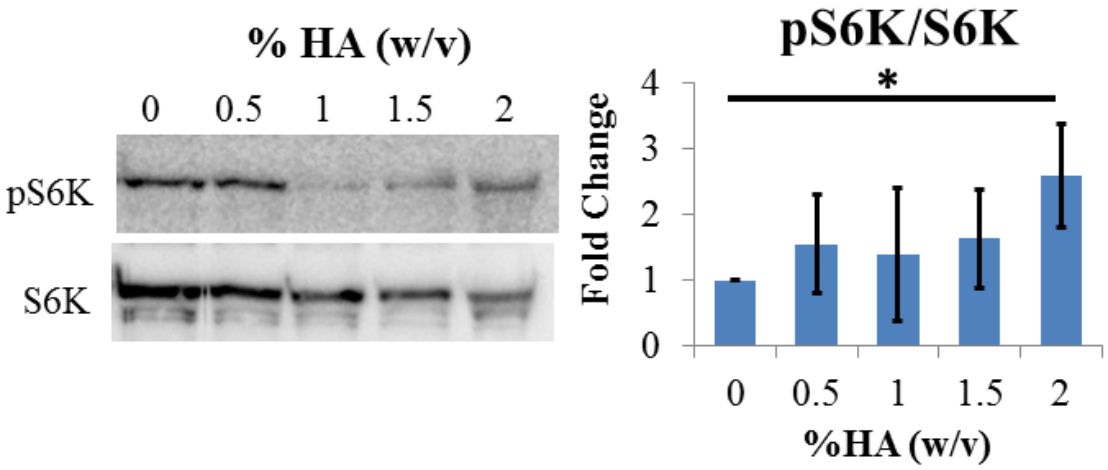

Figure 22, S6K activation in PC3 cells cultured in varying concentrations of HA hydrogel. Left: representative Western blot of phospho-S6K and whole S6K protein content. Right: ratio of phosphor-S6K to whole S6K content. A one-way ANOVA F-test did not find significant differences between hydrogel concentrations, but the 2% condition was found to be significantly different from the control via Student's T-test, $p<0.05$, as indicated by *. Error bars represent standard deviation.

5.2. Materials and Methods

5.2.1. ATP Content Assay

Similar to the procedures described in Sections 4.2.2 and 4.2.3, PC3 cells were cultured in monolayer with 0.5%, 1%, 1.5%, and 2% w/v HA hydrogels. The control condition consisted of PC3 cells cultured in standard monolayer format with liquid culture media only. After one and three days of culture, plates of cells were placed on ice and 40µL of a solution of 0.2g/mL DTT was pipetted into each well. The DTT solution loosened up the hydrogels and allowed them to be gently removed using a standard handheld pipette or plastic transfer pipette, taking care not to disturb the cells underneath. CellTiter-Glo Cell Viability Assay reagent was then immediately added to the cells and the cells were mechanically broken up by scraping and pipetting up and down. Luminescence was then measured using a Filtermax F5 Microplate Reader. Parallel to these experiments, cell lysates were obtained and used for Western blot, as will be described in Section 5.2.3. Blots were probed for histone H3, and protein content was analyzed with densitometry. Using histone H3 content as a measure of cell density, CellTiter-Glo data was normalized to the amount of histone H3 protein per well to obtain average ATP content per cell.

5.2.2. Endpoint Reverse Transcriptase PCR Analysis

PC3 cells were cultured in 0.5%, 1%, 1.5%, and 2% HA hydrogels, as well as the control condition of liquid culture medium. After three days of culture, plates were put on ice and hydrogels were removed from each well, as described earlier. Cellular RNA was extracted using the Aurum Total RNA Mini Kit (Bio-Rad). Briefly, cells were lysed in lysis buffer and lysates were spun through RNA-binding columns with a microcentrifuge. After washing with the provided wash buffer, contaminating genomic DNA was removed via incubation with DNAse. The columns were washed thoroughly and the RNA was eluted using the provided elution buffer.

RNA content of each sample was determined using a SPECTROstar Nano Microplate reader. RNA samples were aliquoted into RNAse-/DNAse-free PCR strip tubes, diluting each sample with

diethyl pyrocarbonate (DEPC) treated water to obtain equal RNA content in each tube with a final volume of 16µL. For the reverse transcriptase reaction, I used qScript cDNA SuperMix (QuantaBio), making cDNA from the collected RNA. Briefly, 4µL of the 5x concentration SuperMix was added to each well, with a final volume of 20µL. Strip tubes were placed into a T100 Thermal Cycler (Bio-Rad) for the following reverse transcriptase reaction cycle: 5min at 25°C, 20min at 46°C, and 1min at 95°C. Strip tubes were removed and placed back on ice to add PCR reagents. PCR primer sequences (Invitrogen) are as follows,

HMBS-forward: 5'-AAGTGCGAGCCAAGGACCAG-3',

HMBS-reverse: 5'-TTACGAGCAGTGATGCCTACCAAC-3'

HIF1A-forward: 5′-CATAAAGTCTGCAACATGGAAGGT-3′

HIF1A-reverse: 5′-ATTTGATGGGTGAGGAATGGGTT-3′

Primers were reconstituted in DEPC-treated water according to the volumes provided by the manufacturer for a primer concentration of 100µM. For a reaction of 20 samples, a mix was made of the following reagents for PCR: 100µL OneTaq reaction buffer, 10µL dNTPs, 2.5µL OneTaq DNA polymerase (New England Biolabs), 1µL forward HIF1A RNA primer, 1µL reverse HIF1A RNA primer, 1µL forward HMBS RNA primer, 1µL reverse HMBS RNA primer, 16µL DEPC-treated water. Each sample received 5µL of the above mix and was placed into the thermal cycler for the following incubation cycle: 1min at 94°C, 2min at 55°C, and 3min at 72°C for 40 cycles.

A solution of 1.6% w/v agarose was made by dissolving 0.64g agarose (Amresco) in 39.4mL Tris-acetate-EDTA (TAE) buffer. The solution was heated in a microwave until melted and homogeneous, and 4µL SYBR Safe DNA Gel Stain (Fisher) was added. The agarose was cast in a DNA electrophoresis gel mould (Bio-Rad) with a 15-well comb. PCR products were run in the gel on a horizontal electrophoresis system (Bio-Rad) for one hour at 100V. Gels were then visualized with blue epifluorescence on an Azure c300 imaging system (Azure Biosystems).

5.2.3. Western Blot Analysis

Cells were cultured, as mentioned, under 80μL of 0.5%, 1%, 1.5%, and 2% HA hydrogels over three days in a standard 96-well plate. The control condition consisted of a standard monolayer culture with liquid culture medium only. After 1 and 3 days of culture, plates were placed on ice and hydrogels were treated with 40μL of 0.2g/mL DTT to loosen up the hydrogels. Hydrogels were removed with a handheld pipette or a plastic transfer pipette. Because of the use of DTT and the mechanical disturbance from hydrogel removal, I decided to not rinse the cells with PBS prior to lysis to prevent loss of sample content. Cells were lysed in radio-immunoprecipitation assay (RIPA) buffer, 10μL per well. Cells were mechanically broken up by scraping and pipetting up and down. Lysates from each conditioned were pooled together and aliquoted into 40μL volumes in PCR strip tubes. Because the cells were not washed with PBS prior to lysis, there was likely contamination of lysates with serum proteins derived from culture media. Thus, normalization of protein content by Bradford assay was not possible.

Cell lysates were mixed at a 1:1 ratio with 2x Laemmli SDS-PAGE sample buffer with 355mM β-mercaptoethanol. Samples were incubated in a T100 Thermal Cycler (Bio-Rad) for 5 minutes at 100°C to denature the proteins. Samples were then run on 4-20% gradient polyacrylamide gels for 1 hour at 100V, then 30 minutes at 200V using a Mini-PROTEAN Tetra Cell system (Bio-Rad). Protein was then transferred onto PVDF membranes (Millipore Sigma) using a Mini Trans-Blot Cell system (Bio-Rad) running at 100V for 80 minutes. Blots were then

After transfer, blots were washed briefly in TBST and then blocked for 1 hour in 5% bovine serum albumin (BSA; Sigma-Aldrich). Primary antibodies were diluted 1:1000 in 1% BSA in TBST and added to blots to incubate overnight on a shaker table at 4°C. The primary antibodies used were all obtained from Cell Signaling Technologies and are as follows: phospho-Akt (Ser473) mouse monoclonal antibody (#12694), phospho-Akt (Thr308) rabbit monoclonal antibody (#4056), Akt rabbit antibody (#9272), p70 S6 Kinase rabbit antibody (#9202), phospho-p70 S6 Kinase (Thr389) rabbit antibody (#9205), phospho-AMPKα rabbit monoclonal antibody (#2535), AMPKα mouse monoclonal antibody

(#2793), and histone H3 rabbit antibody (#9715). The next day, blots were washed three times with TBST, 10 minutes per wash and then underwent secondary incubation for 1 hour with horseradish peroxidase (HRP) -conjugated secondary antibodies diluted 1:1000 in 1% BSA in TBST. The secondary antibodies used were anti-rabbit IgG HRP-conjugated antibody and anti-mouse IgG HRP-conjugated antibody (R&D Systems). After incubation, blots were washed three times in TBST, 10 minutes each wash. ECL Western Blot Substrate (Thermo Fisher) was then added to the blots and incubated for up to 5 minutes. Finally, the blots were visualized via chemiluminescence using an Azure c300 imaging system.

Blots were stripped with house-made acidic glycine stripping buffer, 3 washes of 25 minutes each, then washed in PBS twice for 20 minutes each, then in TBST for 10 minutes before blocking and re-probing. A pair of blots was done per replicate and probed in the following order: one of the two is probed for LC3B, then $pAkt^{S473}$, then $pAkt^{T308}$, then Akt, and finally histone H3; the other is probed for pS6K, then S6K, then pAMPK, then AMPK, and finally histone H3. The blotting order was determined based on strength of signal, strength of antibody binding, host species of antibody, and specifically so that whole proteins were only probed after phosphorylated proteins.

Densitometry was conducted on images of blots using ImageJ, measuring integrated pixel intensity. Protein levels were normalized per blot to the control condition to remove effects of exposure time and antibody avidity. Phosphorylated proteins were normalized to whole protein content to obtain protein activation. LC3B-II was normalized to histone H3 content because the antibody used preferentially bound to LC3B-II and the signal from LC3B-I could not be relied upon to provide accurate whole protein content.

5.3. Discussion

5.3.1. Cell Line Mutations

For this characterization of cell processes in hydrogel culture, I decided to focus on PC3 cells as a model prostate cancer cell line as opposed to working with LNCaP cells. While PC3 cells may not be

reflective of a common prostatic adenocarcinoma due to its similarities to a small cell carcinoma of the prostate, the Akt-mTOR signaling pathway remains entirely intact. In contrast, LNCaP cells express a number of mutations in the Akt-mTOR pathway that have the potential to decouple nutrient sensing from metabolic activity and cell survival.

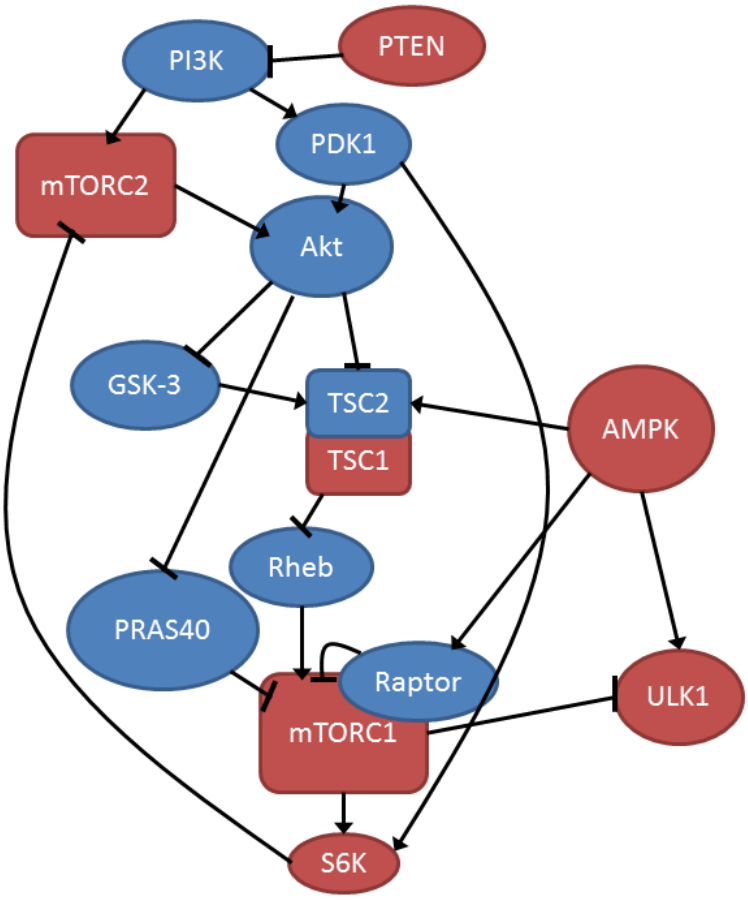

Figure 23, Known mutations in the Akt-mTOR pathway in LNCaP cells. Known mutations expressed by LNCaP cells are shown in red. These mutated elements of the Akt-mTOR pathway could affect nutrient sensing and metabolic activity and not all are well-characterized. Mutations were identified using the Broad Institute Cancer Cell Line Encyclopedia.

LNCaP cells would require more careful and in-depth analysis and interpretation of data due to the possibility of altered protein function. PC3 cells, however, provide a baseline model of metabolism under hydrogel culture.

5.3.2. Expression of HIF-1 in PC3 Cells

There is a caveat with the results of the endpoint PCR experiment, in that PC3 cells are known to overexpress HIF-1 (156). There is also the possibility that upstream signaling could be causing upregulation of HIF-1, downregulation of HMBS, or affecting the degradation of HIF1A mRNA degradation. Of particular interest is the activity of CD44, the main cell receptor for HA and an important marker for cancer cell stemness. Evidence exists of HIF-1 activity affecting CD44 expression and modulating phenotype expression (170,171), though it is unclear whether the reverse is true. Whatever the cause, the data show quite clearly that cells cultured in 2% hydrogels have a significantly higher HIF1A mRNA to HMBS mRNA ratio compared to lower concentration hydrogels and particularly cells cultured in liquid media. This would suggest some relation to the material environment.

5.3.3. S6K Activation amidst Metabolic Stress

Western blot analysis showed that the ratio of pS6K to S6K is higher in cells cultured in 2% HA hydrogels than cells in the control. It is possible, because the antibody signal for S6K content was quite weak, that this is an effect of over-inflation from normalization. The consistency across replicates suggests this is unlikely, however. The lack of a trend and statistical significance with lower hydrogel concentrations is also not surprising, given that it is only in the 2% hydrogel condition that any effect is observed in HIF1A expression and cell viability.

Looking at the data as a whole, it appears the cell death seen in my cell viability experiments is correlated with HIF1A mRNA expression and increased S6K activation despite a lack of significant increase in Akt activity. It is possible that the material environment is directly responsible for both HIF-1 expression and S6K activation, either at once or sequentially. Hypoxia could be driving HIF-1 activity, subsequently leading to S6K activation in a hypoxic response. Cell receptor binding to HA could also have an effect on downstream metabolic activity. Previous studies have reported that CD44, the main cell receptor for HA can enhance glycolytic metabolism in cancer cells (172,173) and CD44 signaling could

affect HIF-1 via NF-κB (130). Finally, the fact that Akt activity did not match up with S6K activity could be the result of decoupling of the Akt-mTOR pathway due to cancer cell mutations. No genes directly involved in the pathway are known to be mutated in PC3 cells, but other genes encoding for adjacent elements could be feeding into the network, bypassing Akt entirely. More work would have to be done to analyze elements upstream of this pathway in more detail. Another possibility is simply the difficulty in obtaining reliable quantitative data from Western blot analysis due to the nature of variable lysate concentrations, antibody binding, and exposure times for obtaining images of blots. While the Akt data shows no significant activation across conditions, it does appear that the hydrogel conditions have higher Akt activity than the control, albeit with high variability. This variability could be a result of differences in initial cell seeding densities between replicates, variabilities in the hydrogel material, or quality of Western blot.

The results from my experiments appear to support the idea that cell metabolic activity is ramping up, or at the very least not decreasing despite adverse growth conditions. It is possible that this metabolic activity is compensatory as cell components are broken down through autophagy or in preparation of proteins and enzymes required for protein scavenging. Perhaps in combination with hypoxia, limited nutrient availability, and environmental acidification from glycolysis, the upregulation of S6K activity caused cells to use up already limited resources and eventually die from metabolic stress. The adverse growth conditions imposed by the 2% HA hydrogel environment has another effect that would not be immediately detectable – hypoxia and limited access to nutrients could be selecting for hardier and more resistant cell types. This could drive cancer cell evolution and generate more aggressive populations of metastatic cells. Indeed, the cell death observed and the increase in S6K activity could be related in that once weaker cells in the population had died off, the cells leftover were more capable of growth and proliferation under adverse conditions.

Chapter 6. Conclusion

6.1. Future Directions

6.1.1. From 2D to 3D

All of the experiments using HA hydrogels discussed have been done on "2.5D" models of prostate cancer tissue – that is, cells are grown in a monolayer culture, but with an ECM-mimicking material overlaid on top. Ideally, this ECM-mimicking material would minimize cell polarization and provide ECM attachment sites that would allow upwards growth and migration of cells into the material. In practice, I never observed upwards growth or invasion of cells into the HA hydrogels. For the most part, cells expressed the spread-out spindle-like or cobblestone-like morphology of adherent cells attached to a stiff TCPS surface. Because of this, I have been able to obtain baseline data of how the material properties of HA hydrogels affect cells grown under 2D conditions. This provides a basis for comparison with cells grown in 3D culture conditions, allowing the study of how 3D orientation can influence cell behaviour.

I have had the chance to conduct pilot experiments growing spheroids in an HA hydrogel environment. As was observed in Section 4.2.2 and discussed in Section 4.3.2, HA hydrogels appear to provide a non- or weakly-adherent environment that would support the development of spheroids. I found, however, that the very soft material caused cells seeded on top to form scattered aggregates with variable shapes and sizes. In contrast, cells grown on stiffer but still non-adherent materials like agarose, as in the liquid overlay method of generating spheroid cultures tend to coalesce and form large single spheroids, as seen in Figure 24. This allows the generation of uniform spheroid cultures, minimizing variability due to cell density and geometry of aggregation. By using an agarose-HA hydrogel "sandwich" culture system, cells can be grown in a 3D, tissue border-mimicking environment, which would allow the study of how cells interact with ECM environments of different composition, as would be found at the border of a solid tumour.

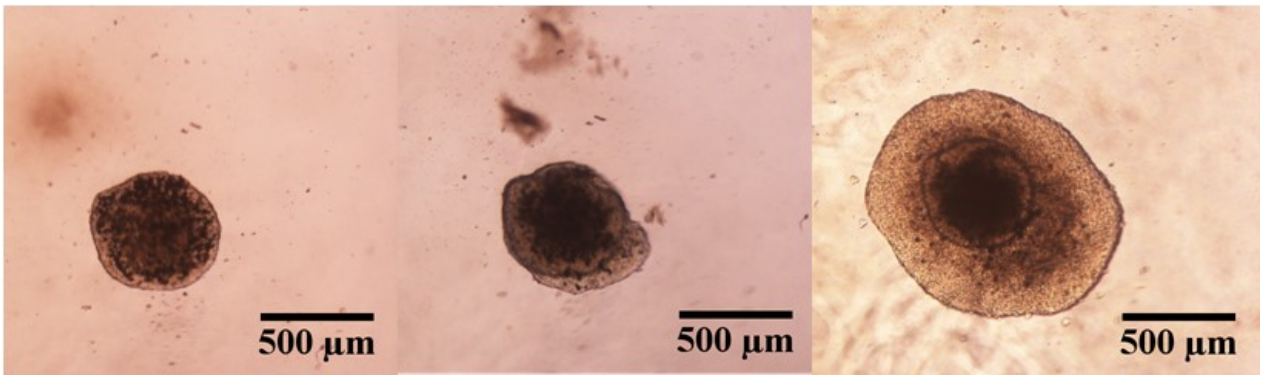

Figure 24, Spheroids grown in agarose-HA hydrogel sandwich culture. LNCaP cells were seeded at a density of 12000 cells/well into the wells of a U-bottom 96-well plate that were coated with 30µL 1% SeaPlaque™ agarose (Lonza) dissolved in PBS. After allowing cells to aggregate overnight, 1% w/v HA hydrogel solutions were mixed, as described previously and added on top. Images are of the same spheroid, corresponding to 6 (left), 10 (middle), and 15 (right) days of culture. Cells were observed to initially condense and form a round spheroid structure after aggregating. Growth of the spheroid after addition of the hydrogel occurred at the edge of the spheroid, growing flat and outwards as opposed to evenly around the spheroid. This suggests that the cells were not able to penetrate the hydrogel, instead growing along the border between the agarose and HA.

The ability to generate uniform spheroids is important for replicability as well as the translation of standard assays developed for 2D cell culture systems to 3D applications.

An advantage of using this tissue ECM-mimicking HA hydrogel material for 3D cultures is the relative ease of fixing and handling spheroid constructs for imaging. Without the hydrogel material, spheroids can easily be lost during liquid handling. During initial experimentation, I found that spheroids in HA hydrogels could easily be fixed with standard paraformaldehyde fixing procedures and could be treated like tissue samples. The HA material was further crosslinked by formaldehyde, making the sample mechanically robust and preventing the loss of the spheroid during liquid handling. The sample could easily be moved around using gentle suction with a plastic transfer pipette and could be sectioned for immunohistochemistry. Immunostaining would need to be optimized for this procedure, especially given that the HA hydrogel has limited protein penetrance.

6.1.2. ECM Additives

Because this HA hydrogel material is well-defined in chemical composition and has non-adherent properties in cell culture, this material would make a good "background" material for the addition of other ECM components. This would allow bottom-up construction of tissue-specific, ECM-mimicking environments based on the addition of materials such as collagen IV and laminin for basement membrane, collagen I and elastin for fibrous tissues, or tenascin and neurocan for brain tissues (174). Especially with the relative ease in preparing uniform 3D sandwich cultures, this platform has potential for use in studying 3D cell-ECM interactions.

6.1.3. Comparing Cell Types

While I have done some work comparing the viability of LNCaP model prostate cancer cells with PC3 cells cultured in HA hydrogels, it would be interesting to further characterize the metabolic activities of both cell lines in light of their different mutations. This can be expanded to include other cell lines with different characterized mutations and levels of malignancy, such as benign prostatic hyperplasia or DU145. Cells with different mutations would likely have different ways of dealing with the lack of nutrients and diffusive environment imposed by the HA hydrogels. Signaling from ECM ligand binding, such as the interaction between CD44 and HA, as well as downstream transduction would also vary across cell lines, especially when such signaling pathways are often restructured from mutational load. Understanding how these differences might contribute to invasiveness, cancer cell dormancy, chemoresistance, and recurrence would provide better understanding of patient-specific disease outcomes. Ultimately, work with primary cells derived from prostate cancer patients would provide the most realistic model of prostate cancer cell behaviour in different ECM environments. While variability with primary cells is much greater, this variability could be an advantage in better understanding the interplay of cell genotype and phenotype within the context of external environmental cues.

6.1.4. HA Hydrogels as Surgical Filler

With the observed limitations on mass transfer, there is potential use of this material as a surgical filler for use after prostatectomy or brachytherapy to treat prostate cancer. This HA hydrogel could be used to smother remaining tumour tissue to help slow or stop recurrent cancer growth. Though I have not observed any evidence of cell invasion in the material, further testing would have to be done to confirm this. As well, it would need to be able to prevent invasion of endothelial cells and angiogenesis in order to starve cancer cells and prevent recurrence. This can be studied with a modified invasion assay to test whether cells are able to penetrate the gel in response to a chemokine gradient. The sequestration observed in the material is also promising, as it would prevent soluble factors released by cancer cells from getting into surrounding tissues. One issue that may arise would be the possible expression of hyaluronidase by cancer cells or surrounding stromal cells, which would compromise the HA material and lead to degradation.

6.2. Limitations of HA Hydrogels

What is still not well-characterized for this HA hydrogel material is the structure of the hydrogel matrix. While the overall effects of HA chain organization may not be entirely relevant in terms of diffusion and mass transfer, as discussed in Chapter Chapter 4, there may be some unknown effects on cells cultured in hydrogel environments, especially in light of CD44 signaling. Study of matrix geometry would be challenging. The material would not lend well to scanning electron microscopy, since it would require specialized drying and fixing procedures to prevent major structural changes in matrix geometry. Regardless, comparisons between HA gels of different concentrations or hydrogels formed through different methods could provide interesting qualitative information on matrix geometry. Atomic force microscopy, on the other hand, may provide some information on surface characteristics, though the low HA content actually used to make the hydrogels might be problematic. It is not well understood how

unmodified HA molecules orient in solution, whether as globules or an amorphous lattice network, for example, so it is not well understood how crosslinking would affect molecular structure.

Bottom-up ECM production and 3D scaffold cultures in general are limited by the inability to recreate *in vivo* conditions of ECM structure and organization. Natural ECM organization can result in localized enrichment of certain components or context-specific presentation of cell receptor ligands. Because ECM is naturally laid down and remodeled by cells in a dynamic nanometre-scale process throughout organ and tissue development, it is very difficult to recreate this level of complexity *in vitro*. This must be taken into consideration with any reconstituted ECM material or ECM-mimicking culture environment, even with complex products like Matrigel. For the HA hydrogel specifically, it is unlikely that the disulfide crosslinking would accurately model how HA is naturally coupled to other ECM components, especially given the size of the DTP crosslink compared to HA-binding proteins like versican or fibronectin. As well, HA-specific binding regions on such proteoglycans likely leave specific free-hanging regions of the HA molecule for cell receptor binding and material sequestration, which would not be represented by the fairly non-specific carbodiimide-hydrazide displacement reaction that couples DTP to HA carboxyl groups. There is also evidence that chemical modification of HA, specifically the conjugation of thiol groups could interfere with cell signaling via CD44 (175). This would lead to the loss of binding motifs that might contribute to cell signaling and motility, which could explain why cells do not seem to be growing into or invading the hydrogel material.

6.3. Is the Future of Cancer Research 3D?

More and more, empirical evidence shows that 2D cell culture models are unable to fully recapitulate the cellular interactions involved in prostate cancer development and progression. Unfortunately, widespread adoption of 3D cell culture models in cancer research remains elusive due to issues of accessibility and replicability. It is important as a designer of a cell culture platform to address the feasibility of using a platform as a general life science researcher.

A general life science lab may not have specialized chemical processing equipment required for in-house generation of cell culture materials. Purchase of commercially-available products may not be a popular option unless that product has been shown to yield scientifically interesting and unique results, as in the case of Matrigel, which is popular as a bio-active substrate that can direct cell organization. Disulfide crosslinked HA hydrogels are also available commercially with the optional addition of other functionalized ECM-derivatives, growth factors, and synthetic polymers (HyStem, Millipore Sigma). The draw of this product is its customizability and versatility in the culture of numerous cell types. Thus, the worth of a cell culture material is closely related to the balance of accessibility and functionality. Simply from a production standpoint, I have shown that disulfide-crosslinked HA hydrogels are a viable option for in-house synthesis, though access to a freeze dryer is required. I have also demonstrated unique material properties of the hydrogel material that could be exploited to model certain tissue characteristics. There is potential to use this material in 3D culture platforms and in combination with other materials as an interpenetrating network of ECM components. On its own, this material is unlikely to be accurately representative of native ECM structure and its use is also limited by its mass transfer properties, which may be problematic for long term cell culture. This hydrogel should only be used up to 1% w/v concentration as a model cell culture environment to avoid the more dramatic effects of limited mass transfer of nutrients leading to starvation that was seen with higher concentration hydrogels. This material would likely be more effective as an ECM-mimicking environment if other ECM components were added to better simulate the mechanical as well as biochemical properties of real tissues.

A major challenge in using 3D cell culture platforms is translating experimental procedures optimized for 2D cell culture for use on 3D cell constructs. Imaging is often a challenge, especially given the opacity of 3D specimens and the difficulty of confocal imaging in a high-throughput capacity. For assays requiring the collection of cell lysates, scaffold materials can contaminate samples or clog up columns and gels used for separating and purifying cell contents. Optimization of experimental procedures has to be done on a per-experiment basis and often comes with extended troubleshooting. With pilot experiments using 3D cell constructs embedded in HA hydrogels, I have successfully fixed and

mounted samples for microscopy, though antibody staining requires more work due to possible entrapment of antibodies in the HA and non-specific binding to the sample. The hydrogel material can also be removed by solubilizing it with a DTT solution, making the collection of lysates much easier. Unfortunately, some experimental measures have to be replaced with indirect methods of quantification due to challenges in obtaining data. An example of this is cell count for spheroids, which technically can be done directly, but requires prior trypsinization and dissociation of cells, which could result in loss of cells and underestimation. Proxies I have previously used for normalization include histone H3 content, whole DNA content, and genes or proteins that have been previously shown to be metabolically stable. I have shown that many standard assays can be reworked to function with 3D culture models, but more work needs to be done to show that this is a viable platform that can work with other experimental procedures.

Another challenge in the adoption of 3D culture models is the lack of standardization and control of existing culture techniques. A wide variety of culture models exist, from scaffold cultures to spherical cultures and beyond. It is often difficult to directly compare experimental results between studies in literature because of the many confounding factors that could affect experimental outcomes. As mentioned previously, cell seeding density in scaffold culture models can override the effects of matrix-derived cell signaling via autocrine and paracrine signaling. In spherical models, variable geometry can greatly affect access to nutrients and diffusion gradients. Variability in material composition, differences in model cell types used, manufacturing processes, and methods for material and cell characterization all result in context-specific results in 3D culture models that cannot be directly compared across studies. There is even much variability in terminology and definitions used, especially in terms of the words “organoid” and “spheroid.” For more widespread adoption of 3D cell culture models, more work needs to be done to compare culture environments and standardize biological assays across different 3D platforms.

In short, 3D cell culture is an exciting way to improve the study of cells in life-like conditions, but it is unlikely that these models will be completely replacing 2D models in the near future. While cells in 2D environments may not accurately reflect *in vivo* cell behaviour, their physiological relevance is far

outweighed by the simplicity and standardization of their use. Improvements in 3D culture models need to be matched by improvements in experimental procedures like imaging technology and protein assay. Furthermore, comparisons of 3D cell culture systems would help in the standardization of experimental procedures and provide better understanding of the different confounding effects of culture environments on experimental results. In the end, the distinction between 2D and 3D cell culture models is not dichotomous; a variety of culture models exists that can be used for the study of biological processes in any kind of environment, physiological or not.

6.4. Final Remarks

Disulfide-crosslinked HA hydrogels are an interesting material that has potential to be used as a model cell culture environment for the study of prostate cancer cells. Diffusion and mass transfer in the material represent unique material characteristics that can be exploited to recreate a tissue environment with limited nutrient access, such as the inside of a prostate tumour. Isolation of cultured cells from liquid media by the hydrogel environment prevents perturbation by fluid flow and bulk mixing, allowing short-to-medium term culture of cells in a tissue-mimicking environment. Study of PC3 model prostate cancer cells cultured in hydrogels reveals interesting metabolic activity despite low energy content, hypoxic stress, and limited access to nutrients. Further study into cell energetics and metabolic pathways would be required to fully understand how prostate cancer cells respond to such an environment and whether such environmental conditions can contribute to cancer malignancy, dormancy, or recurrence.

Importantly, the study and characterization of this material for use as a culture environment will hopefully help with the adoption of 3D cell culture models in general in prostate cancer research. In order to better understand why cancer cells behave the way they do, cancer cell culture models need to be able to recreate the environmental conditions in which cancer cells grow and invade. Understanding the context in which cancer cells behave will allow better understanding of why they do so.

References

1. Canadian Cancer Society's Advisory Committee on Cancer Statistics. Canadian Cancer Statistics 2017 [Internet]. Canadian Cancer Society. 2017. Available from: cancer.ca/Canadian-CancerStatistics-2017-EN.pdf
2. Grönberg H. Prostate cancer epidemiology. Lancet [Internet]. 2003 Mar 8 [cited 2020 Jan 6];361(9360):859–64. Available from: https://www.sciencedirect.com/science/article/pii/S0140673603127134
3. Roehrborn C, Black L. The economic burden of prostate cancer. BJU Int [Internet]. 2011 Aug 25;108(6):806–13. Available from: https://doi.org/10.1111/j.1464-410X.2011.10365.x
4. Lin DW, Porter M, Montgomery B. Treatment and survival outcomes in young men diagnosed with prostate cancer. Cancer [Internet]. 2009 Jul 1;115(13):2863–71. Available from: https://doi.org/10.1002/cncr.24324
5. Salinas CA, Tsodikov A, Ishak-Howard M, Cooney KA. Prostate cancer in young men: an important clinical entity. Nat Rev Urol [Internet]. 2014;11(6):317–23. Available from: https://doi.org/10.1038/nrurol.2014.91
6. Briganti A, Suardi N, Gallina A, Abdollah F, Novara G, Ficarra V, et al. Predicting the risk of bone metastasis in prostate cancer. Cancer Treat Rev [Internet]. 2014 Feb 1;40(1):3–11. Available from: http://dx.doi.org/10.1016/j.ctrv.2013.07.001
7. Tabesh A, Teverovskiy M, Pang H, Kumar VP, Verbel D, Kotsianti A, et al. Multifeature Prostate Cancer Diagnosis and Gleason Grading of Histological Images. IEEE Trans Med Imaging. 2007;26(10):1366–78.
8. Stamey TA, McNeal JE, Yemoto CM, Sigal BM, Johnstone IM. Biological Determinants of Cancer Progression in Men With Prostate Cancer. JAMA [Internet]. 1999 Apr 21;281(15):1395–400. Available from: https://doi.org/10.1001/jama.281.15.1395

9. Lalonde E, Ishkanian AS, Sykes J, Fraser M, Ross-Adams H, Erho N, et al. Tumour genomic and microenvironmental heterogeneity for integrated prediction of 5-year biochemical recurrence of prostate cancer: a retrospective cohort study. Lancet Oncol [Internet]. 2014 Dec 1 [cited 2018 May 3];15(13):1521–32. Available from: https://www.sciencedirect.com/science/article/pii/S1470204514710216

10. Velonas VM, Woo HH, dos Remedios CG, Assinder SJ. Current status of biomarkers for prostate cancer. Int J Mol Sci. 2013;14(6):11034–60.

11. Oellerich M, Schütz E, Beck J, Kanzow P, Plowman PN, Weiss GJ, et al. Using circulating cell-free DNA to monitor personalized cancer therapy. Crit Rev Clin Lab Sci [Internet]. 2017 Apr 3;54(3):205–18. Available from: https://doi.org/10.1080/10408363.2017.1299683

12. Boutros PC, Fraser M, Harding NJ, de Borja R, Trudel D, Lalonde E, et al. Spatial genomic heterogeneity within localized, multifocal prostate cancer. Nat Genet [Internet]. 2015;47(7):736–45. Available from: https://doi.org/10.1038/ng.3315

13. Screening for prostate cancer: U.S. preventive services task force recommendation statement. Ann Intern Med [Internet]. 2012 Jul 17;157(2):120–34. Available from: http://dx.doi.org/10.7326/0003-4819-157-2-201207170-00459

14. Gallaher J, Cook LM, Gupta S, Araujo A, Dhillon J, Park JY, et al. Improving treatment strategies for patients with metastatic castrate resistant prostate cancer through personalized computational modeling. Clin Exp Metastasis [Internet]. 2014;31(8):991–9. Available from: https://doi.org/10.1007/s10585-014-9674-1

15. Kogan Y, Halevi–Tobias K, Elishmereni M, Vuk-Pavlović S, Agur Z. Reconsidering the Paradigm of Cancer Immunotherapy by Computationally Aided Real-time Personalization. Cancer Res [Internet]. 2012 May 1;72(9):2218 LP – 2227. Available from: http://cancerres.aacrjournals.org/content/72/9/2218.abstract

16. Noguchi M, Moriya F, Suekane S, Ohnishi R, Matsueda S, Sasada T, et al. A phase II trial of personalized peptide vaccination in castration-resistant prostate cancer patients: prolongation of prostate-specific antigen doubling time. BMC Cancer [Internet]. 2013;13(1):613. Available from: https://doi.org/10.1186/1471-2407-13-613

17. Arora K, Barbieri CE. Molecular Subtypes of Prostate Cancer. Curr Oncol Rep. 2018;20(8).

18. Tomlins SA, Rhodes DR, Perner S, Dhanasekaran SM, Mehra R, Sun X-W, et al. Recurrent Fusion of TMPRSS2 and ETS Transcription Factor Genes in Prostate Cancer. Science (80-) [Internet]. 2005 Oct 28;310(5748):644 LP – 648. Available from: http://science.sciencemag.org/content/310/5748/644.abstract

19. Abeshouse A, Ahn J, Akbani R, Ally A, Amin S, Andry CD, et al. The Molecular Taxonomy of Primary Prostate Cancer. Cell [Internet]. 2015 Nov 5 [cited 2018 May 3];163(4):1011–25. Available from: https://www.sciencedirect.com/science/article/pii/S0092867415013392#bib20

20. Ramaswamy S, Nakamura N, Vazquez F, Batt DB, Perera S, Roberts TM, et al. Regulation of G1 progression by the PTEN tumor suppressor protein is linked to inhibition of the phosphatidylinositol 3-kinase/Akt pathway. Proc Natl Acad Sci [Internet]. 1999 Mar 2;96(5):2110 LP – 2115. Available from: http://www.pnas.org/content/96/5/2110.abstract

21. Levine AJ, Momand J, Finlay CA. The p53 tumour suppressor gene. Nature [Internet]. 1991;351(6326):453–6. Available from: https://doi.org/10.1038/351453a0

22. Barbieri CE, Baca SC, Lawrence MS, Demichelis F, Blattner M, Theurillat J-P, et al. Exome sequencing identifies recurrent SPOP, FOXA1 and MED12 mutations in prostate cancer. Nat Genet [Internet]. 2012;44(6):685–9. Available from: https://doi.org/10.1038/ng.2279

23. Allott EH, Masko EM, Freedland SJ. Obesity and Prostate Cancer: Weighing the Evidence. Eur Urol [Internet]. 2013 May 1 [cited 2020 Jan 13];63(5):800–9. Available from: https://www.sciencedirect.com/science/article/pii/S0302283812013449

24. Assel MJ, Gerdtsson A, Thorek DLJ, Carlsson S V, Malm J, Scardino PT, et al. Long-term prediction of prostate cancer diagnosis and death using PSA and obesity related anthropometrics at early middle age: data from the malmö preventive project. Oncotarget [Internet]. 2018 Jan 19;9(5):5778–85. Available from: http://www.ncbi.nlm.nih.gov/pmc/articles/PMC5814173/

25. Crewe C, An YA, Scherer PE. The ominous triad of adipose tissue dysfunction: inflammation, fibrosis, and impaired angiogenesis. J Clin Invest [Internet]. 2017/01/03. 2017 Jan 3;127(1):74–82. Available from: https://www.ncbi.nlm.nih.gov/pubmed/28045400

26. Jung UJ, Choi M-S. Obesity and Its Metabolic Complications: The Role of Adipokines and the Relationship between Obesity, Inflammation, Insulin Resistance, Dyslipidemia and Nonalcoholic Fatty Liver Disease. Int J Mol Sci [Internet]. 2014;15(4):6184–223. Available from: https://www.mdpi.com/1422-0067/15/4/6184

27. Sundaram S, Freemerman AJ, Johnson AR, Milner JJ, McNaughton KK, Galanko JA, et al. Role of HGF in obesity-associated tumorigenesis: C3(1)-TAg mice as a model for human basal-like breast cancer. Breast Cancer Res Treat [Internet]. 2013/11/12. 2013 Dec;142(3):489–503. Available from: https://www.ncbi.nlm.nih.gov/pubmed/24218051

28. Quail DF, Dannenberg AJ. The obese adipose tissue microenvironment in cancer development and progression. Nat Rev Endocrinol [Internet]. 2019;15(3):139–54. Available from: https://doi.org/10.1038/s41574-018-0126-x

29. León J, Sáenz JM, Artacho-Cordón F, Fernández MF, Martin-Olmedo P, Salamanca-Fernández E, et al. Contribution of sociodemographic, occupational, lifestyle and dietary characteristics to the oxidative stress microenvironment in adipose tissue. Environ Res [Internet]. 2019 Aug 1 [cited 2020 Jan 13];175:52–62. Available from: https://www.sciencedirect.com/science/article/pii/S0013935119302518

30. Kumar B, Koul S, Khandrika L, Meacham RB, Koul HK. Oxidative Stress Is Inherent in Prostate Cancer Cells and Is Required for Aggressive Phenotype. Cancer Res [Internet]. 2008 Mar 15;68(6):1777 LP – 1785. Available from: http://cancerres.aacrjournals.org/content/68/6/1777.abstract

31. Fiaschi T, Chiarugi P. Oxidative stress, tumor microenvironment, and metabolic reprogramming: A diabolic liaison. Int J Cell Biol. 2012;2012.

32. Bavik C, Coleman I, Dean JP, Knudsen B, Plymate S, Nelson PS. The Gene Expression Program of Prostate Fibroblast Senescence Modulates Neoplastic Epithelial Cell Proliferation through Paracrine Mechanisms. Cancer Res [Internet]. 2006 Jan 15;66(2):794 LP – 802. Available from: http://cancerres.aacrjournals.org/content/66/2/794.abstract

33. Bissell MJ, Hines WC. Why don't we get more cancer? A proposed role of the microenvironment in restraining cancer progression. Nat Med. 2011;17(3):320–9.

34. Frantz C, Stewart KM, Weaver VM. The extracellular matrix at a glance. J Cell Sci. 2010;123(24):4195–200.

35. Wierzbicka-Patynowski I, Schwarzbauer JE. The ins and outs of fibronectin matrix assembly. J Cell Sci. 2003;116(16):3269–76.

36. Orgel JPRO, San Antonio JD, Antipova O. Molecular and structural mapping of collagen fibril interactions. Connect Tissue Res [Internet]. 2011 Feb 1;52(1):2–17. Available from: https://doi.org/10.3109/03008207.2010.511353

37. Wang Z, Chen J-Q, Liu J, Tian L. Exosomes in tumor microenvironment: novel transporters and biomarkers. J Transl Med [Internet]. 2016;14(1):297. Available from: https://doi.org/10.1186/s12967-016-1056-9

38. Vlodavsky I, Folkman J, Sullivan R, Fridman R, Ishai-Michaeli R, Sasse J, et al. Endothelial cell-derived basic fibroblast growth factor: synthesis and deposition into subendothelial extracellular matrix. Proc Natl Acad Sci [Internet]. 1987 Apr 1;84(8):2292 LP – 2296. Available from: http://www.pnas.org/content/84/8/2292.abstract

39. Fornaro M, Plescia J, Chheang S, Tallini G, Zhu YM, King M, et al. Fibronectin Protects Prostate Cancer Cells from Tumor Necrosis Factor-α-induced Apoptosis via the AKT/Survivin Pathway. J Biol Chem. 2003;278(50):50402–11.

40. Bini E, Foo CWP, Huang J, Karageorgiou V, Kitchel B, Kaplan DL. RGD-Functionalized Bioengineered Spider Dragline Silk Biomaterial. Biomacromolecules [Internet]. 2006 Nov 1;7(11):3139–45. Available from: https://doi.org/10.1021/bm0607877

41. Hersel U, Dahmen C, Kessler H. RGD modified polymers: biomaterials for stimulated cell adhesion and beyond. Biomaterials [Internet]. 2003;24(24):4385–415. Available from: http://www.sciencedirect.com/science/article/pii/S0142961203003430

42. Baker BM, Trappmann B, Wang WY, Sakar MS, Kim IL, Shenoy VB, et al. Cell-mediated fibre recruitment drives extracellular matrix mechanosensing in engineered fibrillar microenvironments. Nat Mater. 2015;14(12):1262–8.

43. Farahani E, Patra HK, Jangamreddy JR, Rashedi I, Kawalec M, Rao Pariti RK, et al. Cell adhesion molecules and their relation to (cancer) cell stemness. Carcinogenesis. 2014;35(4):747–59.

44. Chen H, Qu J, Huang X, Kurundkar A, Zhu L, Yang N, et al. Mechanosensing by the α6-integrin confers an invasive fibroblast phenotype and mediates lung fibrosis. Nat Commun [Internet]. 2016;7(1):12564. Available from: https://doi.org/10.1038/ncomms12564

45. Moroz A, Delella FK, Lacorte LM, Deffune E, Felisbino SL. Fibronectin induces MMP2 expression in human prostate cancer cells. Biochem Biophys Res Commun [Internet]. 2013;430(4):1319–21. Available from: http://dx.doi.org/10.1016/j.bbrc.2012.12.031

46. Arpino V, Brock M, Gill SE. The role of TIMPs in regulation of extracellular matrix proteolysis. Matrix Biol [Internet]. 2015 May 1 [cited 2020 Jan 27];44–46:247–54. Available from: https://www.sciencedirect.com/science/article/pii/S0945053X15000566

47. Fraser JRE, Laurent TC, Laurent UBG. Hyaluronan: Its nature, distribution, functions and turnover. J Intern Med. 1997;242(1):27–33.

48. Karsdal MA, Genovese F, Madsen EA, Manon-Jensen T, Schuppan D. Collagen and tissue turnover as a function of age: Implications for fibrosis. J Hepatol [Internet]. 2016 Jan 1 [cited 2020 Jan 27];64(1):103–9. Available from: https://www.sciencedirect.com/science/article/pii/S0168827815005565

49. Zanotelli MR, Goldblatt ZE, Miller JP, Bordeleau F, Li J, Garcia AJ. Regulation of ATP utilization during metastatic cell migration by collagen architecture. 2018;29:1–9.

50. Persad S, Attwell S, Gray V, Delcommenne M, Troussard A, Sanghera J, et al. Inhibition of integrin-linked kinase (ILK) suppresses activation of protein kinase B/Akt and induces cell cycle arrest and apoptosis of PTEN-mutant prostate cancer cells. Proc Natl Acad Sci U S A. 2000;97(7):3207–12.

51. Paszek MJ, Zahir N, Johnson KR, Lakins JN, Rozenberg GI, Gefen A, et al. Tensional homeostasis and the malignant phenotype. Cancer Cell. 2005;

52. Tuxhorn J a, Ayala GE, Smith MJ, Smith VC, Dang TD, Rowley DR. Reactive Stroma in Human Prostate Cancer : Induction of Myofibroblast Phenotype and Extracellular Matrix Remodeling. Clin Cancer Res. 2002;8(September):2912–23.

53. Malik R, Lelkes PI, Cukierman E. Biomechanical and biochemical remodeling of stromal extracellular matrix in cancer. Trends Biotechnol [Internet]. 2015;33(4):230–6. Available from: http://dx.doi.org/10.1016/j.tibtech.2015.01.004

54. Vellinga TT, den Uil S, Rinkes IHB, Marvin D, Ponsioen B, Alvarez-Varela A, et al. Collagen-rich stroma in aggressive colon tumors induces mesenchymal gene expression and tumor cell invasion. Oncogene [Internet]. 2016;35(40):5263–71. Available from: https://doi.org/10.1038/onc.2016.60

55. Kiefer JA, Farach-Carson MC. Type I collagen-mediated proliferation of PC3 prostate carcinoma cell line: implications for enhanced growth in the bone microenvironment. Matrix Biol [Internet]. 2001 Nov 1 [cited 2020 Feb 14];20(7):429–37. Available from: https://www.sciencedirect.com/science/article/pii/S0945053X01001597?via%3Dihub

56. Lieleg O, Baumgärtel RM, Bausch AR. Selective filtering of particles by the extracellular matrix: An electrostatic bandpass. Biophys J. 2009;97(6):1569–77.

57. Philip S, Bulbule A, Kundu GC. Matrix metalloproteinase-2: Mechanism and regulation of NF-κB-mediated activation and its role in cell motility and ECM-invasion. Glycoconj J [Internet]. 2004;21(8):429–41. Available from: https://doi.org/10.1007/s10719-004-5533-7

58. Netti PA, Berk DA, Swartz MA, Grodzinsky AJ, Jain RK. Role of Extracellular Matrix Assembly in Interstitial Transport in Solid Tumors. Cancer Res. 2000;60:2497–503.

59. Yu H, Meyvantsson I, Shkel IA, Beebe DJ. Diffusion dependent cell behavior in microenvironments. Lab Chip. 2005;5(10):1089–95.

60. Kihara T, Ito J, Miyake J. Measurement of biomolecular diffusion in extracellular matrix condensed by fibroblasts using fluorescence correlation spectroscopy. PLoS One [Internet]. 2013 Nov 28;8(11):e82382–e82382. Available from: https://www.ncbi.nlm.nih.gov/pubmed/24312418

61. Mrozik KM, Blaschuk OW, Cheong CM, Zannettino ACW, Vandyke K. N-cadherin in cancer metastasis, its emerging role in haematological malignancies and potential as a therapeutic target in cancer. BMC Cancer [Internet]. 2018;18(1):939. Available from: https://doi.org/10.1186/s12885-018-4845-0

62. Tania M, Khan MA, Fu J. Epithelial to mesenchymal transition inducing transcription factors and metastatic cancer. Tumor Biol [Internet]. 2014;35(8):7335–42. Available from: https://doi.org/10.1007/s13277-014-2163-y

63. Peixoto P, Etcheverry A, Aubry M, Missey A, Lachat C, Perrard J, et al. EMT is associated with an epigenetic signature of ECM remodeling genes. Cell Death Dis [Internet]. 2019;10(3):205. Available from: https://doi.org/10.1038/s41419-019-1397-4

64. Yang M-H, Wu M-Z, Chiou S-H, Chen P-M, Chang S-Y, Liu C-J, et al. Direct regulation of TWIST by HIF-1α promotes metastasis. Nat Cell Biol [Internet]. 2008;10(3):295–305. Available from: https://doi.org/10.1038/ncb1691

65. Gao D, Vahdat LT, Wong S, Chang JC, Mittal V. Microenvironmental Regulation of Epithelial–Mesenchymal Transitions in Cancer. Cancer Res [Internet]. 2012 Oct 1;72(19):4883 LP – 4889. Available from: http://cancerres.aacrjournals.org/content/72/19/4883.abstract

66. Tsai JH, Donaher JL, Murphy DA, Chau S, Yang J. Spatiotemporal Regulation of Epithelial-Mesenchymal Transition Is Essential for Squamous Cell Carcinoma Metastasis. Cancer Cell [Internet]. 2012 Dec 11 [cited 2020 Mar 5];22(6):725–36. Available from: https://www.sciencedirect.com/science/article/pii/S153561081200400X

67. Gao D, Joshi N, Choi H, Ryu S, Hahn M, Catena R, et al. Myeloid Progenitor Cells in the Premetastatic Lung Promote Metastases by Inducing Mesenchymal to Epithelial Transition. Cancer Res [Internet]. 2012 Mar 15;72(6):1384 LP – 1394. Available from: http://cancerres.aacrjournals.org/content/72/6/1384.abstract

68. Reginato MJ, Mills KR, Paulus JK, Lynch DK, Sgroi DC, Debnath J, et al. Integrins and EGFR coordinately regulate the pro-apoptotic protein Bim to prevent anoikis. Nat Cell Biol [Internet]. 2003;5(8):733–40. Available from: https://doi.org/10.1038/ncb1026

69. Paoli P, Giannoni E, Chiarugi P. Anoikis molecular pathways and its role in cancer progression [Internet]. Vol. 1833, Biochimica et Biophysica Acta - Molecular Cell Research. Elsevier B.V.; 2013. p. 3481–98. Available from: http://dx.doi.org/10.1016/j.bbamcr.2013.06.026

70. Gilmore AP. Anoikis. Cell Death Differ [Internet]. 2005 Nov 25;12(S2):1473–7. Available from: http://www.nature.com/articles/4401723

71. Giannoni E, Fiaschi T, Ramponi G, Chiarugi P. Redox regulation of anoikis resistance of metastatic prostate cancer cells: key role for Src and EGFR-mediated pro-survival signals. Oncogene [Internet]. 2009;28(20):2074–86. Available from: https://doi.org/10.1038/onc.2009.77

72. Sakamoto S, McCann RO, Dhir R, Kyprianou N. Talin1 Promotes Tumor Invasion and Metastasis via Focal Adhesion Signaling and Anoikis Resistance. Cancer Res [Internet]. 2010 Mar 1;70(5):1885 LP – 1895. Available from: http://cancerres.aacrjournals.org/content/70/5/1885.abstract

73. Zhao Q, Barclay M, Hilkens J, Guo X, Barrow H, Rhodes JM, et al. Interaction between circulating galectin-3 and cancer-associated MUC1 enhances tumour cell homotypic aggregation and prevents anoikis. Mol Cancer [Internet]. 2010;9(1):154. Available from: https://doi.org/10.1186/1476-4598-9-154

74. Debnath J. Detachment-induced autophagy during anoikis and lumen formation in epithelial acini. Autophagy [Internet]. 2008 Apr 1;4(3):351–3. Available from: https://doi.org/10.4161/auto.5523

75. Saha M, Kumar S, Bukhari S, Balaji SA, Kumar P, Hindupur SK, et al. AMPK – Akt Double-Negative Feedback Loop in Breast Cancer Cells Regulates Their Adaptation to Matrix Deprivation. 2018;(14):1497–511.

76. Gundem G, Van Loo P, Kremeyer B, Alexandrov LB, Tubio JMC, Papaemmanuil E, et al. The evolutionary history of lethal metastatic prostate cancer. Nature. 2015;

77. Hanahan D, Weinberg RA. Hallmarks of cancer: The next generation. Cell [Internet]. 2011;144(5):646–74. Available from: http://dx.doi.org/10.1016/j.cell.2011.02.013

78. Reynolds TY, Rockwell S, Glazer PM. Genetic Instability Induced by the Tumor Microenvironment. Cancer Res [Internet]. 1996 Dec 15;56(24):5754 LP – 5757. Available from: http://cancerres.aacrjournals.org/content/56/24/5754.abstract

79. Bindra RS, Crosby ME, Glazer PM. Regulation of DNA repair in hypoxic cancer cells. Cancer Metastasis Rev [Internet]. 2007;26(2):249–60. Available from: https://doi.org/10.1007/s10555-007-9061-3

80. Min J, Jintaek S, Richard I, Nho S, Hwan Y, Upadhyaya P, et al. Hyaluronan-CD44 / RHAMM interaction-dependent cell proliferation and survival in lung cancer cells. 2018;(July):1–13.

81. Klimkiewicz K, Weglarczyk K, Collet G, Paprocka M, Guichard A, Sarna M, et al. A 3D model of tumour angiogenic microenvironment to monitor hypoxia effects on cell interactions and cancer stem cell selection. Cancer Lett [Internet]. 2017 Jun 28 [cited 2020 Feb 10];396:10–20. Available from: https://www.sciencedirect.com/science/article/pii/S0304383517301702

82. Obenauf AC, Massagué J. Surviving at a Distance: Organ-Specific Metastasis. Vol. 1, Trends in Cancer. Cell Press; 2015. p. 76–91.

83. Fokas E, Engenhart-Cabillic R, Daniilidis K, Rose F, An H-X. Metastasis: the seed and soil theory gains identity. Cancer Metastasis Rev [Internet]. 2007;26(3):705–15. Available from: https://doi.org/10.1007/s10555-007-9088-5

84. Zlotnik A, Burkhardt AM, Homey B. Homeostatic chemokine receptors and organ-specific metastasis. Nat Rev Immunol [Internet]. 2011;11(9):597–606. Available from: https://doi.org/10.1038/nri3049

85. Sun X, Cheng G, Hao M, Zheng J, Zhou X, Zhang J, et al. CXCL12 / CXCR4 / CXCR7 chemokine axis and cancer progression. Cancer Metastasis Rev [Internet]. 2010 Dec;29(4):709–22. Available from: https://www.ncbi.nlm.nih.gov/pubmed/20839032

86. Furusato B, Mohamed A, Uhlén M, Rhim JS. CXCR4 and cancer. Pathol Int [Internet]. 2010 Jul 1;60(7):497–505. Available from: https://doi.org/10.1111/j.1440-1827.2010.02548.x

87. Paget S. THE DISTRIBUTION OF SECONDARY GROWTHS IN CANCER OF THE BREAST. Lancet [Internet]. 1889;133(3421):571–3. Available from: http://www.sciencedirect.com/science/article/pii/S0140673600499150

88. Peinado H, Zhang H, Matei IR, Costa-Silva B, Hoshino A, Rodrigues G, et al. Pre-metastatic niches: organ-specific homes for metastases. Nat Rev Cancer [Internet]. 2017;17(5):302–17. Available from: https://doi.org/10.1038/nrc.2017.6

89. Hoshino A, Costa-Silva B, Shen T-L, Rodrigues G, Hashimoto A, Tesic Mark M, et al. Tumour exosome integrins determine organotropic metastasis. Nature [Internet]. 2015;527(7578):329–35. Available from: https://doi.org/10.1038/nature15756

90. Sánchez CA, Andahur EI, Valenzuela R, Castellón EA, Fullá JA, Ramos CG, et al. Exosomes from bulk and stem cells from human prostate cancer have a differential microRNA content that contributes cooperatively over local and pre-metastatic niche. Oncotarget [Internet]. 2016 Jan 26;7(4):3993–4008. Available from: https://pubmed.ncbi.nlm.nih.gov/26675257

91. Wong CC-L, Gilkes DM, Zhang H, Chen J, Wei H, Chaturvedi P, et al. Hypoxia-inducible factor 1 is a master regulator of breast cancer metastatic niche formation. Proc Natl Acad Sci [Internet]. 2011 Sep 27;108(39):16369 LP – 16374. Available from: http://www.pnas.org/content/108/39/16369.abstract

92. Cox TR, Rumney RMH, Schoof EM, Perryman L, Høye AM, Agrawal A, et al. The hypoxic cancer secretome induces pre-metastatic bone lesions through lysyl oxidase. Nature [Internet]. 2015;522(7554):106–10. Available from: https://doi.org/10.1038/nature14492

93. Peinado H, Zhang H, Matei IR, Costa-Silva B, Hoshino A, Rodrigues G, et al. Pre-metastatic niches: organ-specific homes for metastases. Nat Rev Cancer. 2017;17(5):302–17.

94. Erler JT, Bennewith KL, Cox TR, Lang G, Bird D, Koong A, et al. Hypoxia-Induced Lysyl Oxidase Is a Critical Mediator of Bone Marrow Cell Recruitment to Form the Premetastatic Niche. Cancer Cell [Internet]. 2009 Jan 6 [cited 2020 Feb 19];15(1):35–44. Available from: https://www.sciencedirect.com/science/article/pii/S1535610808003784#bib21

95. Steele JG, Dalton BA, Johnson G, Underwood PA. Polystyrene chemistry affects vitronectin activity: An explanation for cell attachment to tissue culture polystyrene but not to unmodified polystyrene. J Biomed Mater Res [Internet]. 1993 Jul 1;27(7):927–40. Available from: https://doi.org/10.1002/jbm.820270712

96. Steele JG, McFarland C, Dalton BA, Johnson G, Evans MDM, Rolfe Howlett C, et al. Attachment of human bone cells to tissue culture polystyrene and to unmodified polystyrene: the effect of surface chemistry upon initial cell attachment. J Biomater Sci Polym Ed [Internet]. 1994 Jan 1;5(3):245–57. Available from: https://doi.org/10.1163/156856293X00339

97. Curtis AS, Forrester J V, McInnes C, Lawrie F. Adhesion of cells to polystyrene surfaces. J Cell Biol [Internet]. 1983 Nov 1;97(5):1500–6. Available from: https://doi.org/10.1083/jcb.97.5.1500

98. Cukierman E, Pankov R, Stevens DR, Yamada KM. Taking Cell-Matrix Adhesions to the Third Dimension. 2012;294(5547):319–42. Available from: http://dx.doi.org/10.1201/b11532-25

99. Birgersdotter A, Sandberg R, Ernberg I. Gene expression perturbation in vitro — A growing case for three-dimensional (3D) culture systems. 2005;15:405–12.

100. Ihalainen TO, Aires L, Herzog FA, Schwartlander R, Moeller J, Vogel V. Differential basal-to-apical accessibility of lamin A/C epitopes in the nuclear lamina regulated by changes in cytoskeletal tension. Nat Mater [Internet]. 2015;14(12):1252–61. Available from: https://doi.org/10.1038/nmat4389

101. Weiswald LB, Bellet D, Dangles-Marie V. Spherical Cancer Models in Tumor Biology. Neoplasia (United States) [Internet]. 2015;17(1):1–15. Available from: http://dx.doi.org/10.1016/j.neo.2014.12.004

102. Enmon R, O'Connor K, Lacks DJ, Schwartz DK, Dotson RS. Dynamics of Spheroid Self-Assembly in Liquid-Overlay Culture of DU 145 Human Prostate Cancer Cells. 2001;

103. Foty R. A Simple Hanging Drop Cell Culture Protocol for Generation of 3D Spheroids. J Vis Exp [Internet]. 2011 May 6;(51):2720. Available from: http://www.ncbi.nlm.nih.gov/pmc/articles/PMC3197119/

104. Metzger W, Sossong D, Chle ABÄ. The liquid overlay technique is the key to formation of co-culture spheroids consisting of primary osteoblasts , fi broblasts and endothelial cells. 2011;(April):1000–12.

105. Kleinman HK, Martin GR. Matrigel: Basement membrane matrix with biological activity. Semin Cancer Biol [Internet]. 2005 Oct 1 [cited 2018 May 17];15(5):378–86. Available from: https://www.sciencedirect.com/science/article/pii/S1044579X05000313

106. Lang SH, Sharrard RM, Stark M, Villette JM, Maitland NJ. Prostate epithelial cell lines form spheroids with evidence of glandular differentiation in three-dimensional Matrigel cultures. Br J Cancer [Internet]. 2001;85(4):590–9. Available from: https://doi.org/10.1054/bjoc.2001.1967

107. Hughes C, Postovit L, Lajoie G. Matrigel: A complex protein mixture required for optimal growth of cell culture. Proteomics [Internet]. 2010 Apr 28;10(9):1886–90. Available from: https://doi.org/10.1002/pmic.200900758

108. Worthington P, Pochan DJ, Langhans SA. Peptide Hydrogels – Versatile Matrices for 3D Cell Culture in Cancer Medicine [Internet]. Vol. 5, Frontiers in Oncology . 2015. p. 92. Available from: https://www.frontiersin.org/article/10.3389/fonc.2015.00092

109. Ferreira SA, Faull PA, Seymour AJ, Yu TTL, Loaiza S, Auner HW, et al. Neighboring cells override 3D hydrogel matrix cues to drive human MSC quiescence. Biomaterials [Internet]. 2018;176:13–23. Available from: https://doi.org/10.1016/j.biomaterials.2018.05.032

110. Piccoli M, D'Angelo E, Crotti S, Sensi F, Urbani L, Maghin E, et al. Decellularized colorectal cancer matrix as bioactive microenvironment for *in vitro* 3D cancer research. J Cell Physiol [Internet]. 2017;(December):1–27. Available from: http://doi.wiley.com/10.1002/jcp.26403

111. Rodenhizer D, Gaude E, Cojocari D, Mahadevan R, Frezza C, Wouters BG, et al. A three-dimensional engineered tumour for spatial snapshot analysis of cell metabolism and phenotype in hypoxic gradients. Nat Mater. 2016;15(2):227–34.

112. Toivanen R, Taylor RA, Pook DW, Ellem SJ, Risbridger GP. Breaking through a roadblock in prostate cancer research: An update on human model systems. J Steroid Biochem Mol Biol [Internet]. 2012;131(3):122–31. Available from: http://www.sciencedirect.com/science/article/pii/S0960076012000271

113. Gao D, Vela I, Sboner A, Iaquinta PJ, Karthaus WR, Gopalan A, et al. Organoid cultures derived from patients with advanced prostate cancer. Cell [Internet]. 2014;159(1):176–87. Available from: http://dx.doi.org/10.1016/j.cell.2014.08.016

114. Puca L, Bareja R, Prandi D, Shaw R, Benelli M, Karthaus WR, et al. Patient derived organoids to model rare prostate cancer phenotypes. Nat Commun [Internet]. 2018;9(1):2404. Available from: https://doi.org/10.1038/s41467-018-04495-z

115. Drost J, Karthaus WR, Gao D, Driehuis E, Sawyers CL, Chen Y, et al. Organoid culture systems for prostate epithelial and cancer tissue. Nat Protoc [Internet]. 2016;11(2):347–58. Available from: https://doi.org/10.1038/nprot.2016.006

116. Yung CW, Bentley WE, Barbari TA. Diffusion of interleukin-2 from cells overlaid with cytocompatible enzyme-crosslinked gelatin hydrogels. J Biomed Mater Res Part A [Internet]. 2010 Oct 1;95A(1):25–32. Available from: https://doi.org/10.1002/jbm.a.32740

117. Tong Z, Martyn K, Yang A, Yin X, Mead BE, Joshi N, et al. Towards a defined ECM and small molecule based monolayer culture system for the expansion of mouse and human intestinal stem cells. Biomaterials [Internet]. 2018 Feb 1 [cited 2020 Feb 28];154:60–73. Available from: https://www.sciencedirect.com/science/article/pii/S0142961217306877

118. Cowman MK, Lee HG, Schwertfeger KL, McCarthy JB, Turley EA. The content and size of hyaluronan in biological fluids and tissues. Front Immunol. 2015;6(JUN):1–8.

119. Kogan G, Soltes L, Stern R. Hyaluronic acid : a natural biopolymer with a broad range of biomedical and industrial applications. Biotechnol Lett. 2007;29:17–25.

120. Day AJ, Prestwich GD. Hyaluronan-binding Proteins : Tying Up the Giant. 2001;(29):4585–9.

121. Karousou E, Misra S, Ghatak S, Dobra K. Roles and targeting of the HAS / hyaluronan / CD44 molecular system in cancer. Matrix Biol [Internet]. 2017;59:3–22. Available from: http://dx.doi.org/10.1016/j.matbio.2016.10.001

122. Josefsson A, Adamo H, Hammarsten P, Granfors T, Stattin P, Egevad L, et al. Prostate cancer increases hyaluronan in surrounding nonmalignant stroma, and this response is associated with tumor growth and an unfavorable outcome. Am J Pathol [Internet]. 2011;179(4):1961–8. Available from: http://dx.doi.org/10.1016/j.ajpath.2011.06.005

123. Turley EA, Noble PW, Bourguignon LYW. Signaling Properties of Hyaluronan Receptors *. J Biol Chem. 2002;277(7):4589–92.

124. Chen WYJ, Abatangelo G. Functions of hyaluronan in wound repair. Wound Repair Regen. 1999;7(2):79–89.

125. Collins AT, Berry PA, Hyde C, Stower MJ, Maitland NJ. Prospective identification of tumorigenic prostate cancer stem cells. Cancer Res. 2005;65(23):10946–51.

126. Zhao N, Wang X, Qin L, Guo Z, Li D. Effect of molecular weight and concentration of hyaluronan on cell proliferation and osteogenic differentiation in vitro. Biochem Biophys Res Commun [Internet]. 2015 Sep 25 [cited 2020 Feb 26];465(3):569–74. Available from: https://www.sciencedirect.com/science/article/pii/S0006291X15304514

127. Alaniz L, Rizzo M, Malvicini M, Jaunarena J, Avella D, Atorrasagasti C, et al. Low molecular weight hyaluronan inhibits colorectal carcinoma growth by decreasing tumor cell proliferation and stimulating immune response. Cancer Lett [Internet]. 2009 Jun 8 [cited 2020 Feb 26];278(1):9–16. Available from: https://www.sciencedirect.com/science/article/pii/S0304383508009531

128. Misra S, Hascall VC, Berger FG, Markwald RR, Hascall VC, Berger FG, et al. Hyaluronan , CD44 , and Cyclooxygenase-2 in Colon Cancer. 2009;8207:218–24.

129. Lesley J, Hascall VC, Tammi M, Hyman R. Hyaluronan binding by cell surface CD44. J Biol Chem. 2000;275(35):26967–75.

130. Senbanjo LT, Chellaiah MA. CD44: A Multifunctional Cell Surface Adhesion Receptor Is a Regulator of Progression and Metastasis of Cancer Cells . Vol. 5, Frontiers in Cell and Developmental Biology . 2017. p. 18.

131. Wang SJ, Wong G, de Heer A-M, Xia W, Bourguignon LYW. CD44 variant isoforms in head and neck squamous cell carcinoma progression. Laryngoscope. 2009 Aug;119(8):1518–30.

132. Dhir R, Gau J-T, Krill D, Bastacky S, Bahnson RR, Cooper DL, et al. CD44 expression in benign and neoplastic human prostates. Mol Diagnosis. 1997;2(3):197–204.

133. Stevens JW, Palechek PL, Griebling TL, Midura RJ, Rokhlin OW, Cohen MB. Expression of CD44 isoforms in human prostate tumor cell lines. Prostate. 1996 Mar;28(3):153–61.

134. Desai B, Ma T, Zhu J, Chellaiah MA. Characterization of the expression of variant and standard CD44 in prostate cancer cells: Identification of the possible molecular mechanism of CD44/MMP9 complex formation on the cell surface. J Cell Biochem. 2009 Sep;108(1):272–84.

135. Gupta A, Cao W, Chellaiah MA. Integrin αvβ3 and CD44 pathways in metastatic prostate cancer cells support osteoclastogenesis via a Runx2/Smad 5/receptor activator of NF-κB ligand signaling axis. Mol Cancer. 2012;11(1):66.

136. Chu GC-Y, Zhau HE, Wang R, Rogatko A, Feng X, Zayzafoon M, et al. RANK- and c-Met-mediated signal network promotes prostate cancer metastatic colonization. Endocr Relat Cancer. 2014 Mar;21(2):311–26.

137. Bourguignon LYW. Hyaluronan-mediated CD44 activation of RhoGTPase signaling and cytoskeleton function promotes tumor progression. Semin Cancer Biol [Internet]. 2008;18(4):251–9. Available from: http://www.sciencedirect.com/science/article/pii/S1044579X0800028X

138. Okamoto I, Kawano Y, Murakami D, Sasayama T, Araki N, Miki T, et al. Proteolytic release of CD44 intracellular domain and its role in the CD44 signaling pathway . J Cell Biol. 2001 Nov;155(5):755–62.

139. Cho Y, Lee H-W, Kang H-G, Kim H-Y, Kim S-J, Chun K-H. Cleaved CD44 intracellular domain supports activation of stemness factors and promotes tumorigenesis of breast cancer. Oncotarget; Vol 6, No 11. 2015;

140. Lam J, Truong NF, Segura T. Design of cell-matrix interactions in hyaluronic acid hydrogel scaffolds. Acta Biomater [Internet]. 2014;10(4):1571–80. Available from: http://dx.doi.org/10.1016/j.actbio.2013.07.025

141. Tan H, Ramirez CM, Miljkovic N, Li H, Rubin JP, Marra KG. Thermosensitive injectable hyaluronic acid hydrogel for adipose tissue engineering. Biomaterials [Internet]. 2009 Dec 1 [cited 2018 Aug 17];30(36):6844–53. Available from: https://www.sciencedirect.com/science/article/pii/S0142961209009156

142. Xu X, Gurski LA, Zhang C, Harrington DA, Farach-Carson MC, Jia X. Recreating the tumor microenvironment in a bilayer, hyaluronic acid hydrogel construct for the growth of prostate cancer spheroids. Biomaterials [Internet]. 2012;33(35):9049–60. Available from: http://dx.doi.org/10.1016/j.biomaterials.2012.08.061

143. Shu XZ, Liu Y, Luo Y, Roberts MC, Prestwich GD. Disulfide cross-linked hyaluronan hydrogels. Biomacromolecules. 2002;3(6):1304–11.

144. Baier Leach J, Bivens KA, Patrick Jr. CW, Schmidt CE. Photocrosslinked hyaluronic acid hydrogels: Natural, biodegradable tissue engineering scaffolds. Biotechnol Bioeng [Internet]. 2003 Mar 17;82(5):578–89. Available from: https://doi.org/10.1002/bit.10605

145. Zheng Shu X, Liu Y, Palumbo FS, Luo Y, Prestwich GD. In situ crosslinkable hyaluronan hydrogels for tissue engineering. Biomaterials [Internet]. 2004 Mar 1 [cited 2020 Feb 26];25(7–8):1339–48. Available from: https://www.sciencedirect.com/science/article/pii/S0142961203006707#BIB55

146. Oueslati N, Leblanc P, Harscoat-Schiavo C, Rondags E, Meunier S, Kapel R, et al. CTAB turbidimetric method for assaying hyaluronic acid in complex environments and under cross-linked form. Carbohydr Polym [Internet]. 2014;112:102–8. Available from: http://dx.doi.org/10.1016/j.carbpol.2014.05.039

147. Gerecht S, Burdick JA, Ferreira LS, Townsend SA, Langer R, Vunjak-Novakovic G. Hyaluronic acid hydrogel for controlled self-renewal and differentiation of human embryonic stem cells. Proc Natl Acad Sci [Internet]. 2007 Jul 3 [cited 2020 Apr 7];104(27):11298–303. Available from: https://www.pnas.org/content/104/27/11298

148. Tan S, Yamashita A, Gao SJ, Kurisawa M. Hyaluronic acid hydrogels with defined crosslink density for the efficient enrichment of breast cancer stem cells. Acta Biomater [Internet]. 2019 Aug 1 [cited 2020 Apr 7];94:320–9. Available from: https://www.sciencedirect.com/science/article/pii/S1742706119303678

149. Ross D. Glutathione, free radicals and chemotherapeutic agents: Mechanisms of free-radical induced toxicity and glutathione-dependent protection. Pharmacol Ther [Internet]. 1988 Jan 1 [cited 2020 Mar 3];37(2):231–49. Available from: https://www.sciencedirect.com/science/article/abs/pii/0163725888900277

150. Clark AH, Farrer DB. Kinetics of biopolymer gelation—Implications of a cascade theory description for the concentration, molecular weight, and temperature dependences of the shear modulus and gel time. J Rheol (N Y N Y). 1995 Nov;39(6):1429–44.

151. Ross-Murphy SB. Concentration Dependence of Gelation Time. In: Dickinson Gels and Colloids EBT-FP, editor. Woodhead Publishing; 1991. p. 357–68.

152. Xu W, Tang H, Lv H, Li J, Zhao X, Li H, et al. Sol–gel transition of poly(3-hexylthiophene) revealed by capillary measurements: phase behaviors, gelation kinetics and the formation mechanism. Soft Matter [Internet]. 2012;8(3):726–33. Available from: http://dx.doi.org/10.1039/C1SM06482G

153. Ahn B-M, Kim J, Ian L, Rha K-H, Kim H-J. Mechanical Property Characterization of Prostate Cancer Using a Minimally Motorized Indenter in an Ex Vivo Indentation Experiment. Urology [Internet]. 2010 Oct 1 [cited 2020 Mar 9];76(4):1007–11. Available from: https://www.sciencedirect.com/science/article/pii/S0090429510002323?via%3Dihub

154. Bhushan B. Modern Tribology Handbook. Williams JA (Cambridge), Dwyer-Joyce RS (University of S, editors. CRC Press LLC; 2001. 138 p.

155. Horoszewicz JS, Leong SS, Kawinski E, Karr JP, Rosenthal H, Chu TM, et al. LNCaP Model of Human Prostatic Carcinoma. Cancer Res [Internet]. 1983 Apr 1;43(4):1809 LP – 1818. Available from: http://cancerres.aacrjournals.org/content/43/4/1809.abstract

156. Tai S, Sun Y, Squires JM, Zhang H, Oh WK, Liang C-Z, et al. PC3 is a cell line characteristic of prostatic small cell carcinoma. Prostate [Internet]. 2011 Nov 1;71(15):1668–79. Available from: https://doi.org/10.1002/pros.21383

157. Antoniou E, Tsianou M. Solution properties of dextran in water and in formamide. J Appl Polym Sci [Internet]. 2012 Aug 5;125(3):1681–92. Available from: https://doi.org/10.1002/app.35475

158. Axelrod D, Koppel DE, Schlessinger J, Elson E, Webb WW. Mobility measurement by analysis of fluorescence photobleaching recovery kinetics. Biophys J [Internet]. 1976 Sep;16(9):1055–69. Available from: https://pubmed.ncbi.nlm.nih.gov/786399

159. Soumpasis DM. Theoretical analysis of fluorescence photobleaching recovery experiments. Biophys J [Internet]. 1983;41(1):95–7. Available from: http://dx.doi.org/10.1016/S0006-3495(83)84410-5

160. Ferreira LMR. Cancer metabolism: The Warburg effect today. Exp Mol Pathol [Internet]. 2010;89(3):372–80. Available from: http://dx.doi.org/10.1016/j.yexmp.2010.08.006

161. Escudero RM, Amo FH, Martínez MCN, Jiménez JT, Alonso AH, Piniés GO, et al. Metastatic prostate cancer on the thyroid cartilage: unusual symptoms of prostatic adenocarcinoma. Case report. Arch Esp Urol [Internet]. 2011 Mar;64(2):132—135. Available from: http://europepmc.org/abstract/MED/21422500

162. Nohara T, Kawashima A, Takahashi T, Kitamura M, Akai H, Oka T, et al. [Prostate cancer metastasized to thyroid cartilage: a case report]. Nihon Hinyokika Gakkai Zasshi [Internet]. 2005 Nov;96(7):697—700. Available from: https://doi.org/10.5980/jpnjurol1989.96.697

163. Hay N. The Akt-mTOR tango and its relevance to cancer. Cancer Cell. 2005;8(3):179–83.

164. Magnuson B, Ekim B, Fingar DC. Regulation and function of ribosomal protein S6 kinase (S6K) within mTOR signalling networks. Biochem J [Internet]. 2011 Dec 14;441(1):1–21. Available from: https://doi.org/10.1042/BJ20110892

165. Graff JR, Konicek BW, McNulty AM, Wang Z, Houck K, Allen S, et al. Increased AKT activity contributes to prostate cancer progression by dramatically accelerating prostate tumor growth and diminishing p27Kip1 expression. J Biol Chem [Internet]. 2000 Aug 11 [cited 2020 Apr 7];275(32):24500–5. Available from: http://www.ncbi.nlm.nih.gov/pubmed/10827191

166. Guertin DA, Sabatini DM. Defining the Role of mTOR in Cancer. Cancer Cell [Internet]. 2007 Jul 10 [cited 2020 Apr 7];12(1):9–22. Available from: https://www.sciencedirect.com/science/article/pii/S1535610807001511

167. Stephens AS, Stephens SR, Morrison NA. Internal control genes for quantitative RT-PCR expression analysis in mouse osteoblasts, osteoclasts and macrophages. BMC Res Notes [Internet]. 2011;4(1):410. Available from: https://doi.org/10.1186/1756-0500-4-410

168. Cicinnati VR, Shen Q, Sotiropoulos GC, Radtke A, Gerken G, Beckebaum S. Validation of putative reference genes for gene expression studies in human hepatocellular carcinoma using real-time quantitative RT-PCR. BMC Cancer [Internet]. 2008;8(1):350. Available from: https://doi.org/10.1186/1471-2407-8-350

169. Mazure NM, Pouysségur J. Hypoxia-induced autophagy: cell death or cell survival? Curr Opin Cell Biol [Internet]. 2010;22(2):177–80. Available from: http://www.sciencedirect.com/science/article/pii/S0955067409002294

170. Krishnamachary B, Penet M-F, Nimmagadda S, Mironchik Y, Raman V, Solaiyappan M, et al. Hypoxia regulates CD44 and its variant isoforms through HIF-1α in triple negative breast cancer. PLoS One [Internet]. 2012/08/28. 2012;7(8):e44078–e44078. Available from: https://pubmed.ncbi.nlm.nih.gov/22937154

171. Ma Y, Liang D, Liu J, Axcrona K, Kvalheim G, Stokke T, et al. Prostate cancer cell lines under hypoxia exhibit greater stem-like properties. PLoS One [Internet]. 2011/12/28. 2011;6(12):e29170–e29170. Available from: https://pubmed.ncbi.nlm.nih.gov/22216200

172. Nam K, Oh S, Shin I. Ablation of CD44 induces glycolysis-to-oxidative phosphorylation transition via modulation of the c-Src-Akt-LKB1-AMPKα pathway. Biochem J [Internet]. 2016 Jul 25;BCJ20160613. Available from: http://www.biochemj.org/content/early/2016/07/25/BCJ20160613.abstract

173. Tamada M, Nagano O, Tateyama S, Ohmura M, Yae T, Ishimoto T, et al. Modulation of Glucose Metabolism by CD44 Contributes to Antioxidant Status and Drug Resistance in Cancer Cells. Cancer Res [Internet]. 2012 Mar 15;72(6):1438 LP – 1448. Available from: http://cancerres.aacrjournals.org/content/72/6/1438.abstract

174. Bonneh-Barkay D, Wiley CA. Brain extracellular matrix in neurodegeneration. Brain Pathol [Internet]. 2008/07/25. 2009 Oct;19(4):573–85. Available from: https://pubmed.ncbi.nlm.nih.gov/18662234

175. Bhattacharya DS, Svechkarev D, Souchek JJ, Hill TK, Taylor MA, Natarajan A, et al. Impact of structurally modifying hyaluronic acid on CD44 interaction. J Mater Chem B [Internet]. 2017;5(41):8183–92. Available from: http://dx.doi.org/10.1039/C7TB01895A